PHYSICAL REVIEW D **96,** 026001 (2017)

CP-odd sector and θ dynamics in holographic QCD

Daniel Areán,[1] Ioannis Iatrakis,[2] Matti Järvinen,[3] and Elias Kiritsis[4,5,6]
[1]*Max-Planck-Institut für Physik (Werner-Heisenberg-Institut), Föhringer Ring 6, D-80805 Munich, Germany*
[2]*Institute for Theoretical Physics, Utrecht University Leuvenlaan 4, 3584 CE Utrecht, Netherlands*
[3]*Laboratoire de Physique Théorique de l' École Normale Supérieure & Institut de Physique Théorique Philippe Meyer, PSL Research University, CNRS, Sorbonne Universités, UPMC Univ. Paris 06, 24 rue Lhomond, 75231 Paris Cedex 05, France*
[4]*Crete Center for Theoretical Physics, Institute for Theoretical and Computational Physics, Department of Physics, University of Crete, 71003 Heraklion, Greece*
[5]*Crete Center for Quantum Complexity and Nanotechnology, Department of Physics, University of Crete, 71003 Heraklion, Greece*
[6]*APC, Université Paris 7, Diderot, CNRS/IN2P3, CEA/IRFU, Obs. de Paris, Sorbonne Paris Cité, Bâtiment Condorcet, F-75205 Paris Cedex 13, France (UMR du CNRS 7164)*
(Received 25 February 2017; published 7 July 2017)

The holographic model of V-QCD is used to analyze the physics of QCD in the Veneziano large-N limit. An unprecedented analysis of the *CP*-odd physics is performed going beyond the level of effective field theories. The structure of holographic saddle points at finite θ is determined, as well as its interplay with chiral symmetry breaking. Many observables (vacuum energy and higher-order susceptibilities, singlet and nonsinglet masses and mixings) are computed as functions of θ and the quark mass m. Wherever applicable the results are compared to those of chiral Lagrangians, finding agreement. In particular, we recover the Witten-Veneziano formula in the small $x \to 0$ limit, we compute the θ dependence of the pion mass, and we derive the hyperscaling relation for the topological susceptibility in the conformal window in terms of the quark mass.

DOI: 10.1103/PhysRevD.96.026001

I. INTRODUCTION AND OUTLOOK

The axial anomaly plays an important role in the physics of strong interactions and is inherently related to the $U(1)_A$ problem of QCD. The massless QCD Lagrangian enjoys a flavor symmetry, $SU(N_f)_V \times SU(N_f)_A \times U(1)_V \times U(1)_A$. The $U(1)_V$ part is conserved and results in the baryon number conservation. $SU(N_f)_V \times SU(N_f)_A$ is spontaneously broken down to $SU(N_f)_V$. The spontaneous breaking is signaled by the existence of Goldstone bosons in the low energy spectrum of the theory. However, there is neither any trace of $U(1)_A$ symmetry in the spectrum of the theory nor any light Goldstone boson which would signal its spontaneous breaking. Instead, a large mass of η', compared to standard expectations from current algebra [1], was observed experimentally. Historically this is known as the $U(1)_A$ problem in QCD [2].

't Hooft proposed [3] that the nontrivial topological gauge field configurations, instantons, violate the $U(1)_A$ symmetry. Classical instanton solutions lead to nonzero $\int d^4x \mathbb{T}rG \wedge G$, where G is the gluon field strength. This leads to tunneling among different vacua with different topological charge. Most importantly, a nontrivial $\int d^4x \mathbb{T}rG \wedge G$ in QCD results in the nonconservation of the axial current, due to the axial anomaly. This implies that a nonzero *CP*-odd term in the QCD Lagrangian, known as the θ term, $\frac{\theta}{32\pi^2}\mathbb{T}rG \wedge G$, can affect nonperturbatively the dynamics of the theory. In [4], it was pointed out that in the context of the instanton picture, certain anomalous Ward identities are not satisfied and the expectation values of certain operators do not have the correct θ dependence.

The $U(1)_A$ problem was further studied in the large N_c limit where an additional puzzle appeared: if the $U(1)_A$ anomaly is responsible for the would-be Goldstone boson (the η') having a mass, then the mass must be due to the instantons. Therefore it should be proportional to the standard instanton factor that is exponentially small at large N_c. On the other hand, Ward identities seemed to indicate an inverse power law dependence of the η' mass on N_c. Witten [5], by studying a similar model in two dimensions, argued that instantons do not behave as a gas (as is usually assumed in instanton calculations), but rather the instanton number becomes continuous, and this is responsible for the power law dependence of the η' mass.

Along the same line of thought, Veneziano [6] introduced the limit where quark loops contribute to leading order to the $U(1)_A$ anomaly:

$$N_c \to \infty, \qquad N_f \to \infty,$$
$$\frac{N_f}{N_c} = x = \text{fixed}, \qquad \lambda = g_{\rm YM}^2 N_c = \text{fixed}. \quad (1.1)$$

In this limit he was able to resolve the inconsistencies pointed out in [4], to rederive the η'-mass formula,

Eq. (7.21), which was earlier advocated by Witten [7], and to show that the anomalous Ward identities are satisfied.

The dependence of low energy QCD physics on the θ angle was further studied in the context of the low energy effective Lagrangians [8–13]. More recently, lattice field theory methods have also been employed to study the topological dynamics of QCD [14–17].

The inclusion of a θ term in QCD obviously leads to CP violation effects in strong interactions. As it was shown in [18], independently of the confining gluon dynamics, the presence of instantons leads to P- and T-odd effects. However, no such experimental signal has been observed until now: the experimental bound for the value of θ is $|\theta| \leq 3 \times 10^{-10}$. Several attempts have been made to solve the problem [18–26]. The straightforward solution proposes the existence of a (fundamental) pseudoscalar axion field which couples to the topological operator $\mathbb{T}rG \wedge G$. This coupling is suppressed by a large scale, that makes the axion interactions weak. In this way the θ angle becomes now a dynamical variable (the expectation value of the axion field) and the QCD dynamics forces this expectation value to relax to zero [7].

The topological effects in QCD, have recently attracted much attention due to the exciting discovery of the chiral magnetic effect, which takes place when the quark gluon plasma (QGP) moves in a background magnetic field, as soon as there is chiral charge imbalance in the medium. It has been claimed that such an imbalance is created due to topological fluctuations of the medium and their connection to the axial anomaly [27]. Even though it has been argued that the instanton contributions at finite temperature are exponentially suppressed [28], topological fluctuations of the medium, due to sphalerons, at finite temperature [29], lead to a net axial charge [30]. Anomalous conductivities were also studied in holography in [31] and their renormalization for nonconformal theories in [32].

The effects of the axial anomaly and the θ term in low energy QCD have been also studied in the context of holography. In [33], Witten studied the θ dependence of the D_4 brane holographic model, dual to a certain pure four-dimensional Yang Mills theory [34]. The θ angle was introduced as the source of a Ramond-Ramond (RR) bulk field. Then, the energy density of the vacuum was computed as a function of θ and it was shown that for every θ there are infinite distinct vacua. Similar conclusions hold in bottom-up holographic models of pure Yang-Mills theory such as the improved holographic QCD (IHQCD) model [35,36]. In [37], similar observables were computed, building on the background solutions with backreacting θ of [38,39] in the case of $\theta \sim \mathcal{O}(N_c^2)$.

The Witten-Veneziano formula for the mass of η' in the black D_4 brane theory was derived holographically in [40] by including probe D_6 flavor branes in the D_4 background [41]. A similar result was drawn in a different holographic model, where D_3 branes were embedded on a $\mathbb{C}_3/(Z_3 \otimes Z_3)$ orbifold singularity [42]. Later, the Witten-Veneziano formula was verified in more realistic holographic models such as the Witten-Sakai-Sugimoto model [43] and the tachyon AdS/QCD model [44,45], where a θ angle of order $\mathcal{O}(1)$ was considered. The backreaction of the flavor to the geometry in the Witten-Sakai-Sugimoto model and the effect of finite θ angle were considered in [46]. In models with flavors, the coupling of the flavor branes to the RR fields is found by anomaly inflow arguments, which were presented in [47].

The 't Hooft large-N_c limit is a excellent technical tool for studying nonperturbative dynamics. Concerning the physics of the axial $U(1)_A$ anomaly, however, the Veneziano large-N_c limit in (1.1) is more appropriate as in this limit the $U(1)_A$ anomaly is a leading effect. This limit was advocated already in order to describe holographic models similar to QCD that exhibit a conformal window in some part of their phase diagram [48]. This led to a class of holographic theories under the name of V-QCD, whose properties were analyzed in several contexts with interesting and sometimes unexpected results [48–55].

The purpose of the present paper is to fully analyze the CP-odd dynamics of V-QCD associated with the θ dynamics as well as with the dynamics of the phases of the quark mass matrix.

A. Summary of results

We will first describe the complete V-QCD action with CP-odd terms which contains the physics of the axial anomaly and the θ angle. We will use this theory to analyze, among other things, the phase diagram (as a function of the *complex* quark mass and the θ angle) and the meson spectrum. In more detail, the main results are as follows.

In Sec. II we indicate the general structure of CP-odd terms that are added in the V-QCD models. Our method is based on earlier work [44,56,57], and its adaptation to the fully backreacted models was initially studied in [51]. The CP-odd sector arises from the Wess-Zumino-Witten term for the N_f space-filling pairs of $D4 - \overline{D4}$ branes. However, following the reasoning in the glue [35] and flavor [48] sectors, we introduce potential functions depending on the bulk scalars, the dilaton and the tachyon, in the CP-odd action, therefore switching from a top-down to a bottom-up approach. We restrict our study to flavor independent backgrounds [respecting the $SU(N_f)_V$ symmetry], and in particular, to flavor independent quark mass, writing the complex tachyon field as $T = \tau e^{i\xi}\mathbb{I}$, where $\mathbb{I}$ is the unit matrix in flavor space. The final CP-odd action is then given in Eq. (2.15). We stress that full backreaction between all terms in the action (glue, flavor, and CP-odd) is included.

The CP-odd fields are the following:

(i) The axion $\mathfrak{a}$ which is dual to the operator $\mathbb{T}rG \wedge G$ and sources the θ angle on the boundary.

(ii) The phase of the tachyon ξ which is (roughly) dual to the operator $\bar{\psi}\gamma_5\psi$ and sources the phase of the quark mass.

(iii) These are related by the anomaly to the divergence of the axial current [the longitudinal component of the $U(1)_A$ vector of the bulk theory].

The precise dictionary is specified through the boundary coupling to field theory in (2.19). We demonstrate that V-QCD models are consistent with the periodicity of the θ angle in QCD. As expected for QCD in the Veneziano limit [33], the vacua related by $\theta \mapsto \theta + 2\pi$ are not linked by continuous deformation of the θ angle, but there is branch structure instead. Moreover, we argue that the axial anomaly, given in Eq. (2.25), is correctly reproduced. The gauge-independent *CP*-odd source is identified with the gauge invariant $\bar{\theta}$ angle in QCD: $\bar{\theta} = \theta + \arg\det M_q$, where M_q is the (complex) quark mass matrix.

In Sec. III we derive the equations of motion for V-QCD at finite θ angle and analyze their asymptotic solutions. The axial $U(1)_A$ symmetry implies that the *CP*-odd degrees of freedom, the axion and the tachyon phase, can be integrated out. After taking into account symmetry and regularity in the IR, their effect reduces to an additional integration constant C_a, which is seen to be proportional to the VEV of the $\mathbb{T}rG \wedge G$ operator. After solving the background equations, this integration constant can be mapped to the (UV value of the) $\bar{\theta}$ angle.

Perturbative analysis of the solutions near the boundary shows that solutions at finite C_a (and therefore nontrivial $\bar{\theta}$) must always have nonzero quark mass and that $\bar{\theta}$ becomes ambiguous as $m_q \to 0$. This reflects properties of QCD: the θ angle can be gauged away if any of the quarks is massless. We also note that the VEVs of the quark bilinears $\bar{\psi}\psi$, $\bar{\psi}\gamma_5\psi$, and the VEV of $\mathbb{T}rG \wedge G$ respect axial symmetry. The IR regularity of the (fully backreacted) solutions is seen to give constraints to the dependence of the flavor and *CP*-odd terms of the V-QCD action on the dilaton and the tachyon. In particular, we point out that the string theory prediction for the dilaton dependence of the flavor action in the IR falls in the narrow range of acceptable behaviors which produce fully regular solutions, complementing earlier, similar results [35,51].

In Sec. IV we review how the various potentials in the glue and flavor sectors of the V-QCD action are constrained due to regularity, asymptotic behavior near the boundary and in the UV, and by agreement with QCD at the qualitative level. In particular we combine previous results with the additional constraints from the asymptotic analysis of the *CP*-odd solutions in Sec. III. We determine explicit choices for potentials which satisfy the constraints, therefore finalizing the construction of V-QCD at finite $\bar{\theta}$.

In order to compare our results to the chiral Lagrangians, they are derived in the Veneziano limit in Sec. V. We note the following:

(i) There is a delicate issue in the ordering of the chiral ($m_q \to 0$) and 't Hooft or probe ($x \to 0$) limits: the chiral limit needs to be taken before the probe limit or simultaneously with it for the chiral Lagrangians to be applicable. This issue is not relevant in the Veneziano limit, where x is finite.

(ii) Unlike in the 't Hooft limit, the glueballs and mesons mix at leading order in the Veneziano limit. We argue that this mixing does not affect the chiral Lagrangian (5.21) for the Goldstone modes nor the Gell-Mann-Oakes-Renner (GOR) relation.

(iii) The chiral Lagrangian in the Veneziano limit, (5.21), has two important terms which are suppressed in the 't Hooft limit but are leading in the Veneziano limit: one term is responsible for the chiral anomaly and another allows the decay constants of the pions and the η' meson to be different.

In Sec. VI V-QCD is used to analyze (analytically and numerically) the vacuum structure as a function of m_q, $x = N_f/N_c$, and $\bar{\theta}$. As a function of x QCD has two phases of interest: the QCD-like phase for $0 < x < x_c$, and the conformal window for $x_c \le 0 < 11/2 \equiv x_{\rm BZ}$ where the model has an IR fixed point (see [48] and the review in Sec. II B). In addition inside the low-x phase, for $x_c - x \ll 1$, there is a region where the RG flow includes walking, or quasiconformal behavior: the coupling constant varies very slowly for a large range of energies.

A rich and interesting structure is found in the QCD-like phase. We solve numerically the vacua in V-QCD and when applicable we compare the results to those derived from chiral Lagrangians.

The main results from the analysis of V-QCD in the QCD-like phase $x < x_c$ are the following:

(i) In the limit $m_q \to 0$, where chiral Lagrangians for QCD are reliable, they agree with V-QCD. In particular, the leading terms of the free energy as a function of $\bar{\theta}$ and topological susceptibility, which can be derived analytically in V-QCD, match exactly with the predictions of the effective (chiral) theory.

(ii) The analytic agreement with the effective chiral field theory is present both when (only) the pions are light [$m_q \to 0$ with $x = \mathcal{O}(1)$], and also when both the pions and the η' mesons are light ($m_q \to 0$ and $x \to 0$ with $m_q \sim x$).

(iii) We carry out a detailed numerical analysis of the vacua at finite $\bar{\theta}$ in V-QCD in regimes where chiral Lagrangians are not expected do be valid and analytic approximations are not known (e.g., intermediate quark masses), determining key observables such as the topological susceptibility and free energy.

(iv) As $m_q \to \infty$, the quarks decouple and the dynamics becomes that of Yang-Mills theory.[1]

[1]Decoupling here means that observables as functions of the gauge invariant $\bar{\theta}$ angle, such as the topological susceptibility and the free energy, approach their Yang-Mills form. The phase of the quark mass does not decouple but appears only through the gauge invariant variable $\bar{\theta}$.

(v) The final result for the free energy for the energetically favored phase in Eq. (6.16) is similar in form to the result in the 't Hooft limit [33].

(vi) We demonstrate that the dependence between the (complex) source and VEV of the tachyon has a complicated structure, implied by IR regularity, which naturally appears in holographic models but is difficult to describe by using field theory techniques. The results in this article generalize the spiral dependence to complex variables and is linked to a tower of perturbatively unstable Efimov vacua.

The phase structure as a function of x, in the conformal window, and near the conformal transition at $x = x_c$ is studied as well. In the conformal window, the vacuum structure is simpler than in the QCD-like phase as the structure related to the Efimov vacua is absent. In this phase and near the conformal phase transition, the dependence on the quark mass of observables (such as the topological susceptibility) is understood in terms of the separation of UV and IR scales, in agreement with the behavior at $\bar{\theta} = 0$ [55].

Specifically, we find the following:

(i) The scale separation gives rise to the hyperscaling relation for the topological susceptibility in the conformal window:

$$\chi \propto m_q^{\frac{4}{1+\gamma_*}} \quad \text{as} \quad m_q \to 0, \qquad (x_c < x < x_{\rm BZ}), \tag{1.2}$$

where γ_* is the anomalous dimension of the quark mass at the IR fixed point.

(ii) In the walking regime, $x_c - x \ll 1$, the topological susceptibility obeys an intermediate scaling law, $\chi \propto m_q^2$, which holds for longer and longer range of masses as $x \to x_c$ from below.

(iii) The agreement with chiral Lagrangians as $m_q \to 0$ in the QCD-like phase is found for all x within the range $0 < x < x_c$, even in the walking regime. We check this explicitly for the topological susceptibility.

We perform two separate calculations of meson masses. First, in Sec. VII we complete the analysis of [51] by computing at vanishing $\bar{\theta}$ angle the spectra of the flavor singlet pseudoscalar modes, which involve the fields of the CP-odd action S_a. The results are as follows:

(i) The pseudoscalar glueball modes mix with the $\bar{\psi}\gamma_5\psi$ states at generic values of x, and the mixing is suppressed for $x \to 0$.

(ii) The η' meson is identified as the lightest state in this tower as $x \to 0$. It is shown analytically (in Appendix G) and verified numerically that its mass satisfies the Witten-Veneziano relation

$$m_{\eta'}^2 = m_\pi^2 + x\frac{N_f N_c \chi_{\rm YM}}{f_\pi^2}, \tag{1.3}$$

where $\chi_{\rm YM}$ is the Yang-Mills topological susceptibility, when both x and the quark mass are small.

(iii) Apart from the η' meson, a numerical study shows that the dependence on the masses on x and m_q is similar to other sectors, discussed in [51]. In particular, when $m_q = 0$ the dependence on x is mild for $x = \mathcal{O}(1)$, and as $x \to x_c{}^-$ all masses follow the Miransky or Berezinskii-Kosterlitz-Thouless (BKT) scaling law of Eq. (2.33).

Finally, in Sec. VIII, we analyze the spectrum of flavor nonsinglet fluctuations at finite $\bar{\theta}$ angle. Specifically, we use the branch of vacua that are continuous deformations of the "standard" background at $\bar{\theta} = 0$.

(i) At finite $\bar{\theta}$, the scalar and pseudoscalar mesons mix. The mixing vanishes as expected when $\bar{\theta} \to 0$. There is no mixing in the spin-one sector because vectors and axial vectors transform with opposite signs under charge conjugation, which remains as a good quantum number even at finite $\bar{\theta}$ (whereas parity and CP are broken).

(ii) The pion mass is shown to satisfy the generalized Gell-Mann-Oakes-Renner relation

$$f_\pi^2 m_\pi^2 = -\langle\bar{\psi}\psi\rangle|_{m_q=0} m_q \cos\frac{\bar{\theta}}{N_f} + \mathcal{O}(m_q^2) \tag{1.4}$$

analytically and numerically.

(iii) Apart from the pion mode, the dependence of the meson masses on $\bar{\theta}$ is weak.

Briefly the structure of this paper is as follows. In Sec. II we review the V-QCD model and its background solutions for $\bar{\theta} = 0$. In Sec. III we derive the equations of motion with the CP-odd sector included, and analyze their asymptotic solutions. In Sec. IV we present choices of potentials for the V-QCD action which satisfy all known constraints. Section V contains a detailed analysis of the chiral Lagrangians for QCD in the Veneziano limit. In Sec. VI we carry out a detailed analysis of the vacuum structure of the V-QCD models at finite $\bar{\theta}$. In Sec. VII we compute the spectra of flavor singlet CP-odd fluctuations at $\bar{\theta} = 0$. Finally, in Sec. VIII we analyze the flavor nonsinglet meson spectra at finite $\bar{\theta}$.

Technical details are presented in the appendices. In Appendix A, we carry out a detailed analysis of the UV and IR asymptotics of the backgrounds at finite $\bar{\theta}$. In Appendix C we discuss technical details of the vacuum solutions at finite $\bar{\theta}$. Appendix D contains the fluctuation equations for the flavor singlet CP-odd modes. In Appendix E we derive the fluctuation equations for the flavor nonsinglet modes at finite $\bar{\theta}$. Appendix G has details of the proof of the Witten-Veneziano formula for the mass of the η' meson in V-QCD. In Appendix H we prove the Gell-Mann-Oakes-Renner relation at finite $\bar{\theta}$ in V-QCD.

II. V-QCD

We shall start by writing down the action for V-QCD

$$S = S_g + S_f + S_a, \tag{2.1}$$

where S_g and S_f are the pieces corresponding to the glue and flavor sectors, while S_a, which will be the central piece of our analysis, describes the CP-odd sector. The first two contributions have been carefully analyzed in [48], since they are the only ones contributing to the vacuum structure at zero θ angle. We will briefly discuss them before focusing on the CP-odd piece S_a.

The glue action, introduced in [35], takes the form

$$S_g = M^3 N_c^2 \int d^5x\sqrt{-g}\left(R - \frac{4}{3}\frac{(\partial\lambda)^2}{\lambda^2} + V_g(\lambda)\right) \quad (2.2)$$

with $\lambda = e^{\phi}$ the exponential of the dilaton, dual to the operator $\mathbb{T}rF^2$. Hence we identify the background value of λ with the 't Hooft coupling. As for the metric, the Ansatz for the background solution reads

$$ds^2 = e^{2A(r)}(dx_{1,3}^2 + dr^2), \quad (2.3)$$

where the warp factor A is identified with the logarithm of the energy scale in the field theory. In our conventions, the UV boundary is at $r = 0$ (and $A \to \infty$), and the radial coordinate is then in the range $r \in [0, \infty)$. Moreover, the metric will be close to that of AdS near the UV boundary. Therefore $A \sim -\log(r/\ell)$ with ℓ being the (UV) AdS radius, and in the UV r is roughly dual to the inverse of the energy scale of the field theory.

As shown in [51] the fluctuations of the action for the flavor sector S_f mix with those of the CP-odd term S_a. Therefore we first write the action for the flavor sector in general [44] (see also [58]),

$$S_f = -\frac{1}{2}M^3 N_c \mathbb{T}r \int d^4x dr (V_f(\lambda, T^\dagger T)\sqrt{-\det \mathbf{A}_L} + V_f(\lambda, TT^\dagger)\sqrt{-\det \mathbf{A}_R}), \quad (2.4)$$

with the radicands defined as

$$\mathbf{A}_{LMN} = g_{MN} + w(\lambda,T)F^{(L)}_{MN} + \frac{\kappa(\lambda,T)}{2}[(D_M T)^\dagger (D_N T) + (D_N T)^\dagger (D_M T)],$$
$$\mathbf{A}_{RMN} = g_{MN} + w(\lambda,T)F^{(R)}_{MN} + \frac{\kappa(\lambda,T)}{2}[(D_M T)(D_N T)^\dagger + (D_N T)(D_M T)^\dagger], \quad (2.5)$$

and the covariant derivative is given by

$$D_M T = \partial_M T + iTA^L_M - iA^R_M T. \quad (2.6)$$

We notate the five-dimensional indices with capital Latin letters $M, N, \ldots$ and the four-dimensional Lorentz indices with Greek letters $\mu, \nu, \ldots$ throughout the article. The fields A_L, A_R and T are $N_f \times N_f$ matrices in the flavor space, and under the left and right $U(N_f)$ gauge transformations they transform as

$$A_L \to V_L A_L V_L^\dagger - idV_L V_L^\dagger, \quad A_R \to V_R A_R V_R^\dagger - idV_R V_R^\dagger,$$
$$T \to V_R T V_L^\dagger, \quad T^\dagger \to V_L T^\dagger V_R^\dagger, \quad (2.7)$$

with $V_L V_L^\dagger = \mathbb{I} = V_R V_R^\dagger$. A_L, A_R are dual to the left and right flavor currents of the theory while T is dual to the quark mass operator.

It is also useful to define

$$x \equiv \frac{N_f}{N_c}. \quad (2.8)$$

In general, it is not known how to perform the trace in (2.4) when the arguments of the determinants are non-Abelian matrices in flavor space. However, since we will be considering cases where the quarks are either massless or have all the same mass, the background solution will be proportional to the unit matrix. Additionally, for this kind of background, the fluctuations of the Lagrangian are unambiguous up to quadratic order.

As in [51] we will consider the following form of the tachyon potential

$$V_f(\lambda, TT^\dagger) = V_{f0}(\lambda)e^{-a(\lambda)TT^\dagger}, \quad (2.9)$$

and restrict the functions $\kappa(\lambda, T)$ and $w(\lambda, T)$ to be independent of T. Moreover, the functions $V_{f0}(\lambda)$, $a(\lambda)$, $\kappa(\lambda)$, and $w(\lambda)$ are constrained by requiring the agreement with the dynamics of QCD [48,49,51]. We will review the suitable choices for these potentials in Sec. IV.

A. The *CP*-odd sector and the $U(1)_A$ anomaly

The action of the CP-odd sector results from the Wess-Zumino (WZ) term coupling the closed string axion to the phase of the tachyon and the $U(1)_A$ gauge boson. This term was discussed in [44], and further adapted to our model of holographic QCD in [51]. Since we will consider only the case where the quarks are massless, or have all the same mass, we can write the tachyon as

$$T = \tau(r)e^{i\xi(r)}\mathbb{I}_{N_f}, \quad (2.10)$$

where $\mathbb{I}_{N_f}$ denotes the $N_f \times N_f$ unit matrix in flavor space.

Next, following [44,51], we write the action of the CP-odd sector as

$$S_a = S_{\text{closed}} + S_{\text{open}}, \quad S_{\text{closed}} = -\frac{M^3}{2}\int d^5x\sqrt{-g}\frac{|H_4|^2}{Z(\lambda)},$$
$$H_4 = dC_3, \quad (2.11)$$

where C_3 is the RR three-form axion, and

$$S_{\rm open} = i\int C_3 \wedge \Omega_2 = i\int C_3 \wedge d\Omega_1,$$
$$\Omega_1 = iN_f[2V_a(\lambda,\tau)A - \xi dV_a(\lambda,\tau)],$$

where A is the flavor singlet term of the axial gauge boson

$$A_M = \frac{A_M^L - A_M^R}{2}. \tag{2.12}$$

The potential $V_a(\lambda,\tau)$ is known in flat-space tachyon condensation, in which case it is the same as that appearing in the tachyonic Dirac-Born-Infeld (DBI) (i.e., V_f) and is independent of the dilaton [44,59]. Although in our model V_a might be different from V_f, it must satisfy the same basic properties; it becomes a constant (related to the anomaly) at $T=0$, and it vanishes exponentially at $T=\infty$. Hence we will initially take V_a to be of the form

$$V_a(\tau) = e^{-b\tau^2}, \tag{2.13}$$

and discuss possible alternatives in Sec. IV.

After dualizing the three-form C_3 to a pseudoscalar axion field $\tilde{a}$ via

$$\frac{H_4}{Z(\lambda)} = {}^*(d\tilde{a} + i\Omega_1), \tag{2.14}$$

the CP-odd action becomes

$$S_a = -\frac{M^3N_c^2}{2}\int d^5x\sqrt{-g}Z(\lambda)[\partial_M\mathfrak{a} - x(2V_a(\lambda,\tau)A_M - \xi\partial_M V_a(\lambda,\tau))]^2, \tag{2.15}$$

in terms of the QCD axion

$$\mathfrak{a} = \frac{\tilde{a}}{N_c}, \tag{2.16}$$

which, as we will discuss below, is normalized so that $\mathfrak{a}$ is dual to θ/N_c.

In order to establish the holographic dictionary for the CP-odd part of the boundary theory, we start by writing the Lagrangian of QCD as

$$\mathcal{S}_{\rm QCD} = \int d^4x\left[-\frac{1}{2g^2}\mathbb{T}rG_{\mu\nu}G^{\mu\nu} + i\bar{\psi}\not{D}\psi - \bar{\psi}_R M_q\psi_L - \bar{\psi}_L M_q^\dagger\psi_R + \frac{\theta}{32\pi^2}\epsilon^{\mu\nu\rho\sigma}\mathbb{T}rG_{\mu\nu}G_{\rho\sigma}\right] \tag{2.17}$$

where $\psi_L = (1+\gamma^5)\psi/2$, $\psi_R = (1-\gamma^5)\psi/2$, and M_q is the (potentially complex) quark mass matrix.

The bulk action (2.15) is invariant under the gauge transformation

$$A_M \to A_M + \partial_M\varepsilon, \quad \xi\to\xi - 2\varepsilon, \quad \mathfrak{a}\to\mathfrak{a} + 2xV_a\varepsilon, \tag{2.18}$$

where the first two transformations follow from (2.7) for a gauge transformation of the form $V_L = V_R^\dagger = e^{i\varepsilon\mathbb{I}_{N_f}}$. Notice that on the boundary this transformation realizes the QCD axial anomaly upon assuming that the boundary values of the fields $\mathfrak{a}$, A and ξ source the operators $\epsilon^{\mu\nu\rho\sigma}\mathbb{T}r(G_{\mu\nu}G_{\rho\sigma})$, J_μ^5 and $m_q\bar{\psi}\gamma^5\psi$ respectively, according to the following boundary action:

$$S_\delta = \frac{N_c}{32\pi^2}\int_{r=\delta} d^4x\mathfrak{a}\epsilon^{\mu\nu\rho\sigma}\mathbb{T}r(G_{\mu\nu}G_{\rho\sigma}) + \int_{r=\delta} d^4x J_\mu^{(L)ij}A^{(L)\mu ij} + \int_{r=\delta} d^4x J_\mu^{(R)ij}A^{(R)\mu ij} - K_T\int_{r=\delta} d^4x\frac{1}{\ell\delta}\bar{\psi}_R T\psi_L - K_T\int_{r=\delta} d^4x\frac{1}{\ell\delta}\bar{\psi}_L T^\dagger\psi_R \tag{2.19}$$

where δ is a UV cutoff, and $J_\mu^{(L/R)ij} = \bar{\psi}^i\gamma_\mu(1\pm\gamma_5)\psi^j/2$ (with $i,j = 1\ldots N_f$).

The proportionality constants between boundary values of the bulk fields and the sources of their dual operators on the field theory are not fixed in (2.19). They nevertheless disappear from any renormalization group (RG)-invariant quantity (like the product of a source times its VEV). Indeed, we have included the parameter K_T which will appear in the relation between the quark mass and the boundary value of the tachyon.

We could include a second free parameter in front of the term $\sim\mathfrak{a}\epsilon^{\mu\nu\rho\sigma}\mathbb{T}r(G_{\mu\nu}G_{\rho\sigma})$, see [60]. However, we have chosen to fix the normalization of the axion $\mathfrak{a}$ such that its boundary value is precisely θ/N_c, as seen by comparing (2.19) and (2.17). Further requiring that the potential V_a approaches unity at the boundary, $V_a(\lambda, T=0)=1$, the $U(1)_A$ gauge transformation (2.18) implies that the axial anomaly is correctly reproduced. We will see this explicitly below in Eq. (2.25).

The normalization of the couplings of the gauge fields $A^{(L/R)}$ was chosen to be consistent with the gauge transformations (2.7).

Further, recall that the CP transformation of the fermion bilinears is given by

$$\bar{\psi}^i\psi^j(t,\mathbf{x}) \mapsto \bar{\psi}^j\psi^i(t,-\mathbf{x}),$$
$$\bar{\psi}^i\gamma_5\psi^j(t,\mathbf{x}) \mapsto -\bar{\psi}^j\gamma_5\psi^i(t,-\mathbf{x}). \tag{2.20}$$

We require the proportionality coefficient K_T to be real so that the corresponding terms in (2.19) are CP invariant if the tachyon transforms as $T(r,t,\mathbf{x}) \mapsto T(r,t,-\mathbf{x})^*$, which is indeed the transformation found in [44].

Notice also that for a diagonal tachyon as in (2.10), the last two terms of (2.19) take the form

$$-\frac{K_T}{2}\int_{r=\delta} d^4x \frac{1}{\ell\delta}\tau(e^{i\xi}+e^{-i\xi})\bar{\psi}\psi - \frac{K_T}{2}\int_{r=\delta} d^4x \frac{1}{\ell\delta}\tau(e^{i\xi}-e^{-i\xi})\bar{\psi}\gamma^5\psi, \quad (2.21)$$

which in the limit of small phase $\xi \ll 1$ reduce to

$$-K_T\int_{r=\delta} d^4x \frac{1}{\ell\delta}\tau\bar{\psi}\psi - K_T\int_{r=\delta} d^4x \frac{1}{\ell\delta}\xi\tau i\bar{\psi}\gamma^5\psi. \quad (2.22)$$

Finally, we point out that $\mathfrak{a}(r)$ and $\xi(r)$ both transform under (2.18) reflecting the transformation of θ and the quark mass phase ξ under the anomalous $U(1)_{\mathrm{A}}$. It is the gauge invariant combination

$$\tilde{\mathfrak{a}} = \mathfrak{a} + x\xi V_a, \quad (2.23)$$

which is dual to the $U(1)_A$ invariant combination $\bar{\theta}/N_c = \theta/N_c + \arg(\det M_q)/N_c$, upon taking into account that $V_a(\lambda, T=0)=1$.

Notice that because ξ is a phase, any solution is unchanged under the shift $\xi \mapsto \xi + 2\pi$. By using the dictionary, this shift implies $\bar{\theta} \mapsto \bar{\theta} + 2\pi N_f$, so the results in our model will be $2\pi N_f$ periodic in $\bar{\theta}$. But it is known that QCD has a much shorter 2π periodicity in this angle. This periodicity will be less obvious from our analysis, because it is linked to non-Abelian $SU(N_f)$ transformations. We have already restricted our study to backgrounds where the tachyon is proportional to the unit matrix, which effectively excludes such transformations.

In order to see how the 2π periodicity arises, notice that we have made a branch choice when defining the CP-odd action in (2.15). Here the phase of the tachyon could be written for general T as

$$\xi = \frac{1}{2iN_f}(\log\det T - \log\det T^\dagger) = \frac{1}{N_f}\arg\det T. \quad (2.24)$$

We observe that the branch ambiguity of arg in (2.24) corresponds to $\xi \mapsto \xi + 2\pi/N_f$, which gives the desired $\bar{\theta} \mapsto \bar{\theta} + 2\pi$ in the boundary theory. The branches are connected via non-Abelian transformations. To make this explicit, we may start from a background with a diagonal tachyon, choose $V_R = V_L^\dagger = \mathrm{diag}(e^{i\varphi}, \ldots, e^{i\varphi}, e^{-i(N_f-1)\varphi})$ in (2.7), and apply the transformation as φ varies from zero to π/N_f. Since the transformation matrices belong to $SU(N_f)$ the CP-odd action (2.15) transforms trivially. In particular, (2.24) remains constant under the transformation. The end result is, however, that the tachyon changes by $T \mapsto e^{i2\pi/N_f}T$, corresponding to a shift of the tachyon phase by $2\pi/N_f$. Therefore, the transformation connects two "adjacent" branch choices in (2.24).

According to AdS/CFT, the boundary field theory generating functional is given by $W_{\mathrm{QFT}}[\mathfrak{a}(x,\delta), A^\mu(x,\delta), \xi(x,\delta)] \equiv \langle e^{iS_\delta}\rangle = e^{iS_a}$, where the bulk action S_a is taken to be on shell. Applying the transformation (2.18) one obtains $\delta_\varepsilon W_{\mathrm{QFT}} \propto \delta_\varepsilon S_a$, and since S_a is invariant under (2.18), one obtains $\langle e^{iS_\delta}\delta_\varepsilon S_\delta\rangle = 0$. Because $\langle e^{iS_\delta}\rangle$ defines the generating functional, taking functional derivatives with respect to the sources we see that all correlators of the form $\langle \ldots \cdot \delta_\varepsilon S_\delta\rangle$ vanish. Therefore, the following equation holds for all correlators accessible to our holographic model (and thus corresponds to an operator identity in the dual QFT):

$$\partial_\mu J^{(5)\mu} = \frac{N_f}{16\pi^2}\epsilon^{\mu\nu\rho\sigma}\mathbb{T}r(G_{\mu\nu}G_{\rho\sigma}) + 2iK_T\bar{\psi}^i\gamma^5\psi^i\frac{1}{\delta}[\tau\cos(\xi)]_{r=\delta} - 2K_T\bar{\psi}^i\psi^i\frac{1}{\delta}[\tau\sin(\xi)]_{r=\delta}. \quad (2.25)$$

Here $J^5_\mu = \bar{\psi}^i\gamma_\mu\gamma^5\psi^i$, and we have used the fact that $V_a(\lambda, T=0)=1$, and that T vanishes in the UV. Next, upon identifying the energy scale as the metric factor e^A, which behaves as $e^A \sim 1/r$ in the UV, we define the running quark mass (evaluated at the energy scale $\mu = e^A|_{r=\delta}$) as

$$\bar{m}_q|_\mu = K_T\frac{\tau(\delta)}{\ell\delta}, \quad (2.26)$$

while $\xi(\delta) = \xi_0$ denotes the phase of the quarks, and ℓ is the AdS radius introduced below (2.3). Hence we can write

$$\partial_\mu J^{(5)\mu} = \frac{N_f}{16\pi^2}\epsilon^{\mu\nu\rho\sigma}\mathbb{T}r(G_{\mu\nu}G_{\rho\sigma}) + 2i\bar{m}_q\cos(\xi_0)\bar{\psi}^i\gamma^5\psi^i - 2\bar{m}_q\sin(\xi_0)\bar{\psi}^i\psi^i, \quad (2.27)$$

where $\bar{\psi}\psi$ and $\bar{\psi}\gamma^5\psi$ stand for the corresponding renormalized operators at the energy scale μ. Notice that in the following sections we will instead consider the operators sourced by the renormalized mass m_q which is defined through the UV asymptotics of the tachyon (see Appendix A 1 for more details)

$$\frac{1}{\ell}\tau(r) = m_q r(-\log(r\Lambda))^{-\rho}\left[1+\mathcal{O}\left(\frac{1}{\log(r\Lambda)}\right)\right] + \sigma r^3(-\log(r\Lambda))^{\rho}\left[1+\mathcal{O}\left(\frac{1}{\log(r\Lambda)}\right)\right], \quad (2.28)$$

where m_q is a constant and equals the running quark mass $\bar{m}_q$ at some fixed renormalization scale [while σ corresponds to the renormalized chiral condensate $\sim\langle\bar{\psi}\psi\rangle$, and ρ is defined in (A7) in terms of the parameters of the model]. To be precise, in view of (2.26), $\bar{m}_q$ and m_q are related via

$$\bar{m}_q = K_T m_q (-\log(\delta\Lambda))^{-\rho}\left[1+\mathcal{O}\left(\frac{1}{\log(\delta\Lambda)}\right)\right] \quad (2.29)$$

for small δ and this same relation will hold between the renormalized operators sourced by $\bar{m}_q$ [see Eq. (2.27) above], and those sourced by m_q.

Initially, we will be interested in background solutions with both A_μ and ξ vanishing. Therefore, we need solve the equations stemming from the $\mathcal{O}(N_c^2)$ action $S_g + S_f$ to determine $g_{\mu\nu}$, λ, and τ. For the background solutions with a nonzero θ angle analyzed in Sec. VI we will have to consider also a contribution from S_a.

B. The background solutions at $\theta = 0$

In this subsection we review some general features of the background solutions of V-QCD at zero θ angle. We will only consider the standard case that displays a phase diagram similar to what is expected in QCD (see [51] for a thorough analysis of the constraints this requirement imposes on the different potentials entering the theory).

The background solutions follow from an Ansatz where λ, A, and T are functions of the radial coordinate r, while the rest of the fields in the model are consistently set to zero. The Ansatz for the tachyon is further restricted to $T = \tau(r)\mathbb{I}_{N_f}$, corresponding to all quarks having the same real-valued mass [hence setting $\xi = 0$ in (2.10)]. Two types of (zero temperature) vacuum solutions were found in [48]:

(1) Backgrounds with identically zero tachyon and nontrivial $\lambda(r)$, $A(r)$. These solutions correspond to chirally symmetric vacua with zero quark mass. In this case, analytical integration of the equations of motion leaves us with a single first order differential equation that can be easily solved numerically.
(2) Solutions with nonzero $\lambda(r)$, $A(r)$ and $\tau(r)$. These describe vacua with broken chiral symmetry, with the quark mass and the chiral condensate corresponding respectively to the non-normalizable and normalizable modes of the tachyon [51]. These backgrounds follow from the numerical integration of a set of coupled differential equations.

As shown in Appendix A, we can obtain analytic expansions of the solutions in the UV and IR regions of the geometry (see [48,51] for more detailed analyses).

The standard phase diagram of the theory at zero quark mass is parametrized in terms of the ratio $x = N_f/N_c$, which is constrained to the range $0 \le x < 11/2 = x_{\rm BZ}$ since with our normalization the upper bound corresponds to the Banks-Zaks (BZ) value in QCD for which the leading coefficient of the β function becomes positive.

The phase diagram within this range consists of two phases, corresponding to the two types of backgrounds above, separated by a phase transition at a critical value $x = x_c$.

(i) For the range $x_c \le x < x_{\rm BZ}$, the dominant vacuum solution (at zero quark mass) is of the first type above, with an identically zero tachyon, and therefore chiral symmetry is preserved [61]. The IR geometry is asymptotically AdS_5.
(ii) For $0 < x < x_c$ the dominant background corresponds to solutions of the second kind, hence the tachyon presents a nontrivial profile even if the quark mass is zero. Chiral symmetry is broken in this phase and the geometry ends in a singularity in the IR.

The phase transition at $x = x_c$ (only present at zero quark mass [55]) displays BKT [62] or Miransky [63] scaling, in accordance with predictions from the Schwinger-Dyson approach (see, e.g., [64]). The chiral condensate $\sigma \sim \langle\bar{\psi}\psi\rangle$, which is the order parameter of the phase transition, vanishes exponentially as $x \to x_c$ from below. As shown in [48],

$$\sigma \sim \exp\left(-\frac{2\hat{K}}{\sqrt{x_c - x}}\right), \quad (2.30)$$

with $\hat{K}$ being a positive constant, while σ vanishes identically in the region $x > x_c$ where chiral symmetry is unbroken. Linked to this scaling is the "walking" behavior of the coupling constant for $x \lesssim x_c$. The field $\lambda(r)$ dual to the coupling constant becomes approximately constant, $\lambda \sim \lambda_*$, for a large range of r, and the size of this scaling region enjoys the same scaling as (the square root of) the condensate (2.30). The physics near the transition has also been studied in other models: a top-down setup [65], using a tachyonic DBI action without backreaction [66], models with Einstein-dilaton gravity tuned to produce walking [67], and in dynamic AdS/QCD models which are simple bottom-up models where the holographic RG flow is tuned to match with QCD [68].

The appearance of a region displaying walking behavior and the mechanism for the phase transition at $x = x_c$, are related to the existence of an IR fixed point for $x \ge x_c$. First, notice that for the first type of backgrounds in the classification above, $\lambda(r) \to \lambda_*$ as $r \to \infty$, and the solution becomes AdS also in the IR. The region $x \ge x_c$ is therefore called the "conformal window." Second, the violation of the Breitenlohner-Freedman (BF) bound by the tachyon in the IR fixed point gives rise to an instability that is responsible for the phase transition at the end of the conformal window ($x = x_c$).

The BF bound is given in terms of the effective IR mass of the tachyon $m_{\tau*}$ as

$$-m_{\tau*}^2 \ell_*^2 < 4, \quad (2.31)$$

where ℓ_* is the radius of the IR AdS geometry. When the bound is violated, solutions where the tachyon has been turned on are favored, implying spontaneous breaking of chiral symmetry (remember that we are setting the source of the tachyon—corresponding to the quark mass—to zero). In [48] it was indeed found that the bound (2.31)

is saturated exactly at $x = x_c$, where the BKT transition described above occurs. This is in agreement with general arguments showing that the violation of the BF bound at an IR fixed point leads to a BKT transition [69]. Additionally, in [48] the constant $\hat{K}$ of (2.30) was expressed in terms of $m_{\tau *}$ and ℓ_*, which are functions of x, as

$$\hat{K} = \frac{\pi}{\sqrt{\frac{d}{dx}(m_{\tau *}^2 \ell_*^2)|_{x=x_c}}}. \tag{2.32}$$

In [48] it was also shown how the Miransky scaling manifests itself in the ratio of the scales of the model as $x \to x_c$. One can define the UV and IR scales $\Lambda_{\rm UV} = \Lambda$, $\Lambda_{\rm IR} = 1/R$, in terms of the constants appearing respectively in the UV and IR solutions (see Appendix A). For the solutions with $x < x_c$ and $x_c - x$ large enough, $\Lambda_{\rm IR}/\Lambda_{\rm UV} = \mathcal{O}(1)$, reflecting the fact that there is only one scale in the model, as happens normally in QCD (where the single scale is denoted by $\Lambda_{\rm QCD}$). Instead, when $x \to x_c$, there is a clear separation of scales, and their ratio behaves as

$$\frac{\Lambda_{\rm UV}}{\Lambda_{\rm IR}} \sim \exp\left(\frac{\hat{K}}{\sqrt{x_c - x}}\right), \tag{2.33}$$

hence featuring Miransky scaling.

It is worth pointing out that even as $x \to x_c$, $\Lambda_{\rm UV}$ is still the scale at which the coupling constant becomes small. In that limit, the range where the coupling "walks" is characterized by the two scales as $\Lambda_{\rm UV}^{-1} \ll r \ll \Lambda_{\rm IR}^{-1}$, and the coupling diverges for $r \gtrsim \Lambda_{\rm IR}^{-1}$. Moreover, in terms of the two scales, the chiral condensate can be expressed as $\sigma \sim \Lambda_{\rm UV}(\Lambda_{\rm IR})^2$. Therefore, the Miransky scaling featured in Eq. (2.30) follows from (2.33) when the condensate is expressed in units of $\Lambda_{\rm UV}$, i.e. for $\sigma/(\Lambda_{\rm UV})^3$.

When the quark mass is nonzero, the phase transition at $x = x_c$ becomes a crossover: chiral symmetry is broken and the dominant solution changes smoothly as x is varied. Even though there are no transitions, one can identify various regions where the dependence of the background on the quark mass is different [55]:

(1) In the QCD-like regime, with $0 < x < x_c$, the background at finite m_q approaches the solution at $m_q = 0$ uniformly as $m_q \to 0$. For small enough m_q the mass dependence is therefore perturbative. A characteristic feature in this regime is the light pion mode.
(2) Adding a finite quark mass in the conformal window drives the model away from the IR fixed point. For $m_q \ll \Lambda_{\rm UV}$ the background walks, and the amount of walking is controlled by the value of the quark mass. This leads to the hyperscaling relations [55,70] for the meson masses.
(3) At large quark mass, $m_q \gg \Lambda_{\rm UV}$, the background solution of the tachyon field is large (except for very close to the UV boundary) which leads to the decoupling of quarks from the gluons and a large mass gap for the meson states.

The results at finite quark mass agree with other approaches, in regimes of parameter space where such approaches can be trusted. In particular, the behavior within the conformal region and close to the critical value $x = x_c$ is in agreement with the analysis of RG flows [71,72].

Finally, there also exist solutions corresponding to subdominant vacua of the model. Allowing for a finite quark mass, one finds the following generic structure [48]:

(i) For $x_c \le x < x_{\rm BZ}$, only one vacuum solution exists, even at finite quark mass.
(ii) When $0 < x < x_c$ and the quark mass is zero, there is an infinite tower of (unstable) Efimov saddle-point solutions in addition to the standard, dominant solution.[2]
(iii) When $0 < x < x_c$ and the quark mass is nonzero, there is an even number (possibly zero) of Efimov vacua. The number of vacua increases with decreasing quark mass for fixed x.

The subdominant Efimov vacua at finite (real) quark mass were carefully studied in [55]. In Sec. VI E we will generalize that analysis to the case of a complex quark mass.

III. EQUATIONS OF MOTION AND ASYMPTOTIC SOLUTIONS AT FINITE θ ANGLE

A. Equations of motion for the background

In order to study the physics of the model at finite θ angle, we will solve the equations of motion when the QCD axion $\mathfrak{a}$ is finite [and $\mathcal{O}(1)$ in the large N_c expansion]. As implied by the axial anomaly (2.18) we must also allow for a nonzero overall phase of the tachyon, and then all three sectors, glue, flavor and *CP*-odd, contribute to the action. We also need to consider a $U(1)_A$ flavor singlet gauge field given in (2.12), while the other components of the gauge field are set to zero. Notice that we consider a tachyon field of the form $T = \tau e^{i\xi}\mathbb{I}$ corresponding to all the quarks having equal complex mass. This allows us to write the action as

$$\begin{aligned} S &= S_g + S_a + S_f \\ &= M^3 N_c^2 \int d^5x \Big\{ \sqrt{-g}\Big[R - \frac{4}{3}\frac{(\partial_M \lambda)^2}{\lambda^2} + V_g(\lambda) \\ &\quad - \frac{Z(\lambda)}{2}(\partial_M \mathfrak{a} + x\xi \partial_M V_a(\lambda,\tau) - 2x A_M V_a(\lambda,\tau))^2 \Big] \\ &\quad - \frac{x V_f(\lambda,\tau)}{2}\left[\sqrt{-\det \mathbf{A}_{(+)}} + \sqrt{-\det \mathbf{A}_{(-)}}\right]\Big\}, \end{aligned} \tag{3.1}$$

where

[2]For simplicity it is assumed that there exists an IR fixed point for any positive value of x, and that the BF bound is violated at the fixed point for any x down to $x = 0$.

$$\mathbf{A}_{(\pm)MN} = g_{MN} + \kappa(\lambda)[(\partial_M\tau)(\partial_N\tau) + \tau^2(\partial_M\xi + 2A_M)(\partial_N\xi + 2A_N)] \pm w(\lambda)F_{MN}, \tag{3.2}$$

with $F_{MN} = \partial_M A_N - \partial_N A_M$.

We list the full equations of motion in Appendix B, and restrict our discussion here to the case (relevant for the background) where all fields only depend on the radial coordinate r. We set the sources for the four-vector A_μ to zero, and as argued in Appendix B, the solution for A_μ then vanishes in the bulk also. Moreover, we choose the gauge $A_r = 0$.

Taking the Ansatz (2.3) for the metric, we are then left with the five fields $A(r)$, $\lambda(r)$, $\mathfrak{a}(r)$, $\tau(r)$, and $\xi(r)$. The equation of motion for $\mathfrak{a}$ [Eq. (B1) in Appendix B] allows us to solve for $\mathfrak{a}'$ as

$$\mathfrak{a}' = \frac{C_a e^{-3A}}{Z} - x\xi V_a', \tag{3.3}$$

where C_a is a constant. Moreover, substituting this solution into the equation of motion for A_r (B11), we obtain

$$\frac{e^{3A}}{\tilde{G}}\kappa V_f \tau^2 \xi' - C_a V_a = 0, \tag{3.4}$$

where

$$\tilde{G}(r) = \sqrt{1 + \kappa e^{-2A}(\tau'^2 + \tau^2\xi'^2)}. \tag{3.5}$$

Solving for ξ' we arrive at

$$\xi' = \frac{C_a V_a \sqrt{e^{2A} + \kappa\tau'^2}}{\kappa^{1/2}\tau\sqrt{e^{8A}V_f^2\kappa\tau^2 - C_a^2 V_a^2}}. \tag{3.6}$$

As we will see below when analyzing the asymptotic behavior, the requirement of finding regular solutions with nonvanishing ξ' restricts the form of the potentials in our model.

For the equations of motion of the other fields we obtain

$$6A'' + 6A'^2 = -\frac{4}{3}\frac{\lambda'^2}{\lambda^2} + e^{2A}V_g - xe^{2A}V_f\tilde{G} - C_a^2\frac{e^{-6A}}{2Z}, \tag{3.7}$$

$$12A'^2 = \frac{4}{3}\frac{\lambda'^2}{\lambda^2} + e^{2A}V_g - xV_f\frac{e^{2A}}{\tilde{G}} + C_a^2\frac{e^{-6A}}{2Z}, \tag{3.8}$$

$$\lambda'' - \frac{\lambda'^2}{\lambda} + 3A'\lambda' = \frac{3}{8}e^{2A}\lambda^2\left\{-\frac{\partial V_g}{\partial\lambda} + x\frac{\partial V_f}{\partial\lambda}\tilde{G} + \frac{x}{2}e^{-2A}\frac{\partial\kappa}{\partial\lambda}\frac{V_f}{\tilde{G}}(\tau'^2 + \tau^2\xi'^2) + C_a^2\frac{e^{-8A}}{2Z^2}\frac{\partial Z}{\partial\lambda} - xC_a e^{-5A}\xi'\frac{\partial V_a}{\partial\lambda}\right\}, \tag{3.9}$$

$$\partial_r\left(\frac{e^{3A}}{\tilde{G}}\kappa V_f\tau'\right) - e^{5A}\tilde{G}\frac{\partial V_f}{\partial\tau} - \frac{e^{3A}}{\tilde{G}}V_f\kappa\tau\xi'^2 - e^{3A}\frac{V_f}{2\tilde{G}}(\tau'^2 + \tau^2\xi'^2)\frac{\partial\kappa}{\partial\tau} + C_a\xi'\frac{\partial V_a}{\partial\tau} = 0, \tag{3.10}$$

where we eliminated $\mathfrak{a}$ by using (3.3).

Notice that as the potentials of the action (3.1) are independent of $\mathfrak{a}$ and ξ, it is invariant under the reflection $\mathfrak{a} \mapsto -\mathfrak{a}$, $\xi \mapsto -\xi$, which corresponds to the CP transformation on the field theory side. This is reflected in the invariance of the equations of motion (3.6) and (3.7)–(3.10) under $C_a \mapsto -C_a$, $\xi \mapsto -\xi$.

B. Asymptotics

We will now analyze the asymptotic solutions corresponding to backgrounds at finite θ angle. We concentrate on the asymptotics which are affected nontrivially by finite $\bar{\theta}$. Other results are listed in Appendix A.

1. UV

We begin by considering the effect of a nonzero ξ on the UV solutions of the equations (3.7)–(3.9) for $A(r)$ and $\lambda(r)$. It is easy to check that the standard ($\theta = 0$) UV asymptotics for $A(r)$ and $\lambda(r)$, Eqs. (A2), (A3)), solve those equations in the UV upon assuming that τ vanishes at least as $\tau \sim r$ and ξ' is regular there (the new terms sourced by ξ' are suppressed at least as r^2).

Next, assuming that the UV metric is close to AdS, namely $e^A \simeq \ell/r$ as implied by the standard UV asymptotics of $A(r)$, and that the tachyon is at most $\tau \sim r$, Eqs. (3.6) and (3.10) for the modulus and phase of the tachyon become

$$\tau'' + \partial_r \log(e^{3A}\kappa V_{f0})\tau' - e^{2A}m_\tau^2\tau - \tau(\xi')^2 \simeq 0,$$
$$\xi' \simeq \frac{C_a}{\kappa V_{f0}e^{3A}\tau^2}, \tag{3.11}$$

where

$$m_\tau^2 = -\frac{2a}{\kappa}. \tag{3.12}$$

These two real equations are equivalent to the single linear complex valued equation

$$(\tau e^{i\xi})'' + \partial_r \log(e^{3A}\kappa V_{f0})(\tau e^{i\xi})' - e^{2A}m_\tau^2\tau e^{i\xi} \simeq 0. \tag{3.13}$$

Therefore, towards the UV boundary the complex tachyon satisfies this linearized equation of motion where C_a does not appear explicitly. In particular, the equation is the same as that for the (real) tachyon at zero θ angle or equivalently at zero C_a.

Inserting the UV asymptotics of $A(r)$ and $\lambda(r)$ in (3.13), we obtain the UV asymptotic solution for the complex tachyon,

$$\frac{1}{\ell}\tau e^{i\xi} = e^{i\xi_0} m_q r(-\log(\Lambda r))^{-\rho}(1+\mathcal{O}(\log(\Lambda r)^{-1})) + e^{i\xi_0}\hat{\sigma} r^3(-\log(\Lambda r))^{\rho}(1+\mathcal{O}(\log(\Lambda r)^{-1})), \tag{3.14}$$

in terms of two real valued constants m_q and ξ_0, and one complex constant $\hat{\sigma}$ while ρ is defined in Eq. (A7). Notice that m_q and ξ_0 are the modulus and phase of the source dual to the complex tachyon, and thus correspond to the absolute value of the mass of the quarks and its phase. This solution satisfies the assumptions we made above and is therefore valid, as can also be verified by inserting it together with the asymptotics for $A(r)$ and $\lambda(r)$ in the full system (3.7)–(3.10).

To obtain the relation between the integration constant C_a and the coefficients of the expansion, we insert it in the second equation in (3.11), which gives

$$C_a = 2\ell^5 \kappa_0 W_0 m_q \mathrm{Im}\hat{\sigma}, \tag{3.15}$$

where $\kappa_0 = \kappa(\lambda=0)$ and $W_0 = V_{f0}(\lambda=0)$. For positive quark mass, the UV expansion of ξ' can be read from (3.14):

$$\xi' = r(-\log(\Lambda r))^{2\rho}\left[\frac{C_a}{\ell^5\kappa_0 W_0 m_q^2}\right](1+\mathcal{O}(\log(\Lambda r)^{-1})). \tag{3.16}$$

Similarly, the expansion of the absolute value is

$$\frac{1}{\ell}\tau = m_q r(-\log(\Lambda r))^{-\rho}(1+\mathcal{O}(\log(\Lambda r)^{-1})) + \sigma r^3(-\log(\Lambda r))^{\rho}(1+\mathcal{O}(\log(\Lambda r)^{-1})), \tag{3.17}$$

where $\sigma = \mathrm{Re}\hat{\sigma}$. At nonzero quark mass, the relations between the VEVs can therefore be written as

$$\hat{\sigma} = \sigma + \frac{iC_a}{2\ell^5\kappa_0 W_0 m_q}. \tag{3.18}$$

In the case of massless quarks ($m_q = 0$), as the form of the complex tachyon solution already makes clear, the physical solution corresponds to a constant $\xi = \xi_0$, for which $C_a = 0$, in agreement with (3.15). Notice finally that a constant ξ can be gauged away via (2.18) as expected for QCD with massless quarks.

We shall finish this subsection by discussing the relation between the subleading terms in the UV asymptotics of the complex tachyon and the corresponding VEVs on the field theory side. To establish that relation we compare the variation of the free energies of the field theory and its holographic dual. We allow the quark mass m_q, the phase ξ_0, and the boundary value of the axion a_0 to vary keeping Λ fixed.

Then, for an IR regular variation, the free energy density satisfies the standard formula

$$\delta\mathcal{E} = -\delta\bar{\mathfrak{a}}(r)\frac{\partial\mathcal{L}}{\partial\bar{\mathfrak{a}}'(r)}\Big|_{r=0}^{\infty} - \delta\xi(r)\frac{\partial\mathcal{L}}{\partial\xi'(r)}\Big|_{r=0}^{\infty} - \delta\tau(r)\frac{\partial\mathcal{L}}{\partial\tau'(r)}\Big|_{r=0}^{\infty}, \tag{3.19}$$

where $\mathcal{L}$ is the (complete) V-QCD Lagrangian, and $\bar{\mathfrak{a}}$ was defined in (2.23). Here the second term vanishes due to the A_r equation of motion.[3] The third term is UV divergent and needs to be regulated. We should also make sure that the variation of the metric does not enter the formula when $\Lambda = \Lambda_{\mathrm{UV}}$ is kept fixed. These issues were analyzed in detail for the case of zero θ angle in [55]. By using the UV expansion of the phase in (3.16) we observe that the nontrivial phase or the *CP*-odd action do not add any nonzero contributions to this analysis, and the result for the regularized third term is unchanged. That is, (3.19) becomes

$$\delta\mathcal{E} = -M^3 N_c^2 C_a(\delta\mathfrak{a}_0 + x\delta\xi_0) - 2M^3 N_c N_f W_0\kappa_0\ell^5\sigma\delta m_q, \tag{3.20}$$

where the first term arises from the first term of (3.19) and the second term can be computed as in [55]. As a check, this result may also be written as

$$\delta\mathcal{E} = -M^3 N_c^2 C_a\delta\mathfrak{a}_0 - 2M^3 N_c N_f W_0\kappa_0\ell^5\mathrm{Re}[\hat{\sigma}^* e^{-i\xi_0}\delta(m_q e^{i\xi_0})], \tag{3.21}$$

i.e. the terms involving the tachyon admit a simple expression in terms of the complex source and VEV in (3.14), which is consistent with the complex tachyon being the natural field to consider in the UV as seen from Eq. (3.13).

By using the QCD Lagrangian (2.17), and the Feynman-Hellmann theorem, or equivalently by using the dictionary implied by (2.19), we obtain

$$\langle\bar{\psi}_R\psi_L\rangle = \frac{e^{i\xi_0}}{2}\left(\frac{\partial\mathcal{E}}{\partial m_q} + \frac{i}{m_q}\frac{\partial\mathcal{E}}{\partial\xi_0}\right) = -M^3 N_c N_f W_0\kappa_0\ell^5 e^{i\xi_0}\hat{\sigma} = -M^3 N_c N_f W_0\kappa_0\ell^5 e^{i\xi_0}\left(\sigma + \frac{iC_a}{2\ell^5\kappa_0 W_0 m_q}\right), \tag{3.22}$$

so that the expectation value is given by the coefficient of the subdominant term of the complex tachyon in (3.14). The other condensates are found similarly, e.g.,

[3] After switching to the gauge invariant axion $\bar{\mathfrak{a}}$, the action only depends on ξ through its derivative and invariance under (2.18) implies that $\frac{\partial\mathcal{L}}{\partial\xi'(r)} = \frac{1}{2}\frac{\partial\mathcal{L}}{\partial A_r}$.

$$\langle\bar{\psi}\psi\rangle = -2M^3N_cN_fW_0\kappa_0\ell^5\mathrm{Re}\left[e^{i\xi_0}\left(\sigma+\frac{iC_a}{2\ell^5\kappa_0W_0m_q}\right)\right], \tag{3.23}$$

$$i\langle\bar{\psi}\gamma_5\psi\rangle = -2M^3N_cN_fW_0\kappa_0\ell^5\mathrm{Im}\left[e^{i\xi_0}\left(\sigma+\frac{iC_a}{2\ell^5\kappa_0W_0m_q}\right)\right], \tag{3.24}$$

$$\langle\epsilon^{\mu\nu\rho\sigma}\mathbb{T}r(G_{\mu\nu}G_{\rho\sigma})\rangle = 32\pi^2M^3N_cC_a. \tag{3.25}$$

The relation between the VEVs

$$\frac{N_f}{32\pi^2}\langle\epsilon^{\mu\nu\rho\sigma}\mathbb{T}r(G_{\mu\nu}G_{\rho\sigma})\rangle = m_q\sin\xi_0\langle\bar{\psi}\psi\rangle - im_q\cos\xi_0\langle\bar{\psi}\gamma_5\psi\rangle \tag{3.26}$$

is consistent with (2.27).

The results above show that the phase of the tachyon is a perturbative correction in the UV when $m_q\sigma \gg C_a$, under the natural assumption that the factor $\ell^5W_0\kappa_0$ is of order one. It can be fixed by requiring the UV behavior of the scalar two-point correlator to match with perturbative QCD [51], which results in

$$M^3W_0\kappa_0\ell^5 = \frac{1}{4\pi^2}. \tag{3.27}$$

The value of M^3 can also be constrained independently by comparing the pressure of the model to that of high temperature QCD [49,73].

2. IR

We then consider the asymptotic solutions in the IR ($r\to\infty$) at finite θ angle. For physically relevant solutions we expect that the tachyon diverges in the IR as it does for $\theta = 0$ [51][4] so the tachyon potentials V_f and V_a vanish in the IR (and this is indeed what we will find for all regular solutions in the IR). This together with the regularity of ξ' implies that the glue degrees of freedom $A(r)$ and $\lambda(r)$ satisfy the same asymptotics as at $\theta = 0$, given in Eqs. (A9), (A10) in Appendix A. The asymptotics of the tachyon field is, however, modified as one turns on a finite θ angle.

The most relevant IR constraint arises as the requirement of having a regular ξ' from Eq. (3.6). Indeed, by demanding that the denominator of (3.6) does not become complex one obtains the inequality

$$e^{4A}V_f\sqrt{\kappa}\tau - |C_a|V_a > 0, \qquad (r\gg\Lambda_{\mathrm{IR}}^{-1}). \tag{3.28}$$

We have identified two choices for the potentials that satisfy this inequality and lead to sensible IR solutions. First, if one considers an Ansatz where the exponential factors in V_f and V_a can be different functions of τ, the inequality will be satisfied by a V_a that vanishes faster than V_f for an IR diverging tachyon. A simple choice would be to take $V_f\propto\exp(-a\tau^2)$ and $V_a = \exp(-b\tau^2)$ where a and b are constants satisfying $b > a$. Another choice, which we will use below, is to modify the tachyon dependence of V_a, to, e.g., $V_a = \exp(-a_q\tau^2 - a_l|\tau|)$.

Second, if one insists on keeping the same exponential factors [see (2.9) and (2.13)], and then $V_a\sim e^{-a\tau^2}$ as in flat space string theory [59], then the inequality above will constrain V_{f0}. Namely, the inequality (3.28) reduces to

$$e^{4A}V_{f0}\sqrt{\kappa}\tau > |C_a|, \tag{3.29}$$

and this condition results in a constraint on the potential V_{f0} as we now explain. In [51] it was shown that in order to have linear meson trajectories, κ should behave in the IR as $\sim\lambda^{-4/3}$, while for the flavor potential we had $V_{f0}\sim\lambda^{v_p}$. Although v_p was not fixed by the spectrum analysis of [51], it was already shown in [48] that for $v_p > 10/3$ no acceptable solutions existed. Potentials with $\kappa\sim\lambda^{-4/3}$ and $v_p < 10/3$ were indeed analyzed in [51], and shown to display linear meson trajectories. However, after inserting the IR asymptotic expansions of $A(r)$, $\lambda(r)$ and $\tau(r)$ for that case, the inequality (3.29) would only be satisfied if we had $v_p\geq 10/3$. This leads one to consider potentials having $v_p = 10/3$:

$$\kappa\sim\kappa_c\lambda^{-4/3}(\log\lambda)^{-\kappa_\ell}, \qquad V_{f0}\sim v_c\lambda^{10/3}(\log\lambda)^{-v_\ell}; \qquad (\lambda\to\infty). \tag{3.30}$$

As shown in Appendix A 2, this choice results in regular IR asymptotics if certain constraints for κ_ℓ and v_ℓ are fulfilled. In particular, the asymptotics for the phase is

$$\xi'\sim\left(\frac{2}{3}\right)^{v_l+\frac{\kappa_\ell}{2}}\frac{C_ae^{-4A_c-\frac{8}{3}\lambda_c}}{v_c\sqrt{\kappa_c}}\frac{\tau'}{r^{2-2v_l-\kappa_\ell}\tau^2}, \qquad (r\to\infty). \tag{3.31}$$

However, we have not been able to find potentials with $v_p = 10/3$ for which the (numerically constructed) solutions would have been regular both in the IR and in the UV. Regular solutions are found for $4/3\leq v_p\lesssim 3$. The prediction from string theory, $v_p = 7/3$ (see Sec. 2. 4 in [51]) falls in the middle of the acceptable range. Similar observations have been made earlier for the other potentials V_g, a, and κ in the model: the power laws given by string theory arguments, possibly with multiplicative logarithmic corrections, give the best match with QCD physics. The result for V_{f0} is, however, different from those for the other potentials, because the power law is nontrivial (i.e., having power different from zero) even after the transformation from Einstein frame to a string frame. That is, choosing all

[4]The stable minimum of the tachyon potential is at $T\to\infty$.

potentials to have exactly "critical" asymptotics in the string frame does not lead to regular solutions, but following the string theory prediction does, and even results in physics which is close to QCD.

In the numerical analysis below, we will consequently use the first option discussed above and choose the tachyon dependence in the exponential factor of V_a so that (3.28) is satisfied independently of the asymptotic form of V_{f0}.

IV. CHOICE OF POTENTIALS

In this section we present concrete choices for the potentials appearing in the action of our holographic model. These choices will be used in the numerical analysis of subsequent sections, and largely agree with those introduced in [48], and further constrained in [49,51], as we now review.

Two classes of potentials V_g, V_{f0}, κ, and a were considered in [48,49,51]; they are called potentials I and potentials II.

(i) Potentials I were chosen such that the IR power behavior of $\kappa(\lambda) \sim \lambda^{-4/3}$ and $a(\lambda) \sim \lambda^0$ is the critical one; as shown in [51] these values correspond to the critical point at the edge of the region of acceptable IR asymptotics. These potentials admit a regular IR solution with exponential tachyon, $\tau \sim \tau_0 e^{C_{\rm I} r}$, where $C_{\rm I}$ can be computed in terms of the potentials, and τ_0 is an integration constant (see Appendix D of [51] for details). For the resulting mesonic spectra, the asymptotic trajectories of masses in all towers are linear but have logarithmic corrections. Exactly linear asymptotic trajectories for the mesons can be obtained by considering a slight modification of potentials I such that $\kappa(\lambda) \sim \lambda^{-4/3}(\log\lambda)^{1/2}$ in the IR.

(ii) Potentials II behave instead as $\kappa(\lambda) \sim \lambda^{-4/3}$ and $a(\lambda) \sim \lambda^{2/3}$ in the IR. These potentials admit a regular IR solution with $\tau \sim \sqrt{C_{\rm II} r + \tau_0}$, and the asymptotic trajectories of masses in all towers are quadratic.

In order to fully fix the action for this article we will also need to specify the potentials appearing in the CP-odd action (2.15). Notice that he function $Z(\lambda)$ there contributes even when $x = 0$, and therefore has been considered in the context of IHQCD [35,60,73]. In [73] it was shown that the asymptotic behavior of Z at $\lambda \to 0$ and $\lambda \to \infty$ was fixed from general principles. We adopt a similar Ansatz compatible with the asymptotic behaviors as was used there:

$$Z(\lambda) = Z_0\left[1 + c_a\left(\frac{\lambda}{\lambda_0}\right)^4\right]. \tag{4.1}$$

For the physics at finite x the choice of V_a is even more relevant. Based on earlier studies and observations made above, we can immediately set some constraints. As pointed out in Sec. II A, for the anomaly structure to be reproduced correctly we need $V_a(\lambda, \tau = 0) = 1$. That is, in the UV we must have $V_a = 1$ up to terms suppressed by powers of τ, and in particular the leading term is independent of λ. Dependence on λ would have introduced perturbative corrections to triangle diagrams giving rise to the axial anomaly, which would have conflicted with our knowledge of QCD. Here we will impose the stricter but natural constraint that V_a only depends on τ. The independence of V_a on λ is consistent with the analysis of boundary string field theory [59] where the flavor and CP-odd potentials were found to be $\propto \exp(-a\tau^2)$ with the same λ-independent factor a in both potentials. The λ independence of the flavor potential in V-QCD is also supported by the analysis of the asymptotic radial trajectories of the meson spectrum [51] and the behavior of the meson masses at high quark mass [55].

As we have seen in Sec. III B 2, extra constraints result from demanding a regular solution for ξ' in the IR; in particular, the inequality (3.28) must be satisfied. The options which lead to regular IR asymptotics can be summarized as follows:

(1) Choose $V_{f0}(\lambda)$ with the asymptotics (3.30), take $V_a = \exp(-a\tau^2)$, and use potentials I for the other functions.

(2) Add a linear term in the exponential factor of the CP-odd potential: $V_a = \exp(-a\tau^2 - a_l|\tau|)$ (or modify the tachyon dependence in some other way such that V_a is suppressed with respect to V_f). Then the IR behavior $V_{f0}(\lambda)$ can be chosen more freely, e.g., as in previous work [51].

We show in Appendix A 2 that the first choice still gives regular IR asymptotics for a vanishing θ angle, and with a good choice of v_ℓ the tachyon phase is also regular when $\theta \neq 0$. The second option above is nonanalytic at $\tau = 0$, but the extra linear term in the exponential guarantees that the term involving V_a in (3.28) is suppressed, and the inequality is fulfilled. As we mentioned above, we have not found potentials satisfying the first option for which the solutions would have been regular both in the IR and in the UV. Therefore we selected the latter option when performing the numerical analysis of vacua at finite θ angle.

Next we summarize the explicit choices of potentials that were used to carry out the numerical analysis of Secs. VI, VII, and VIII.

A. Potentials I

The motivation for this choice is to mimic (at qualitative level, without fitting any of the numerical results to QCD data) the physics of real QCD in the Veneziano limit [51].

With potentials I we have used in this article the choice $V_a = \exp(-a_q\tau^2 - a_l|\tau|)$, suggested above, which also makes the backgrounds at finite θ angle well defined. As pointed out above, we require that the leading dependence on the tachyon in V_a is the same as in V_f, i.e.

$a_q = \text{const} = a$. In addition, we choose a_l to be a constant having a sufficiently large value so that $e^{4A}V_f\sqrt{\kappa}\tau$ in (3.28) dominates over V_a for all $r \gtrsim 1/\Lambda_{\rm IR}$. A convenient choice is $a_l = 10/C_{\rm I}$, where $C_{\rm I}$ is the coefficient in the IR asymptotics of the tachyon: $\tau \sim e^{C_{\rm I} r}$. For the numerical coefficients in the function $Z(\lambda)$ of (4.1) we chose $Z_0 = 1$ and $c_a = 0.1$. This choice was seen to lead to reasonable behavior for all observables depending on this function.

In summary, the potentials I are given by

$$V_g(\lambda) = V_0\left[1 + V_1\lambda + V_2\lambda^2\frac{\sqrt{1+\log(1+\frac{\lambda}{\lambda_0})}}{(1+\frac{\lambda}{\lambda_0})^{2/3}}\right], \quad (4.2)$$

$$V_{f0}(\lambda) = W_0[1 + W_1\lambda + W_2\lambda^2],$$
$$a(\lambda) = a_0, \qquad \kappa(\lambda) = \frac{1}{(1+\frac{3a_1}{4}\lambda)^{4/3}} = w(\lambda), \quad (4.3)$$

$$Z(\lambda) = Z_0\left[1 + c_a\left(\frac{\lambda}{\lambda_0}\right)^4\right],$$
$$V_a(\tau) = \exp(-a_q\tau^2 - a_l|\tau|), \quad (4.4)$$

where the coefficients satisfy

$$V_0 = 12, \qquad V_1 = \frac{11}{27\pi^2}, \qquad V_2 = \frac{4619}{46656\pi^4};$$
$$W_1 = \frac{24 + (11-2x)W_0}{27\pi^2 W_0},$$
$$W_2 = \frac{24(857-46x) + (4619 - 1714x + 92x^2)W_0}{46656\pi^4 W_0};$$
$$a_0 = \frac{12 - xW_0}{8} = a_q, \qquad a_1 = \frac{115 - 16x}{216\pi^2},$$
$$\lambda_0 = 8\pi^2; \quad (4.5)$$

$$Z_0 = 1, \qquad c_a = 0.1, \quad (4.6)$$

and with a_l chosen as explained above. For potentials I we have used[5] $W_0 = 3/11$.

All computations at finite θ angle in this article were done by using this choice of potentials.

B. Potentials II

This choice might not model QCD as well as potentials I, but the motivation is to pick a background with different IR structure in order to see how much this affects our results for the backgrounds at zero θ angle. The numerics for potentials II in this article were done with the choice $V_a = \exp(-a(\lambda)\tau^2)$, where $a(\lambda)$ is the same function which appears in V_f and is given explicitly in (4.7).

Explicitly we used

$$a(\lambda) = a_0\frac{1 + a_1\lambda + \frac{\lambda^2}{\lambda_0^2}}{(1+\frac{\lambda}{\lambda_0})^{4/3}},$$
$$\kappa(\lambda) = \frac{1}{(1+\frac{\lambda}{\lambda_0})^{4/3}}, \qquad w(\lambda) = 1; \quad (4.7)$$

$$V_a = \exp(-a(\lambda)\tau^2), \quad (4.8)$$

and all the other functions as for potentials I above, except that we chose

$$W_0 = \frac{12}{x}\left[1 - \frac{1}{(1+\frac{7}{4}x)^{2/3}}\right] \quad (4.9)$$

instead of $W_0 = 3/11$. With this choice, the pressure agrees with the Stefan-Boltzmann (SB) result at high temperatures [49] (without the need to introduce an x dependence in the normalization of the action). In this article, we used potentials II in the numerical analysis of Sec. VII (at zero θ angle).

V. THE CHIRAL LAGRANGIAN ANALYSIS IN THE VENEZIANO LIMIT

In this section we will take a detour and consider the problem from the effective chiral theory point of view. To do this, we must assume that the bare quark masses $m \ll \Lambda_{\rm UV}$ so that the pions are very light compared to other particles, and therefore it makes sense to write down an effective action for them integrating out all other particles. This analysis is useful as we can see what can be determined from low energy symmetries alone and what needs a full nonperturbative computation (using holography in this paper). Moreover the chiral Lagrangian results provide consistency checks for our holographic analysis.

We will start by writing the effective action for the expectation values of the QCD order parameters W_{ij} which is an $N_f \times N_f$ complex matrix (the expectation value of $\bar\psi_R^i\psi_L^j$), as well as G and Θ the pseudoscalar and scalar glueball related expectation values following [74] and references therein.

We start from the $U(1)_A$ anomaly equation that can be written as

$$\langle\partial_\mu J_5^\mu\rangle = \frac{g^2 N_f}{16\pi^2}\langle\mathbb{T}r[F\tilde F]\rangle + i(M_{ij}\langle\bar\psi_R^i\psi_L^j\rangle - M_{ij}^\dagger\langle\bar\psi_L^i\psi_R^j\rangle)$$
$$= N_f N_c G + i\mathbb{T}r[\bar M W - \bar M^\dagger W^\dagger], \quad (5.1)$$

$$\text{with} \quad W_{ij} \equiv \langle\bar\psi_R^j\psi_L^i\rangle, \qquad W_{ij}^\dagger \equiv \langle\bar\psi_L^j\psi_R^i\rangle, \quad (5.2)$$

as well as the conformal anomaly equation (in flat space)

[5] As was shown in [49], the finite temperature phase diagram is not of the standard type for potentials I if W_0 is close to its upper limit $24/11$; a chirally symmetric phase is present at small x. Therefore we pick a value near the lower end of the possible range.

$$\langle T^{\mu}{}_{\mu}\rangle = -\frac{\beta(g)}{2g}\langle \mathbb{T}r[F^2]\rangle + (1+\gamma(g))(M_{ij}\langle\bar{\psi}^i_R\psi^j_R\rangle + \text{c.c.})$$
$$= N_c\Theta + (1+\gamma(g))\mathbb{T}r[\bar{M}W + \bar{M}^\dagger W^\dagger], \tag{5.3}$$

where Θ, G were defined so that they are $\mathcal{O}(1)$ in the Veneziano limit and $\bar{M}$ is the quark mass matrix. Here $\beta(g)$ is the QCD β function and $\gamma(g)$ is the fermion anomalous dimension. Because of energy and charge conservation G and H have canonical dimension 4. Note that although the product $\mathbb{T}r[\bar{M}W]$ is RG invariant, W is RG dependent. For the purposes of an effective theory, W will be defined at low energies and therefore $\bar{M}$ will be the renormalized quark matrix at low energies. It will be linearly related to the UV quark mass matrix for small enough quark masses.

Flavor $U(N_f)_L \times U(N_f)_R$ transformations act as

$$W \to V_L W V_R^\dagger, \tag{5.4}$$

where V_L, V_R are $U(N_f)$ matrices. G, Θ are flavor invariants. We can also construct flavor invariants from the matrix W

$$I_n \equiv \frac{1}{N_f(g^2N_c)^{6n}}\mathbb{T}r[(WW^\dagger)^n] \tag{5.5}$$

which are also $\mathcal{O}(1)$ in the Veneziano limit. In the absence of masses and the anomaly, the effective potential takes the following form:

$$V_{\text{eff}}(G,\Theta,I_n) = N_c^2 V_0(G,\Theta,I_n), \tag{5.6}$$

where V_0 is an arbitrary function that due to parity invariance must satisfy

$$V_0(G,\Theta,I_n) = V_0(-G,\Theta,I_n). \tag{5.7}$$

To accommodate the $U(1)_A$ anomaly we must consider that the $U(1)_A$ transformation acts as

$$W \to e^{i\epsilon}W, \qquad G \to G + \epsilon. \tag{5.8}$$

Therefore the full effective potential that includes the anomaly is

$$V_{\text{eff}} = N_c^2 V_0\left(\Theta, I_n, G + \frac{i}{2N_f}\log\det\frac{W}{W^\dagger}\right). \tag{5.9}$$

In the presence of a (complex) mass matrix $\bar{M}$ at linear order, we have in addition the associated term from the QCD Lagrangian

$$V_{\text{eff}} = N_c^2 V_0\left(\Theta, I_n, G + \frac{i}{2N_f}\log\det\frac{W}{W^\dagger}\right) + \mathbb{T}r[\bar{M}W + \bar{M}^\dagger W^\dagger]. \tag{5.10}$$

By a chiral rotation we can also introduce the θ angle:

$$V_{\text{eff}} = N_c^2 V_0\left(\Theta, I_n, G + \frac{i}{2N_f}\log\det\frac{W}{W^\dagger} - \frac{\theta}{N_f}\right) + \mathbb{T}r[\bar{M}W + \bar{M}^\dagger W^\dagger] \tag{5.11}$$

and by a phase redefinition of W it can be moved to the masses

$$V_{\text{eff}} = N_c^2 V_0\left(\Theta, I_n, G + \frac{i}{2N_f}\log\det\frac{W}{W^\dagger}\right) + \mathbb{T}r[e^{i\frac{\theta}{N_f}}\bar{M}W + e^{-i\frac{\theta}{N_f}}\bar{M}^\dagger W^\dagger]. \tag{5.12}$$

When quark masses are small (compared to Λ_{QCD}) the G and Θ glueballs are much heavier than the mesons. We will therefore neglect their kinetic terms and their equations of motion amount to minimizing their potential. It is interesting that there seems to be more things that can be said about the dependence of this action concerning its dependence on the G and Θ condensates. A glimpse of this was indicated first in [75] and in a more targeted way in [76] where the effective potential for the trace of the stress tensor was calculated holographically in a single scalar gravitational theory.

We next move to the two derivative level. We will concentrate on the kinetic terms of the quark condensate W which is the only light remaining field. To write such kinetic terms, we must introduce flavor invariants with up to two derivatives

$$I^n_\mu \equiv \frac{1}{N_f}\mathbb{T}r[(WW^\dagger)^n(\partial_\mu W)W^\dagger],$$
$$\bar{I}^n_\mu \equiv \frac{1}{N_f}\mathbb{T}r[(WW^\dagger)^n W(\partial_\mu W^\dagger)], \tag{5.13}$$

and

$$J_{mn} \equiv \frac{1}{N_f}\mathbb{T}r[(WW^\dagger)^m(\partial_\mu W)(WW^\dagger)^n(\partial^\mu W^\dagger)], \tag{5.14}$$

and then

$$S_2 = \int d^4x \sum_{m,n=0}^{\infty}[C_{nm}J_{mn} + \hat{C}_{mn}I_\mu\bar{I}^\mu]. \tag{5.15}$$

We now decompose W as a product of an Hermitian (H) and a unitary matrix (U)

$$W = HU, \qquad W^\dagger = U^\dagger H, \tag{5.16}$$

and thus,

$$WW^\dagger = HUU^\dagger H = H^2, \qquad \det\frac{W}{W^\dagger} = (\det U)^2. \quad (5.17)$$

Moreover, we shall write U as

$$U = \exp\left[\frac{i}{\sqrt{N_f}}\eta' + i\pi^a T^a\right], \qquad \mathbb{T}r[T^a T^b] = \delta^{ab}, \quad (5.18)$$

where T^a are the (traceless) generators of $SU(N_f)$.

Chiral symmetry breaking will give an expectation value to H, while U remains free and parametrizes the Goldstone bosons, namely, η' and the generalized pions.

Minimizing now the potential in the massless case (by setting first $\bar{M} = 0$) with respect to the "heavy" fields Θ, G, H_{ij} we will obtain nontrivial VEVs for G, Θ and H that are functions only of $\Lambda_{\rm QCD}$.[6] In particular,

$$\langle H_{ij}\rangle = \sigma\delta_{ij}. \quad (5.19)$$

The VEV of G can be absorbed in the θ phase changing it to $\bar{\theta}$. The only part of U that appears in the potential is $\log\det U$ due to the anomaly. As argued in the end of Sec. VI B the dependence in the Veneziano limit is quadratic like in the 't Hooft limit,

$$V_{\rm eff} = \kappa N_c N_f(-i\log\det U)^2 + \cdots. \quad (5.20)$$

A. The effective action for the Goldstone modes

We now set Θ, G and H equal to their VEVs and we rewrite the effective Lagrangian (up to two derivatives) for the Goldstone modes described by an $N_f \times N_f$ unitary matrix U as[7] [8–11,77]

$$\begin{aligned}\mathcal{L}_{\rm chiral} = {}& \frac{\hat{f}_\pi^2}{2}[\mathbb{T}r[\partial_\mu U\partial^\mu U^{-1}] + \mathbb{T}r[\hat{M}U + \hat{M}^\dagger U^\dagger]] \\ & - \frac{a\hat{f}_\pi^2}{2N_c}(-i\log\det U)^2 \\ & + \frac{\hat{f}_{\eta'}^2 - \hat{f}_\pi^2}{2N_f}\mathbb{T}r[U^\dagger\partial_\mu U]\mathbb{T}r[U\partial^\mu U^\dagger]. \end{aligned} \quad (5.21)$$

The last term in (5.21) originates in the factorized terms in (5.15), and although it is subleading in the 't Hooft limit, it is $\mathcal{O}(1)$ in the Veneziano limit. It is responsible for the fact that the decay constant of the η' is different from the rest of the Goldstone modes (pions).

The term $\propto(\log\det U)^2$ in (5.21) is the anomaly term and is of order $\mathcal{O}(\eta'^2)$ giving a mass to the η'. As discussed in the end of Sec. VI B this is a good estimate also in the Veneziano limit. The matrix $\hat{M}$ is a renormalized quark mass matrix. We lump the θ parameter inside $\hat{M}$ via a chiral rotation. We will consider the $SU(N_f)$ invariant case where all quark masses are equal to m_q.

Finally, the coefficients are written in terms of the physical pion and η' decay constants, $\hat{f}_{\pi,\eta'}$, as well as the parameter a that as we will soon see is related to the topological susceptibility. It should be noted that in the Veneziano limit

$$\hat{f}_\pi^2 \sim \hat{f}_{\eta'}^2 \sim N_c, \qquad m_{\eta'} \sim \mathcal{O}(1). \quad (5.22)$$

We now consider the case explored in this paper: quark masses that are $SU(N_f)$ invariant. In this case the mass term in the effective chiral Lagrangian can be parametrized in terms of the pion mass m_π as

$$\hat{M}_{ij} = e^{i\frac{\theta}{N_f}}m_\pi^2\delta_{ij}. \quad (5.23)$$

We now transform $U \to Ue^{-i\frac{\theta}{N_f}}$ to obtain

$$\begin{aligned}\mathcal{L}_{\rm chiral} = {}& \frac{\hat{f}_\pi^2}{2}\left[\mathbb{T}r[\partial_\mu U\partial^\mu U^{-1}] + m_\pi^2\mathbb{T}r[U + U^\dagger]\right. \\ & \left. - \frac{a}{N_c}(-i\log\det U - \theta)^2\right] \\ & + \frac{\hat{f}_{\eta'}^2 - \hat{f}_\pi^2}{2N_f}\mathbb{T}r[U^\dagger\partial_\mu U]\mathbb{T}r[U\partial^\mu U^\dagger], \end{aligned} \quad (5.24)$$

from which the pion potential reads

$$V(U) = \frac{\hat{f}_\pi^2}{2}\left[m_\pi^2\mathbb{T}r[U + U^\dagger] - \frac{a}{N_c}(-i\log\det U - \theta)^2\right]. \quad (5.25)$$

By symmetry we should look for a minimum of V of the form $U_{ij} = e^{i\phi}\delta_{ij}$. However, we should remember that 2π rotations of individual masses give the same theory. Therefore, a better parametrization of the vacua is

$$U_{ij} = e^{i\phi}e^{2\pi i n_i}\delta_{ij}. \quad (5.26)$$

Then the potential becomes

$$V(\phi) = \hat{f}_\pi^2\left[-N_f m_\pi^2\cos\phi + \frac{a}{2N_c}(\theta - N_f\phi - 2\pi N)^2\right] \quad (5.27)$$

with $N = \sum_{i=1}^{N_f} n_i$. In the sequel, we will set $N = 0$, but we will consider all branches with θ shifted by multiples of 2π.

[6] Once quark masses are turned on, there will be $\mathcal{O}(m^2)$ corrections to such VEVs.

[7] The pion decay constant $\hat{f}_\pi$ which is normalized as is usual for chiral Lagrangians differs from the constant f_π used elsewhere in this article by $N_f\hat{f}_\pi^2 = f_\pi^2$.

We define

$$\tilde{\theta} = \frac{\theta}{N_f}, \qquad x = \frac{N_f}{N_c}, \tag{5.28}$$

and obtain

$$V(\phi) = N_f \hat{f}_\pi^2 \left[-m_\pi^2 \cos\phi + \frac{xa}{2}(\tilde{\theta} - \phi)^2 \right] = f_\pi^2 \left[-m_\pi^2 \cos\phi + \frac{xa}{2}(\tilde{\theta} - \phi)^2 \right]. \tag{5.29}$$

Note that $V \sim \mathcal{O}(N_c N_f)$.

Consider first the case with zero quark mass. In this case $m_\pi = 0$ and the extremum is at $\phi = \tilde{\theta}$. Hence the vacuum energy is independent of θ as expected.

When $m_\pi \neq 0$, the extrema satisfy the equation

$$m_\pi^2 \sin\phi = ax(\tilde{\theta} - \phi), \tag{5.30}$$

which can be rewritten as

$$\sin\phi - \zeta(\tilde{\theta} - \phi) = 0, \quad \text{with} \quad \zeta = \frac{ax}{m_\pi^2}, \tag{5.31}$$

ζ being a dimensionless parameter which is $\mathcal{O}(1)$ in the Veneziano limit. There are three different parameters that enter in ζ: the QCD scale as $a \sim \Lambda_{\rm QCD}^2$, the bare quark masses m_q, and the flavor parameter x. For small m_q, $m_\pi^2 \sim m_q$. The assumption for the validity of the effective chiral theory implies that $a \gg m_\pi^2$. Therefore, for generic values of x, $\zeta \gg 1$. Only in the 't Hooft limit, $x \to 0$, can ζ become much smaller than one.

When $\zeta \geq 1$ there is a unique solution to (5.30) as the left-hand side of (5.31) is monotonic. But for $\zeta < 1$ there is a range of values of θ where there are two or more minima. We denote these extrema, which are functions of $\tilde{\theta}$, as $\phi_i(\tilde{\theta})$. They are minima of the potential if

$$V''(\phi_i) = f_\pi^2 m_\pi^2 [\cos\phi_i + \zeta] \geq 0. \tag{5.32}$$

The deepest minimum is the one that minimizes

$$V(\phi) = f_\pi^2 m_\pi^2 \left[-\cos\phi + \frac{\zeta}{2}(\tilde{\theta} - \phi)^2 \right]. \tag{5.33}$$

Therefore, the θ-dependent vacuum energy is

$$E(\tilde{\theta}) = \min_\phi f_\pi^2 m_\pi^2 \left[-\cos\phi + \frac{\zeta}{2}(\tilde{\theta} - \phi)^2 \right]. \tag{5.34}$$

In Fig. 1 we present a calculation for the energy as a function of $\tilde{\theta}$ for $\zeta = 2$, where we now have added the $\frac{2\pi}{N_f}$

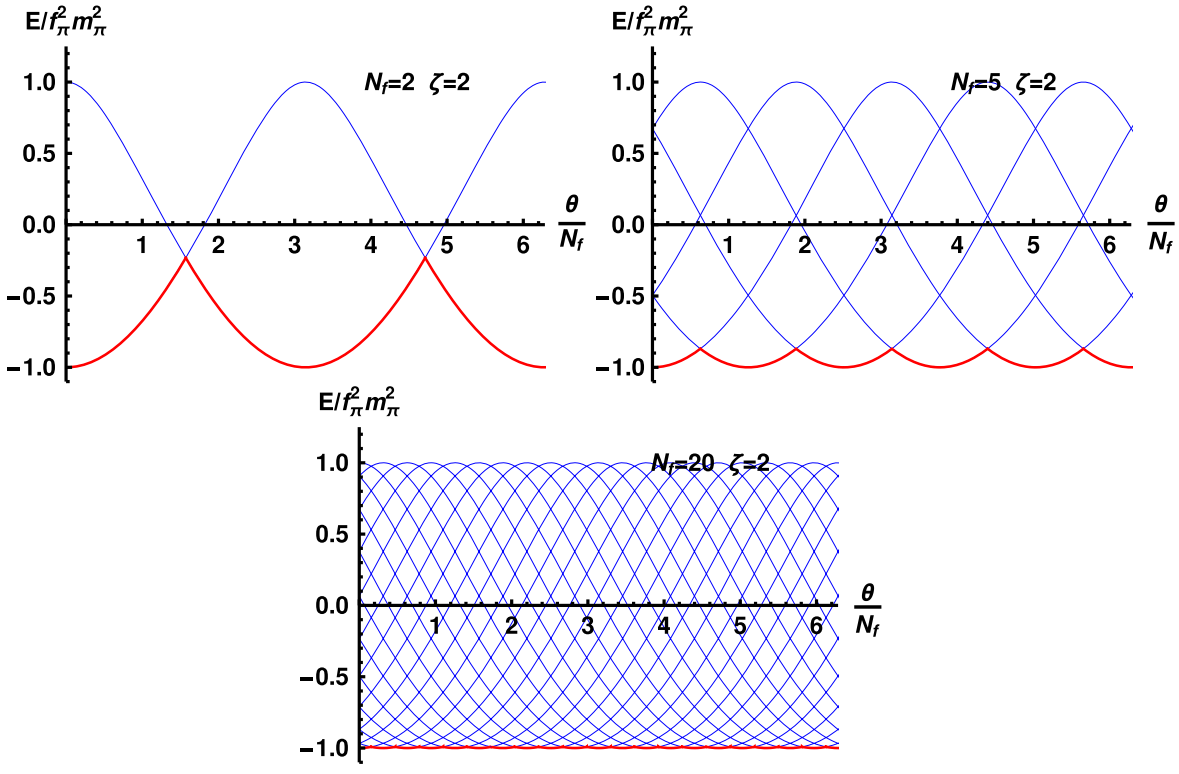

FIG. 1. The branches of vacua according to the chiral Lagrangian analysis. The thin blue lines show (normalized) energy for all branches, and the thick red line is the final energy for the dominant vacuum. We chose $\zeta = 2$ in all plots with $N_f = 2$, 5, and 20, in the top-left, top-right, and bottom plots, respectively.

shifts as argued above, and we have denoted by red lines the minimum values that indicate the true $\tilde{\theta}$ dependence of the ground state energy.

To compute the derivatives of the vacuum energy we need the derivatives of ϕ from (5.31)

$$\frac{\partial\phi}{\partial\tilde{\theta}}=\frac{\zeta}{\zeta+\cos\phi},\qquad \frac{\partial^2\phi}{\partial\tilde{\theta}^2}=\frac{\zeta^2\sin\phi}{(\zeta+\cos\phi)^3}. \tag{5.35}$$

We obtain

$$\frac{\partial E}{\partial\tilde{\theta}}=f_\pi^2 ax(\tilde{\theta}-\phi),\qquad \hat{\chi}_{\rm top}(\tilde{\theta})\equiv\frac{\partial^2 E}{\partial\tilde{\theta}^2}=f_\pi^2 m_\pi^2\frac{\zeta\cos\phi}{\zeta+\cos\phi}. \tag{5.36}$$

At $\tilde{\theta}=0$ we have $\phi=0$ and

$$\left.\frac{\partial E}{\partial\tilde{\theta}}\right|_{\tilde{\theta}=0}=0,$$
$$\hat{\chi}_{\rm top}(\tilde{\theta}=0)\equiv\left.\frac{\partial^2 E}{\partial\tilde{\theta}^2}\right|_{\tilde{\theta}=0}=f_\pi^2 m_\pi^2\frac{\zeta}{1+\zeta}\geq 0. \tag{5.37}$$

The topological susceptibility in the normalization used in the latter sections of the article is then

$$\chi(\tilde{\theta})\equiv\chi_{\rm top}(\tilde{\theta})\equiv\frac{\partial^2 E}{\partial\theta^2}=\frac{\hat{\chi}_{\rm top}(\tilde{\theta})}{N_f^2}. \tag{5.38}$$

Note that $\chi_{\rm top}=\mathcal{O}(1)$ and $\hat{\chi}_{\rm top}=\mathcal{O}(N_f^2)$.

We can now compute the meson masses in the nontrivial vacuum by expanding U around it

$$U=e^{i\phi}\cdot\exp\left[\frac{i}{\sqrt{N_f}}\eta'+i\pi^a T^a\right]. \tag{5.39}$$

We obtain

$$V=E(\tilde{\theta})-\frac{1}{2}\hat{f}_\pi^2[m_\pi^2\cos\phi\pi^a\pi^a+(m_\pi^2\cos\phi+ax)\eta'^2]+\cdots. \tag{5.40}$$

From (5.24) we observe that f_π and $f_{\eta'}$ are θ independent.

We obtain for the $\tilde{\theta}$-dependent meson masses

$$m_\pi^2(\tilde{\theta})=m_\pi^2\cos\phi,\qquad m_{\eta'}^2(\tilde{\theta})=\frac{f_\pi^2}{f_{\eta'}^2}[m_\pi^2(\tilde{\theta})+ax], \tag{5.41}$$

where $f_{\eta'}^2=N_f\hat{f}_{\eta'}^2$. The last relation can be written in terms of the topological susceptibility by solving (5.36)

$$ax=\frac{m_\pi^2(\tilde{\theta})\hat{\chi}_{\rm top}(\tilde{\theta})}{f_\pi^2 m_\pi^2(\tilde{\theta})-\hat{\chi}_{\rm top}(\tilde{\theta})}, \tag{5.42}$$

as

$$m_{\eta'}^2(\tilde{\theta})=\frac{f_\pi^2}{f_{\eta'}^2}\frac{f_\pi^2 m_\pi^2(\tilde{\theta})}{f_\pi^2 m_\pi^2(\tilde{\theta})-\hat{\chi}_{\rm top}(\tilde{\theta})}m_\pi^2(\tilde{\theta}). \tag{5.43}$$

Equation (5.43) is the analogue of the Witten-Veneziano formula in the Veneziano limit. In the 't Hooft limit, $x\to 0$, we find that

$$\hat{\chi}_{\rm top}=f_\pi^2 ax[1+\mathcal{O}(x)],$$
$$\chi_{\rm top}=\frac{f_\pi^2}{N_f N_c}a+\mathcal{O}(x),$$
$$m_\pi^2(\tilde{\theta})=m_\pi^2+\mathcal{O}(x^2), \tag{5.44}$$

where in the last estimate we used (5.55). Since the kinetic and mass terms of mesons are group theoretically similar we also have

$$f_\pi=f_{\eta'}[1+\mathcal{O}(x^2)], \tag{5.45}$$

and then (5.43) can be written as

$$m_{\eta'}^2(\tilde{\theta})=m_\pi^2(0)+\frac{\hat{\chi}_{\rm top}(0)}{f_\pi^2}+\mathcal{O}(x^2)$$
$$=m_\pi^2(0)+x\frac{N_f N_c\chi_{\rm top}(0)}{f_\pi^2}+\mathcal{O}(x^2), \tag{5.46}$$

which is the standard Witten-Veneziano relation and is also in agreement with (G15).

B. The large ζ limit

We will investigate now the limit where $\zeta\gg 1$. This is reached when the masses of the quarks are much smaller than the characteristic QCD scale. For $\zeta\gg 1$ the unique solution of (5.31) is

$$\phi_*=\tilde{\theta}-\frac{\sin\tilde{\theta}}{\zeta}+\frac{1}{2}\frac{\sin(2\tilde{\theta})}{\zeta^2}+\frac{\sin\tilde{\theta}-3\sin(3\tilde{\theta})}{8\zeta^3}+\cdots, \tag{5.47}$$

and

$$V''(\phi_*)=f_\pi^2 m_\pi^2\left[\zeta+\cos\tilde{\theta}+\frac{\sin^2\tilde{\theta}}{\zeta}+\cdots\right]>0, \tag{5.48}$$

while

$$E(\tilde\theta)=V(\phi_*)=-f_\pi^2m_\pi^2\left[\cos\tilde\theta+\frac{\sin^2\tilde\theta}{2\zeta}-\frac{\cos\tilde\theta\sin^2\tilde\theta}{2\zeta^2}+\frac{1}{6\zeta^3}\sin^2\tilde\theta(1+2\cos(2\tilde\theta))+\cdots\right]. \tag{5.49}$$

From (5.36) and (5.41) we obtain

$$\chi_{\rm top}=f_\pi^2m_\pi^2\left[\cos\tilde\theta-\frac{\cos(2\tilde\theta)}{\zeta}+\mathcal{O}(\zeta^{-2})\right], \tag{5.50}$$

$$m_\pi^2(\tilde\theta)=m_\pi^2\left[\cos\tilde\theta+\frac{\sin^2\tilde\theta}{\zeta}+\mathcal{O}(\zeta^{-2})\right]. \tag{5.51}$$

In the large N_f limit $\tilde\theta\to 0$, and (5.49) becomes

$$E(\theta)=-f_\pi^2m_\pi^2\left[1+\left(-1+\frac{1}{\zeta}-\frac{1}{\zeta^2}+\cdots\right)\frac{\theta^2}{2N_f^2}+\mathcal{O}(N_f^{-4})\right]. \tag{5.52}$$

In this case, if we are interested in the limit $\tilde\theta\to 0$ we can solve (5.31) to all orders in $1/\zeta$ as follows:

$$\phi=\frac{\zeta}{\zeta+1}\tilde\theta+\frac{\zeta^3}{6(\zeta+1)^4}\tilde\theta^3+\mathcal{O}(\tilde\theta^5), \tag{5.53}$$

obtaining the following formula for the energy density:

$$\begin{aligned}E(\tilde\theta)&=-f_\pi^2m_\pi^2\left[1-\frac{\zeta}{2(1+\zeta)}\tilde\theta^2+\frac{\zeta^4}{4(1+\zeta)^4}\tilde\theta^4+\mathcal{O}(\tilde\theta^6)\right]\\&=-f_\pi^2m_\pi^2\left[1-\frac{ax}{2(m_\pi^2+ax)}\tilde\theta^2+\frac{(ax)^4}{4(m_\pi^2+ax)^4}\tilde\theta^4+\mathcal{O}(\tilde\theta^6)\right],\end{aligned} \tag{5.54}$$

where in the second line we substituted the value of ζ from (5.31).

C. The $\zeta\to 0$ limit

This limit can be reached as $x\to 0$ and coincides with the 't Hooft large-N_c limit. In this limit, $\zeta\to 0$, there is an infinite number of extrema that can be found perturbatively in ζ

$$\phi_n=n\pi+(-1)^n(\tilde\theta-n\pi)\zeta-(\tilde\theta-n\pi)\zeta^2+\cdots, \tag{5.55}$$

and thus

$$V''\sim(-1)^n+\zeta+\cdots \tag{5.56}$$

which implies that only $n=$ even are minima. Evaluating the vacuum energy at the 2n-th minimum we obtain

$$V_n=-f_\pi^2m_\pi^2\left[1-\frac{\zeta-\zeta^2}{2}(\tilde\theta-2n\pi)^2+\cdots\right], \tag{5.57}$$

and

$$E(\tilde\theta)=\min_n\left\{-f_\pi^2m_\pi^2\left[1-\frac{\zeta-\zeta^2}{2}(\tilde\theta-2n\pi)^2+\cdots\right]\right\}. \tag{5.58}$$

VI. VACUA OF V-QCD AT FINITE θ ANGLE

In this section we analyze vacuum solutions of V-QCD at finite θ angle. First we write down explicitly the solutions for the axion $\mathfrak{a}$ and the phase ξ. We denote

$$f_a(r)\equiv\frac{V_a\sqrt{e^{2A}+\kappa\tau'^2}}{\kappa^{1/2}\tau\sqrt{e^{8A}V_f^2\kappa\tau^2-C_a^2V_a^2}} \tag{6.1}$$

so that (3.6) implies

$$\xi'(r)=C_af_a(r),\qquad \xi(r)=\xi_0+C_a\int_0^r dr'f_a(r'). \tag{6.2}$$

Here ξ_0 is identified as the phase of the quark mass on the field theory side. The solution for $\mathfrak{a}$ can be obtained from (3.3)

$$\begin{aligned}&\mathfrak{a}=\bar{\mathfrak{a}}_0-x\xi V_a+C_a\int_0^r\frac{dr'}{e^{3A}Z}+xC_a\int_0^r dr'f_aV_a,\\&\bar{\mathfrak{a}}_0\equiv\mathfrak{a}_0+x\xi_0,\end{aligned} \tag{6.3}$$

where the integration constant $\mathfrak{a}_0$ is related to the standard θ angle by $\mathfrak{a}_0=\mathfrak{a}(r=0)=\theta/N_c$, and as explained in Sec. II A, the gauge invariant combination $\bar{\mathfrak{a}}_0$ is related to the gauge invariant $\bar\theta$ angle through $\bar{\mathfrak{a}}_0=\bar\theta/N_c$. Recall that $\bar\theta=\theta+\arg\det M_q$, where M_q is the quark mass matrix. We could use the transformation (2.18) to set either ξ_0 or $\mathfrak{a}_0$ to zero, but equivalently we can postpone the gauge fixing and continue working with $\bar{\mathfrak{a}}_0$. The value of $\mathfrak{a}$ at the tip (which will be determined below) is then given by

$$\mathfrak{a}(\infty)=\bar{\mathfrak{a}}_0+C_a\int_0^\infty dr\left(\frac{1}{e^{3A}Z}+xf_aV_a\right). \tag{6.4}$$

Notice that it is also gauge invariant.

In order to demonstrate the dependence of the free energy on $\bar\theta$, we first analyze the contribution solely from S_a which is obtained from the on-shell value of the Euclidean action [the overall sign of which is opposite that of (3.1)]:

$$\mathcal{E}_a = \frac{1}{2}M^3N_c^2\int_0^\infty dre^{3A}Z(\mathfrak{a}' + x\xi V_a')^2$$
$$= \frac{1}{2}M^3N_c^2C_a\int_0^\infty dr(\mathfrak{a}' + x\xi V_a')$$
$$= \frac{1}{2}M^3N_c^2C_a\left(\mathfrak{a}(\infty) - \bar{\mathfrak{a}}_0 - xC_a\int_0^\infty drf_aV_a\right), \quad (6.5)$$

where we used (3.3) to obtain the expression on the second line. We stress that this expression is not the complete free energy, which will be analyzed below, but it is the most important contribution for the $\bar{\theta}$ dependence. By using (6.4) the result may be written as

$$\mathcal{E}_a = \frac{1}{2}M^3N_c^2\frac{\int_0^\infty dre^{-3A}Z^{-1}}{[\int_0^\infty dr(e^{-3A}Z^{-1} + xf_aV_a)]^2}(\bar{\mathfrak{a}}_0 - \mathfrak{a}(\infty))^2. \quad (6.6)$$

This result is analogous to what was found for the θ dependence in the Yang-Mills case in [35]. Similarly as in that case, we expect that the contribution to the energy from the IR singularity, i.e. $\mathfrak{a}(\infty)$, vanishes. Otherwise, the IR singularity would play the role of a second boundary. Vanishing of $\mathfrak{a}(\infty)$ also leads to $\mathcal{E}_a \propto \bar{\mathfrak{a}}_0^2 \propto \bar{\theta}^2$ [for small $\bar{\theta}$ so that the implicit dependence of the integrals in (6.6) on $\bar{\theta}$ can be neglected] which agrees with the large N_c analysis of QCD [33]. We will argue below that after setting $\mathfrak{a}(\infty)$ to zero, also the full free energy, not only $\mathcal{E}_a$, has quadratic behavior for small $\bar{\mathfrak{a}}_0$.

The issue described above applies to all string theory "axions," namely scalars without a potential. As argued above, in all such cases, an explicit boundary condition must be imposed in the IR that is not dictated by regularity. In many cases such axions are internal components of gauge fields or higher forms (even the ten-dimensional IIB axion can be T-dualized to such a form). A concrete example of this is the case of the black D_4 soliton where the θ angle is generated by a six-dimensional vector field [33]. In all such cases, the usual regularity condition for the form field indicates that it should vanish on the extremal horizon, not unlike the boundary condition we chose above.

Setting $\mathfrak{a}(\infty) = 0$, the relation between the source $\bar{\mathfrak{a}}_0$ and the VEV C_a follows from (6.4)

$$\frac{\bar{\theta}}{N_c} = \bar{\mathfrak{a}}_0 = -C_a\int_0^\infty dr\left(\frac{1}{e^{3A}Z} + xf_aV_a\right), \quad (6.7)$$

where one should recall that the integral also depends implicitly on C_a so that the relation is not exactly linear.

A. Construction of backgrounds and their generic properties

Recall that at zero $\bar{\theta}$, the chirally broken backgrounds could be parametrized in terms of a single variable defined through the IR asymptotics of the solution [48]. For potentials I, this variable was denoted by T_0 and controlled the normalization of the tachyon in the IR. The value of T_0 could be mapped to the physical parameter in QCD, the quark mass, after constructing the background solution. At zero $\bar{\theta}$ it was natural to choose the tachyon to be real, and to define τ as the real part of the complex field, so that it could become negative. The source of τ in the earlier work, i.e. the quark mass, consequently maps to the real part of the source of the complex tachyon. An example of the dependence of the quark mass on T_0 (in the QCD regime $0 < x < x_c$) is given in Fig. 2. Notice also that negative values of T_0 were allowed, but the solutions with opposite values of T_0 were related by the reflection $\tau \mapsto -\tau$ which left the action invariant.

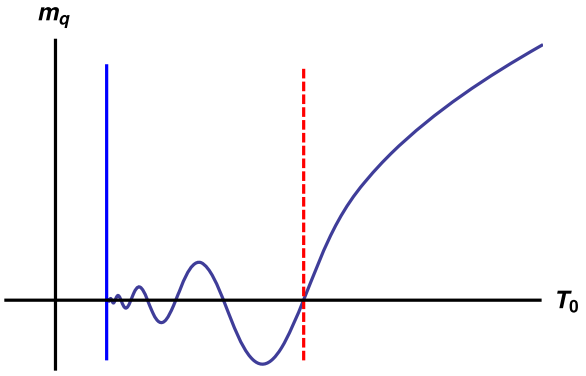

FIG. 2. Sketch of the dependence of the quark mass on T_0 for $C_a = 0 = \bar{\theta}$, i.e. on the horizontal axis of Fig. 3 (left). Solutions exist right of the vertical blue line. The dashed red vertical line denotes the location of the standard vacuum with zero quark mass.

Implementation of the CP-odd sector removes the reflection symmetry: Because the phase of the tachyon is nontrivial, it is natural that τ is the absolute value of the complex tachyon. Therefore the quark mass is also defined as the absolute value of the source for the complex tachyon, and $T_0 > 0$. At finite $\bar{\theta}$ angle we also have a second variable, the integration constant C_a, which controls the value of the $\bar{\theta}$ angle. More precisely, the pair (T_0, C_a) can be mapped to $(m_q, \bar{\theta})$ after the background has been constructed.

We have studied the CP-odd backgrounds numerically, restricting our study to the region with positive C_a—the solutions at negative C_a can be obtained by applying the CP transformation as pointed out at the end of Sec. III A. The procedure for creating the numerical solutions is essentially the same as discussed in [48,51,55]—the solutions are obtained by shooting from near the IR singularity, and the boundary conditions there are given by the known IR asymptotic expansions. As the axion and the phase of the tachyon could be integrated out of the equations of motion, there are essentially only two differences with respect to the equations at zero $\bar{\theta}$ angle: there is a new integration constant C_a and the tachyon equation of motion is now written in

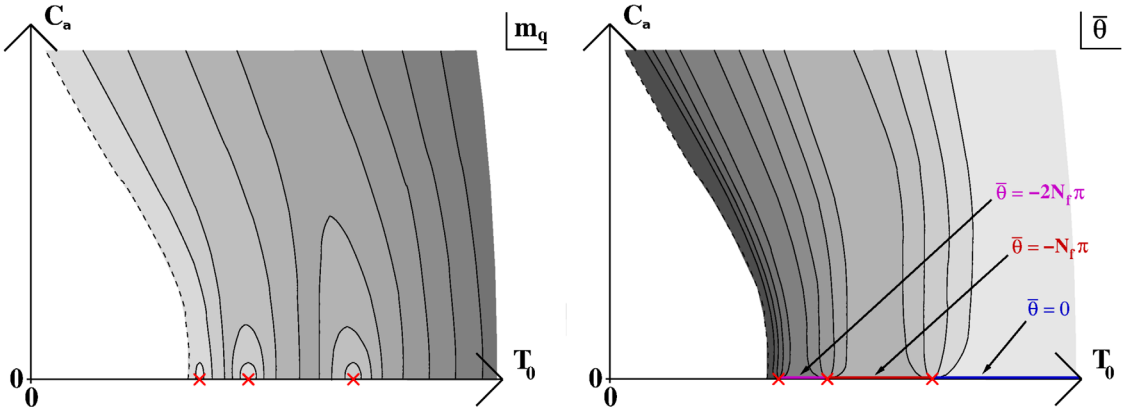

FIG. 3. Sketch of the dependence of the quark mass (left-hand plot) and the $\bar{\theta}$ angle (right-hand plot) on the parameters T_0 and C_a (with C_a given in IR units). The contours lie at fixed quark mass or $\bar{\theta}$ angle, and the red crosses denote points where the quark mass vanishes. Solutions exist in the shaded region. The $\bar{\theta}$ angle takes piecewise constant values on the intervals of the horizontal axis between the crosses as indicated in the right-hand plot.

terms of the absolute value of the complex tachyon rather than its real part. As we have demonstrated above in Sec. III the IR asymptotics (and therefore also the IR boundary conditions) are unchanged, up to the possible appearance of some special solutions which will be discussed below. When presenting the numerical data, dimensionful quantities can be given either in UV units (Λ_{UV}) or in IR units (Λ_{IR}), which are discussed in Sec. II B and defined precisely in (A4) and (A12) in Appendix A.

We discuss first details in the QCD-like phase [$0 < x < x_c$ with $x_c - x = \mathcal{O}(1)$], where a rich structure is found, and return to the dependence of the backgrounds on x below. In this phase, the absolute value of the quark mass and the $\bar{\theta}$ angle depend on T_0 and C_a as depicted schematically in Fig. 3. Recall first what happens on the horizontal axis ($C_a = 0$) where the $\bar{\theta}$ angle vanishes and the tachyon is real. The real quark mass as a function of T_0 in this case is given in Fig. 2; see [48]. As we have already pointed out, at finite C_a we define m_q as the absolute value of the source of the complex tachyon, whereas Fig. 2 shows the dependence of the real part of the source on T_0. Therefore, in order to compare to Fig. 3 (left), one needs first take the absolute value so that the negative values of m_q in Fig. 2 are reflected to positive values.

Solutions are only found for $T_0 > T_{0c}$, where the critical value T_{0c} is the endpoint of the dashed curve in Fig. 3 and denoted by the vertical blue line in Fig. 2. The value of the quark mass oscillates as $T_0 \to T_{0c}$ from above, so that there are infinitely many zeroes (of which the three which occur at largest T_0's are shown as red crosses in Fig. 3). The first node (largest value of T_0) is the standard stable vacuum at zero quark mass, whereas the other nodes are unstable Efimov vacua. As one approaches the critical value T_{0c}, the background flows closer and closer to the IR fixed point but misses it eventually due to the nonzero tachyon. It is also possible that there is only a finite amount of nodes on the horizontal axis. This can happen if the bulk mass of the tachyon satisfies the BF bound at the IR fixed point [48,51], as is the case for potentials I at low values of x [49].

Extending to the solutions with $C_a \neq 0$ and therefore finite $\bar{\theta}$ angle, the nodes are smoothed out, but the region at small T_0, where no regular solutions exist (white in Fig. 3), remains at least for small C_a. The structure of the sketch in Fig. 3 can be confirmed numerically for the concrete choices of potentials I that we have introduced. As an example we show the dependence of the quark mass and the $\bar{\theta}$ angle on T_0 and C_a for the QCD-like potentials I in Fig. 4. The range of T_0 was chosen in the vicinity of the "standard" zero mass vacuum, which is denoted by the rightmost cross in Fig. 3 and by the vertical dashed red line in Fig. 2. It can also be verified analytically that $\bar{\theta}$ is quantized in units of $N_f\pi$ on the $C_a = 0$ axis, as shown in Fig. 3 (right); see Appendix C. The uniqueness and stability of the solutions is discussed in the same appendix.

Notice that there are two types of curves of constant m_q in Fig. 3 (left). First, some of the curves start from the horizontal axis, circle around some of the nodes, and return to the axis. Second, some curves start from the horizontal axis and exit the plot at its upper edge. We plot in Fig. 5 the value of the $\bar{\theta}$ angle at constant m_q, i.e., along the curves, for potentials I. The plots for $m_q/\Lambda_{\mathrm{UV}} = 0.0001$, $m_q/\Lambda_{\mathrm{UV}} = 0.01$, and $m_q/\Lambda_{\mathrm{UV}} = 0.025$ correspond to contours in Fig. 3 (left) which start from the standard $\bar{\theta} = 0$ solutions, i.e. on the interval marked with dark blue color, and return on the horizontal axis on the dark red interval, having $\bar{\theta} = -N_f\pi$. We will also show in Appendix C why these curves end exactly at $\bar{\theta} = -N_f\pi$. The remaining plot at $m_q/\Lambda_{\mathrm{UV}} = 1$ in Fig. 5 corresponds to a curve in Fig. 3 (left) which starts from the dark blue interval and exits the

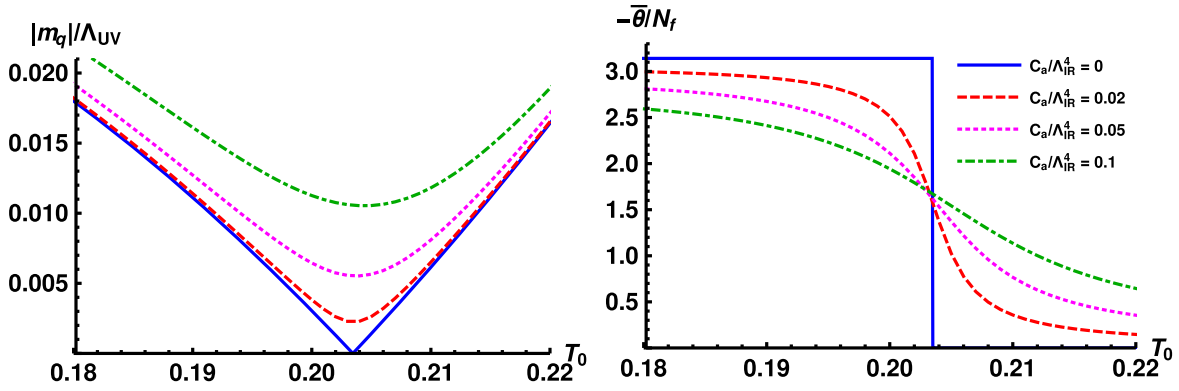

FIG. 4. The behavior of the quark mass (left-hand plot) and the $\bar{\theta}$ angle (right-hand plot) for the "QCD-like" potentials I with $x = 2/3$ near the rightmost node in Fig. 3 (left), i.e. the standard zero mass vacuum. The solid blue, dashed red, dotted magenta, and dot-dashed green curves have $C_a/\Lambda_{IR}^4 = 0$, 0.02, 0.05, and 0.1, respectively.

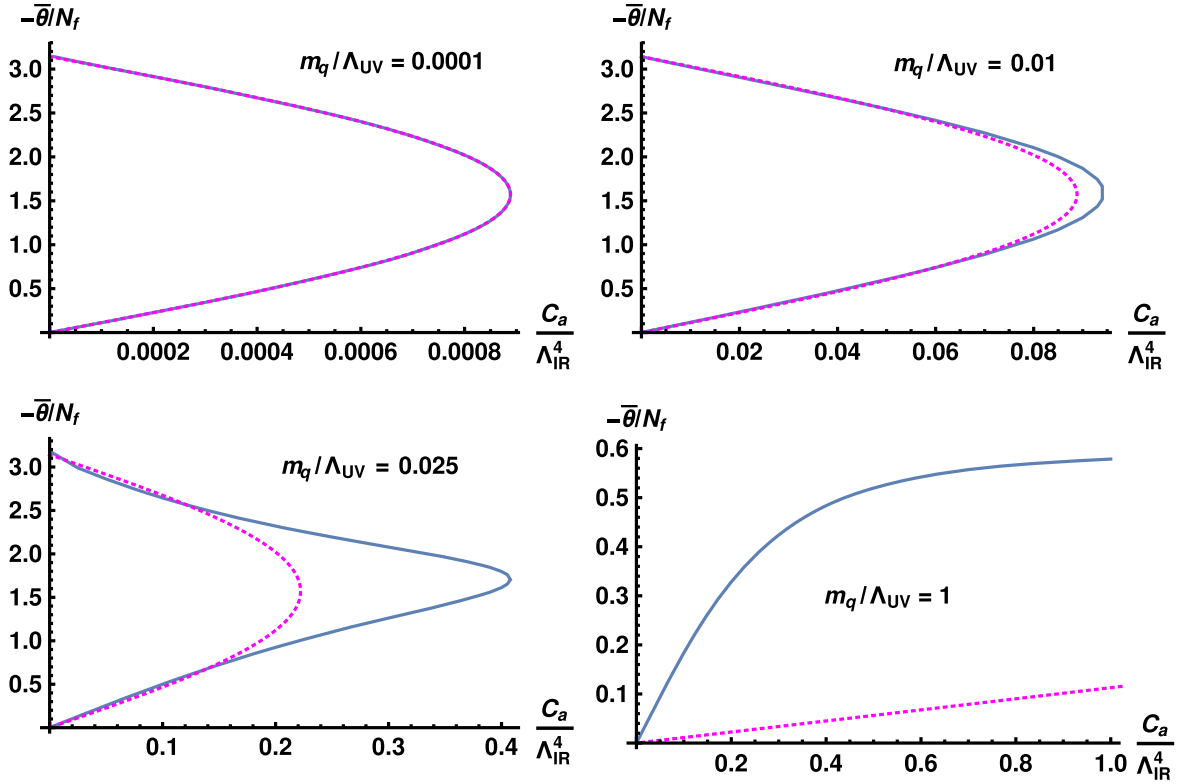

FIG. 5. The dependence of the (gauge invariant) $\bar{\theta}$ angle on C_a for the QCD-like potentials I at $x = 2/3$ and for various fixed values of the quark mass as indicated in the plots. The blue curves are numerical data, and the dotted magenta curves are determined by the analytic approximation at small m_q from (6.24).

plot without returning to the horizontal axis, which leads to the solutions being found only for a finite[8] range of $\bar{\theta}$. We also show the analytic small m_q approximation [given below in (6.24)] as dashed magenta curves. The value $m_q/\Lambda_{UV} = 1$ is so large already that the small m_q result does not work even as a rough approximation. If the value of m_q is increased further the plot will remain essentially unchanged.

In Fig. 6 we study numerically the holographic RG flow of the field $\tilde{\mathfrak{a}} = \mathfrak{a} + x\xi V_a$ which is invariant under the $U(1)_A$ transformation (2.18). The field vanishes in the IR due to the boundary condition $\tilde{\mathfrak{a}}(\infty) = \mathfrak{a}(\infty) = 0$, and its

[8]Notice that this is the case only for a single branch of solutions, which are connected by continuous deformations of the parameters. As argued in Sec. II, there are also disconnected branches which realize the 2π periodicity of $\bar{\theta}$, an taking them into account solutions are found for all values of $\bar{\theta}$.

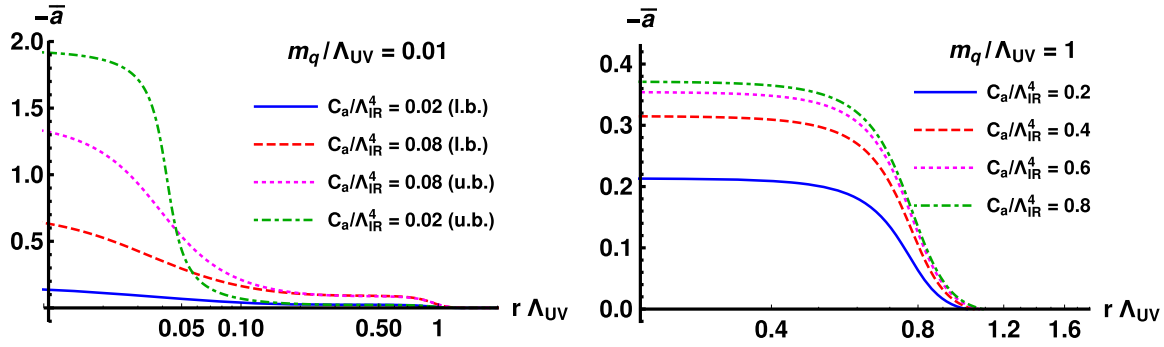

FIG. 6. The holographic RG flow of the gauge invariant field $\bar{\mathfrak{a}}$ for potentials I at $x = 2/3$. Left: $\bar{\mathfrak{a}}(r)$ at $m_q/\Lambda_{UV} = 0.01$. The solid blue and dot-dashed green curves have $C_a/\Lambda_{IR}^4 = 0.02$, while the dashed red and dotted magenta curves have $C_a/\Lambda_{IR}^4 = 0.08$. The solid blue and dashed red curves are for the lower branch (as denoted by "l.b." in the legend) in the top right plot of Fig. 5, while the dotted magenta and dot-dashed green curves are for the upper branch (denoted by "u.b." in the legend). Right: $\bar{\mathfrak{a}}(r)$ at $m_q/\Lambda_{UV} = 1$. The solid blue, dashed red, dotted magenta, and dot-dashed green curves have $C_a/\Lambda_{IR}^4 = 0.2$, 0.4, 0.6, and 0.8, respectively.

boundary value is $\bar{\mathfrak{a}}_0 = \bar{\theta}/N_c$. For the left-hand plot we have picked four points from the curve in the top right plot of Fig. 5 at $m_q/\Lambda_{UV} = 0.01$, which have pairwise the values $C_a/\Lambda_{IR}^4 = 0.02$ and $C_a/\Lambda_{IR}^4 = 0.08$ but are on different branches of the curve. The flow of $\bar{\mathfrak{a}}$ is determined by (6.3). When $m_q/\Lambda_{UV} \ll 1$, the two integrals in this equation affect the flow at different scales of r, which can also be seen from Fig. 6. The first integral is the only finite term in the probe limit $x \to 0$. It adds a contribution to the flow at $r \sim 1/\Lambda_{UV}$, which is roughly proportional to C_a. Indeed the curves having the same C_a overlap in Fig. 6 (left) when $r \sim 1/\Lambda_{UV}$. The second integral is the flavor contribution which affects the flow mostly at $r \sim \sqrt{m_q/\sigma}$. This term is dominant at small r in the plot, and results in a different flow for the curves which have the same C_a but different branch. We will see in Sec. VI D that this structure is analytically tractable in the limit $m_q \to 0$. Also, one can show that the flow on the upper branch of Fig. 5 approaches a step function as $C_a \to 0$ (see Appendix C) and indeed the flow at $C_a/\Lambda_{IR}^4 = 0.02$ (dot-dashed green curve) in the left-hand plot of Fig. 6 is already reminiscent of a step function. In the right-hand plot of Fig. 6 we plot $\bar{\mathfrak{a}}(r)$ for $m_q/\Lambda_{UV} = 1$ and for various values of C_a. In this case the RG flow is significant only for $r \sim 1/\Lambda_{UV}$. One can check that the first integral in (6.3) dominates.

B. Free energy and topological susceptibility

We analyzed above the contribution to the free energy from the CP-odd action S_a. However, the dependence of the free energy density on $\bar{\mathfrak{a}}_0$ is not fully captured by this contribution when x is nonzero. This is the case because S_f depends on the derivative of the phase, ξ', whose source varies as $\bar{\mathfrak{a}}_0$ is varied. Therefore, we need to study the full energy density. This can be done quite simply since we only allow a variation of $\bar{\mathfrak{a}}_0$ while keeping the other sources (in particular m_q and Λ_{UV}) fixed. In this case we can read from (3.20) that

$$\delta\mathcal{E} = -M^3 N_c^2 C_a \delta\bar{\mathfrak{a}}_0 = -M^3 N_c C_a \delta\bar{\theta}. \tag{6.8}$$

Notice that this result is valid for any value of $\bar{\mathfrak{a}}_0$. Since the integral in (6.7) is positive, $\bar{\mathfrak{a}}_0 = 0$ is the only minimum of the energy (for the branch of solutions continuously connected to $\bar{\mathfrak{a}}_0 = 0$).

We may write the relation (6.7) as

$$-M^3 C_a = G_\chi(\bar{\theta})\bar{a}_0 = \frac{G_\chi(\bar{\theta})\bar{\theta}}{N_c} \tag{6.9}$$

where

$$G_\chi(\bar{\theta}) = M^3\left[\int_0^\infty dr\left(\frac{1}{e^{3A}Z} + x f_a V_a\right)\right]^{-1}. \tag{6.10}$$

The topological susceptibility (generalized to nonzero $\bar{\theta}$) therefore becomes, in terms of G_χ,

$$\chi(\bar{\theta}) \equiv \bar{\mathcal{E}}''(\bar{\theta}) = G_\chi(\bar{\theta}) + \bar{\theta} G_\chi'(\bar{\theta}) \tag{6.11}$$

where we used (6.8) and (6.10).

For small $\mathfrak{a}_0$ integrating (6.8) gives

$$\bar{\mathcal{E}}(\bar{\theta}) - \bar{\mathcal{E}}(0) = \frac{1}{2}N_c^2 \chi \bar{\mathfrak{a}}_0^2 + \mathcal{O}(\bar{\mathfrak{a}}_0^4) = \frac{1}{2}\chi\bar{\theta}^2 + \mathcal{O}(\bar{\theta}^4), \tag{6.12}$$

where $\chi = \chi(\bar{\theta} = 0) = G_\chi(\bar{\theta} = 0)$. We denote the energy in (6.12) by $\bar{\mathcal{E}}$ rather than $\mathcal{E}$ in order to stress that it is the energy of the configuration obtained from the solution at $\bar{\theta} = 0$ by continuously varying $\bar{\theta}$. In order to determine the final free energy in the dominant vacuum, $\mathcal{E}$, we will need to take into account the other branches of solutions.

We plot the topological susceptibility for potentials I at $x = 2/3$ as a function of the quark mass at $\bar{\theta} = 0$ in Fig. 7 and as a function of $\bar{\theta}$ at fixed m_q in Fig. 8. The magenta curves are given by the small m_q approximation which will

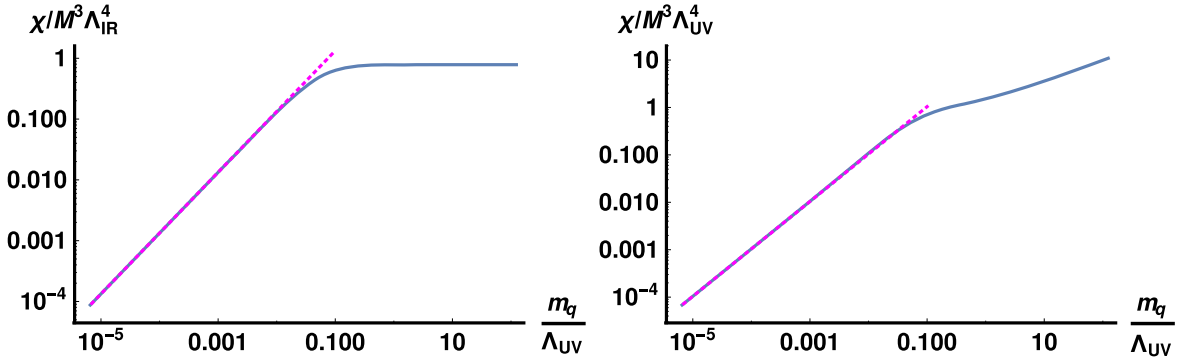

FIG. 7. The dependence of the topological susceptibility on the quark mass in IR units (left-hand plot) and in UV units (right-hand plot) in the standard, dominant vacuum for potentials I with $x = 2/3$. The units were discussed in Sec. II B and they are defined in terms of the asymptotic expansions of Appendix A. The blue solid curves are numerical data and the dashed magenta curves follow the approximation at small m_q given in Eq. (6.29).

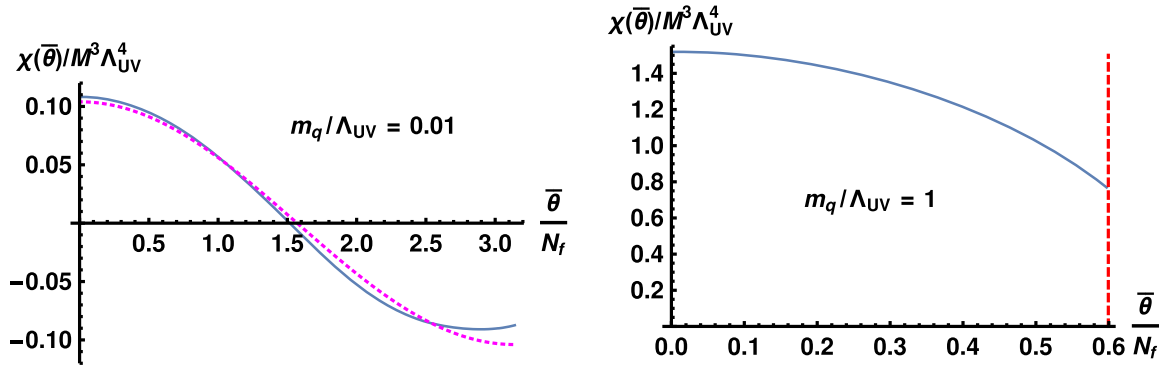

FIG. 8. The dependence of χ on the $\bar{\theta}$ angle for small (left-hand plot) and relatively large (right-hand plot) quark mass for potentials I with $x = 2/3$. On the left-hand plot, the magenta curve is given by (6.28). The dashed red vertical line denotes the limiting value of the $\bar{\theta}$ angle as $C_a \to -\infty$ along the curve of the fixed mass value.

be discussed in Sec. VI D and matches with effective field theory (this curve lies above the range of the plot in the right-hand plot of Fig. 8). We also notice that the susceptibility in IR units shown in Fig. 7 (left) approaches a constant value at large m_q. This signals the decoupling of quarks, and the value is that of the YM limit (i.e. IHQCD), which can be seen as follows. As the quark mass grows, the tachyon is sizeable except for a short interval up to $r \simeq 1/m_q$ in the UV. Outside this interval, the exponential behavior of the potential V_a suppresses the second term in the integrand in (6.10). Therefore the second term is suppressed, and the leading contribution arises from the first term, which has the same functional form as the expression for χ in IHQCD [35]. Because this integral is dominated in the IR where the background approaches smoothly the YM (or IHQCD) background as the quark mass grows [55], the result for χ in this limit agrees with that of YM.

A comparison of the two plots in Fig. 7 at large mass shows that χ only approaches a constant value when measured in IR units, which signals the fact that Λ_{UV} and Λ_{IR} are different at large quark mass as we now explain. The difference between these two scales might be surprising, since a large mass decouples the quarks so that the low energy dynamics is that of the YM theory, which only has a single energy scale. The UV scale Λ_{UV} differs from Λ_{IR} because it is defined through the running of the 't Hooft coupling asymptotically in the UV where the quarks are not decoupled: the definition (A4) is not directly affected by the quark mass for any value of m_q. This can be seen explicitly in the UV expansions (A2)–(A3): for $r \ll 1/m_q$ the backreaction of the tachyon is suppressed, no matter how large m_q is. The relation between the energy scales can be found by requiring continuity between the YM and full QCD behavior of the coupling at $r \sim 1/m_q$, which leads to [55]

$$\frac{\Lambda_{UV}}{\Lambda_{IR}} \sim \left(\frac{m_q}{\Lambda_{UV}}\right)^{b_0/b_0^{YM}-1} = \left(\frac{m_q}{\Lambda_{UV}}\right)^{-2x/11}, \tag{6.13}$$

where b_0 and b_0^{YM} are the leading coefficients of the beta functions of QCD and YM theory, respectively. It was observed in [55] that observables such as the glueball masses and thermodynamic variables similarly approach their YM values in IR units at large m_q, and Λ_{IR} is therefore identified as the single energy scale of the YM theory.

Using $\chi \sim \Lambda_{IR}^4$ at large quark mass, together with the relation (6.13), gives the asymptotic large m_q behavior of χ:

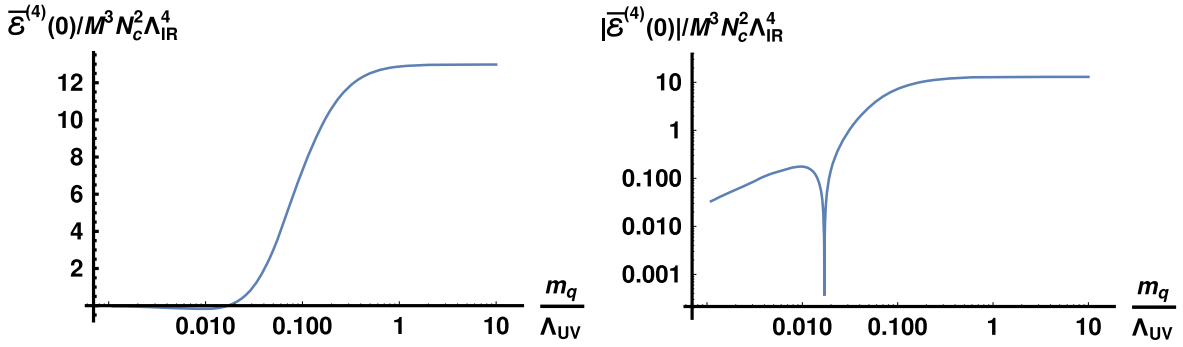

FIG. 9. The dependence of the fourth order derivative of the free energy at $\bar{\theta} = 0$ as a function of m_q for potentials I with $x = 2/3$. Left: linear scale. Right: logarithmic scale.

$$\frac{\chi}{\Lambda_{\mathrm{UV}}^4} \sim \left(\frac{m_q}{\Lambda_{\mathrm{UV}}}\right)^{4(1-b_0/b_0^{\mathrm{YM}})} = \left(\frac{m_q}{\Lambda_{\mathrm{UV}}}\right)^{8x/11}, \quad \left(\frac{m_q}{\Lambda_{\mathrm{UV}}} \gg 1\right). \tag{6.14}$$

We also show the m_q dependence of the fourth order coefficient in the expansion of the free energy around $\bar{\theta} = 0$ in Fig. 9. For $m_q/\Lambda_{\mathrm{UV}} \gg 1$, the coefficient approaches a constant in IR units, as was the case for topological susceptibility in Fig. 7. For small m_q the coefficient vanishes in accordance with effective field theory [11].

The free energy for solutions at finite $\bar{\mathfrak{a}}_0$ can be obtained by integrating the differential (6.8) numerically, using the dependence between C_a and $\bar{\mathfrak{a}}_0$ (or equivalently $\bar{\theta}/N_f$) given in Fig. 5. We present the results as a function of $\bar{\theta}/N_f$ at fixed quark mass in Fig. 10. The blue curves are numerical data and magenta dashed curves are given by the analytic result (6.26) at small m_q. We notice that the approximation works slightly better for the integrated energy than for the relation between the $\bar{\theta}$ angle and C_a of Fig. 5 where there is already significant deviation between the numerical data and the analytic approximation at $m_q/\Lambda_{\mathrm{UV}} = 0.025$.

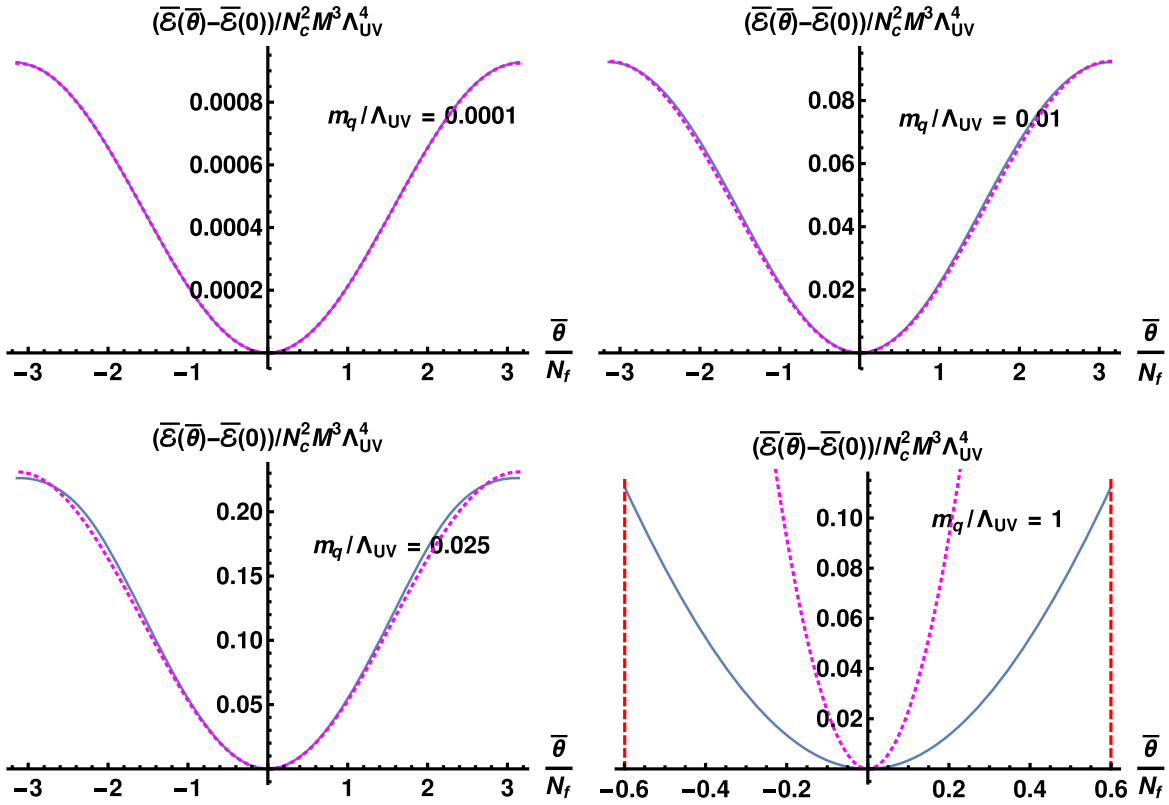

FIG. 10. The dependence of the free energy on the $\bar{\theta}$ angle for potentials I at $x = 2/3$ and for various fixed values of the quark mass as indicated in the plots. (Notation as in Fig. 5). The dashed red vertical lines denote the limiting values of the $\bar{\theta}$ angle as $C_a \to \pm\infty$ along the curve of the fixed mass value.

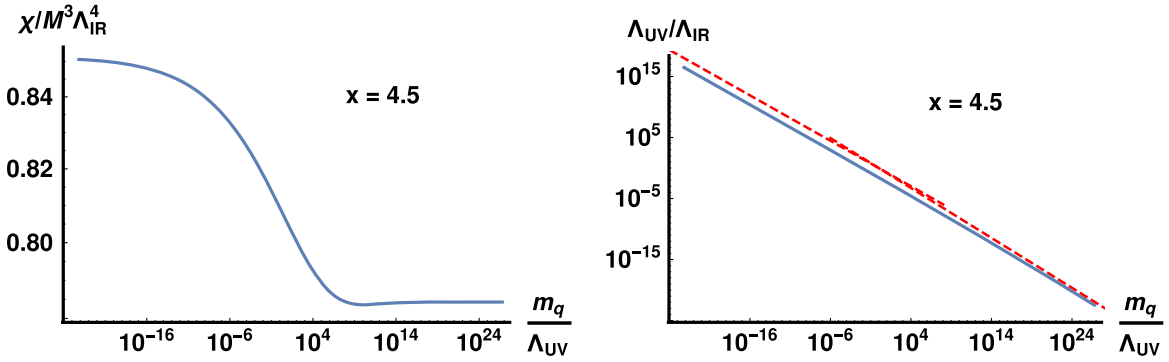

FIG. 11. Conformal window, $x = 4.5$. Left: dependence of the topological susceptibility on the quark mass in IR units for potentials I. Right: ratio $\Lambda_{\rm UV}/\Lambda_{\rm IR}$ as a function of the quark mass (blue solid curve). The red dashed lines show the scaling relations (6.17) and (6.13) at small and large quark masses, respectively.

The numerical result agrees with the generic argument presented above: the energy is minimized at $\bar{\theta} = 0$ for each value of the quark mass. For very small m_q there are also additional Efimov vacua, which we will discuss more in Sec. VI E and in Appendix C, and argue that they are also subleading. The final expression for the energy is then obtained by taking into account the periodicity of the theta angle (see Sec. II and [33]):

$$\mathcal{E}(\bar{\theta}) = \min_{k\in\mathbb{Z}} \bar{\mathcal{E}}\left(\frac{\bar{\theta}+2\pi k}{N_f}\right). \tag{6.15}$$

When writing down the last expression we recalled that for a single branch the free energy is naturally a function of $\bar{\mathfrak{a}}_0 = \bar{\theta}/N_f$. Therefore the derivatives with respect to this variable are of the same order as the function, $\mathcal{O}(N_c^2)$. We have found that the global minimum of $\bar{\mathcal{E}}$ is $\bar{\mathcal{E}}(0)$, so (6.15) is minimized for some k which satisfies approximately $k \simeq -\bar{\theta}/2\pi$. Then the argument of $\bar{\mathcal{E}}$ in (6.15) is $\mathcal{O}(1/N_f)$: there is always some value of k such that $|\bar{\theta}+2\pi k| \leq \pi$. Therefore we may apply Taylor expansion for $\bar{\mathcal{E}}$ around the origin, which gives the final result for the free energy

$$\mathcal{E}(\bar{\theta}) = \bar{\mathcal{E}}(0) + \frac{1}{2}\chi \min_{k\in\mathbb{Z}}(\bar{\theta}+2\pi k)^2 \tag{6.16}$$

in the Veneziano limit. Here we recalled that the second derivative of $\bar{\mathcal{E}}$ is the topological susceptibility. The result is similar in form to that obtained in the 't Hooft limit [33].

C. Dependence on x and hyperscaling

Above we restricted ourselves to the QCD-like regime with $x = \mathcal{O}(1)$, but it is also interesting to study the vacua as a function of x.

It was found [48,55] that there is a BKT-type transition at some $x = x_c$ between the QCD-like phase and the conformal window as x varies (at zero temperature). In the QCD phase, the vacua with nontrivial tachyon and zero quark mass (corresponding to the crosses of Fig. 3) only exist in the chirally broken phase where one of them is the energetically favored vacuum.

On the other hand, in the conformal window ($x_c < x < 11/2 = x_{\rm BZ}$), the picture is much simpler. At zero $\bar{\theta}$, there is no spontaneous chiral symmetry breaking and the quark mass grows monotonically with T_0. When $\bar{\theta}$ is nonzero, the situation is similar: in Fig. 3 the nodes on the horizontal axis are absent and the quark mass grows monotonically with T_0 for fixed C_a.

The topological susceptibility in the conformal window ($x = 4.5$) is shown for the QCD-like potentials I in Fig. 11 (left). For large quark mass, $m_q/\Lambda_{\rm UV} \gg 1$, the susceptibility approaches the YM value as was the case in the QCD-like phase $0 < x < x_c \simeq 4.083$. Consequently, the susceptibility in UV units obeys (6.14) in this limit. When $m_q/\Lambda_{\rm UV} \to 0$ the susceptibility also approaches a finite, nonzero value in IR units. This is in agreement with earlier observations that mass gaps and decay constants are of order $\Lambda_{\rm IR}$ for small m_q in the conformal window [55]. Note that the vertical axis of the plot does not start from the origin, and the UV and IR limiting values are actually rather close.

Overall, the dependence of CP-odd observables on m_q is weak, when the observables are expressed in units of $\Lambda_{\rm IR}$. For example, the relation between the source $\bar{\theta}$ and the VEV C_a is similar to that of the bottom-right plot of Fig. 5 for all values of m_q. The relation is determined by the IR behavior of the solutions of the various fields which are weakly dependent on m_q. While most observables are therefore proportional to the scale $\Lambda_{\rm IR}$, the ratio $\Lambda_{\rm UV}/\Lambda_{\rm IR}$ depends strongly on the quark mass as shown in Fig. 11 (right). The ratio obeys different power laws for $m_q/\Lambda_{\rm UV} \ll 1$ and $m_q/\Lambda_{\rm UV} \gg 1$, given in (6.17) and (6.13), respectively, and shown as red dashed lines in Fig. 11 (right).

The hyperscaling relation (see [72]) for χ can be found by taking into account the dependence of the scales on m_q in the limit of small m_q,

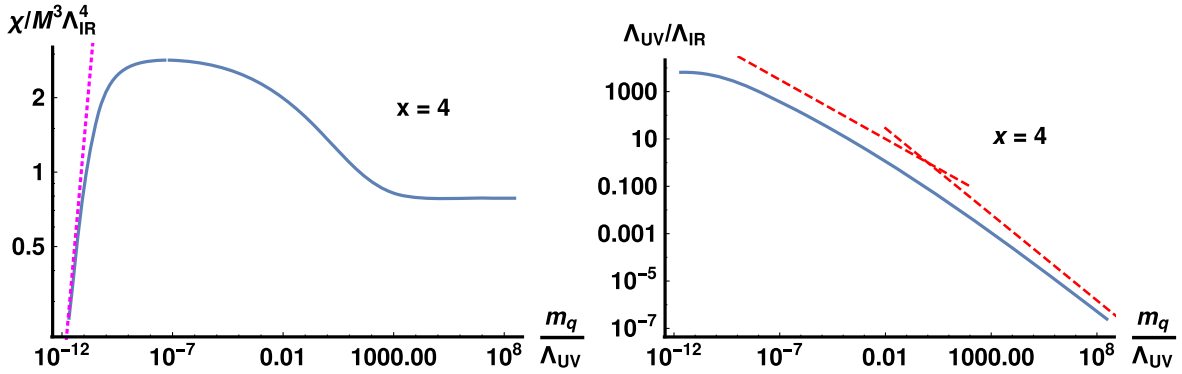

FIG. 12. Walking regime, $x = 4$. Left: dependence of the topological susceptibility on the quark mass in IR units for potentials I. The dashed magenta curve is given by the approximation at small m_q given in Eq. (6.29). Right: ratio $\Lambda_{\rm UV}/\Lambda_{\rm IR}$ as a function of the quark mass (blue solid curve). The red dashed lines show the scaling relations (6.17) (with $\Delta_* = 2$) and (6.13) at intermediate and large quark masses, respectively.

$$\frac{\Lambda_{\rm IR}}{\Lambda_{\rm UV}} \sim \left(\frac{m_q}{\Lambda_{\rm UV}}\right)^{\frac{1}{\Delta_*}}, \tag{6.17}$$

where Δ_* is the dimension of the quark mass at the IR fixed point [55]. Because $\chi \sim \Lambda_{\rm IR}^4$,

$$\frac{\chi}{\Lambda_{\rm UV}^4} \sim \left(\frac{m_q}{\Lambda_{\rm UV}}\right)^{\frac{4}{\Delta_*}} \sim \left(\frac{m_q}{\Lambda_{\rm UV}}\right)^{\frac{4}{1+\gamma_*}}, \qquad \left(\frac{m_q}{\Lambda_{\rm UV}} \ll 1\right) \tag{6.18}$$

where γ_* is the anomalous dimension of the quark mass at the fixed point.

We then discuss the phase diagram near the conformal transition and, in particular, in the regime with walking behavior ($x_c - x \ll 1$). As we have already pointed out, the diagram of Fig. 3 has nodes for all x within the interval $0 < x < x_c$. However, they approach the dashed line where the solution ceases to exist as $x \to x_c$ from below.

We demonstrate the approach to $x = x_c$ by studying numerically the topological susceptibility in the dominant vacuum. It is shown at $\bar{\theta} = 0$ as a function of the quark mass in Fig. 12 (left). We chose $x = 4$, which is close to the critical value $x_c \simeq 4.083$ for the potentials I used here. Three separate regimes can be identified as the quark mass varies. For very small[9] m_q, the topological susceptibility is proportional to m_q and obeys the relation (6.29) as in the QCD-like phase. In the intermediate regime, the topological susceptibility is close to the constant value associated with the IR CFT (that is approached in the walking region). Finally, for large m_q, $\chi/\Lambda_{\rm IR}^4$ approaches the constant value associated with the QCD-like IR regime. In contrast, for lower values of x, far from the walking regime, the topological susceptibility (see the left plot in Fig. 7) contains only the first and third regimes above, while the intermediate regime is (not surprisingly) absent.

The dependence of the ratio $\Lambda_{\rm UV}/\Lambda_{\rm IR}$ on $m_q/\Lambda_{\rm UV}$ is shown in Fig. 12. We observe that the ratio takes a finite value in the limit $m_q \to 0$, as in the QCD-like phase, and shows similar behavior to the conformal window in the intermediate and large m_q regimes. In particular, the scaling relation (6.17) with $\Delta_* = 2$ [55] (shown as the dashed red line at intermediate quark masses), is consistent with the numerical results. Consequently, we obtain a hyperscaling-like relation

$$\chi/\Lambda_{\rm UV}^4 \propto (m_q/\Lambda_{\rm UV})^2 \tag{6.19}$$

in the intermediate regime.

In summary, the dependence of the topological susceptibility (and the *CP*-odd physics in general) on x and m_q is qualitatively similar to that obtained for other observables (such as meson masses) at $\bar{\theta} = 0$; see Fig. 2 in [55].

D. The chiral limit and comparison to effective field theory

The solutions for the *CP*-odd fields can be studied analytically at small m_q, i.e. in the vicinity of the nodes of Fig. 3 (left). As shown in Sec. III B 1, in the UV, the complex tachyon satisfies the linearized Eq. (3.13), where C_a does not appear explicitly. In particular, that equation has the same form as the equation for the (real) tachyon at zero $\bar{\theta}$ angle or equivalently at zero C_a. The UV boundary data for the complex tachyon (but not necessarily for its absolute value and its phase) is expected to behave smoothly as the IR boundary conditions are varied. For small m_q (that is for $m_q/\Lambda_{\rm UV} \ll \sigma_0/\Lambda_{\rm UV}^3$), we may therefore write the asymptotic solution as

$$\frac{1}{\ell}\tau e^{i\xi} \simeq e^{i\xi_0} m_q r(-\log(\Lambda r))^{-\rho} + \sigma_0 r^3(-\log(\Lambda r))^{\rho}, \tag{6.20}$$

[9]As shown in [55], the boundaries between the three regimes are roughly at $m_q \sim \Lambda_{\rm UV}\exp(-2\hat{K}/\sqrt{x_c - x})$ with $\hat{K}$ given in (2.32), and at $m_q \sim \Lambda_{\rm UV}$.

where σ_0 is the real valued VEV for the standard solution at $m_q = 0$, and we neglected $\mathcal{O}(m_q)$ corrections to the VEV term.[10]

Recall that (6.20) is not gauge invariant: in particular ξ_0, or equivalently the phase of the quark mass, transforms under $U(1)_A$. So far we have not worried about gauge dependence, because we were mostly using gauge invariant variables, but it is convenient to fix the gauge now. We do this by requiring that the tachyon phase vanishes in the IR, $\xi \to 0$ as $r \to \infty$. This makes sense even when working with the UV expansions, because the phase ξ only varies significantly in the UV region when the quark mass is small. That is, the tachyon is real up to $\mathcal{O}(m_q)$ corrections in the IR region for this gauge choice. Continuity at $r \sim 1/\Lambda_{\rm IR}$ implies the VEV term of the tachyon and σ_0 are real up to $\mathcal{O}(m_q)$ corrections.

Inserting the phase and absolute value from (6.20) in the phase equation of (3.11) we find that

$$C_a = -2m_q\sigma_0\kappa_0 W_0 \ell^5 \sin\xi_0 + \mathcal{O}(m_q^2). \tag{6.21}$$

Moreover, for the current gauge choice (6.7) implies

$$\bar{\mathfrak{a}}_0 = x\xi_0 - C_a \int_0^\infty dr \left(\frac{1}{e^{3A} Z} + x f_a (V_a - 1) \right), \tag{6.22}$$

where the second term vanishes as $m_q \to 0$ [because $C_a \to 0$ in this limit as seen from (6.21)]—the possible singular contributions from f_a near the tachyon nodes are regulated by the factor $1 - V_a$ which also vanishes at the nodes. Therefore we find

$$\bar{\theta} = N_c \bar{\mathfrak{a}}_0 = N_f \xi_0 + \mathcal{O}(m_q). \tag{6.23}$$

Notice, however, that the first term in (6.22) vanishes as $x \to 0$—the integral which we dropped is actually much smaller than the term $x\xi_0$ if $x \gg m_q\sigma/\Lambda_{\rm IR}^4$. That is, the limits $x \to 0$ and $m_q \to 0$ do not commute. We will take $x = \mathcal{O}(1)$ first and return to the case of small x below.

1. Limit of small m_q for $x = \mathcal{O}(1)$

The relation between the VEV C_a and the source $\bar{\theta}$ becomes

$$C_a = -2m_q\sigma_0\kappa_0 W_0 \ell^5 \sin\frac{\bar{\theta}}{N_f} + \mathcal{O}(m_q^2). \tag{6.24}$$

The free energy at small, constant m_q can be then obtained[11] by integrating (6.8):

$$\bar{\mathcal{E}}(\bar{\theta}) - \bar{\mathcal{E}}(0) = 2N_c N_f M^3 m_q \sigma_0 \kappa_0 W_0 \ell^5 \left(1 - \cos\frac{\bar{\theta}}{N_f}\right) + \mathcal{O}(m_q^2) \tag{6.25}$$

$$= -\langle\bar{\psi}\psi\rangle|_{m_q=0} \left(1 - \cos\frac{\bar{\theta}}{N_f}\right) m_q + \mathcal{O}(m_q^2). \tag{6.26}$$

Here we recall that the proportionality constant between the VEV σ_0 and the chiral condensate (for the standard solution at $m_q = 0$) is $-2N_c N_f M^3 \kappa_0 W_0 \ell^5$ [45,55]. The same result is also found by using chiral effective Lagrangians in the limit of small m_q [10,11] (see also the review [14]).

The (generalized) topological susceptibility reads

$$\chi(\bar{\theta}) = -M^3 N_c \frac{dC_a}{d\bar{\theta}} = \frac{2M^3 m_q \sigma_0 \kappa_0 W_0 \ell^5}{x} \cos\frac{\bar{\theta}}{N_f} + \mathcal{O}(m_q^2) \tag{6.27}$$

$$= -\frac{\langle\bar{\psi}\psi\rangle|_{m_q=0}}{N_f^2} m_q \cos\frac{\bar{\theta}}{N_f} + \mathcal{O}(m_q^2). \tag{6.28}$$

Taking here $\bar{\theta} \to 0$ we obtain

$$\chi = \chi(\bar{\theta} = 0) = -\frac{\langle\bar{\psi}\psi\rangle|_{m_q=0}}{N_f^2} m_q + \mathcal{O}(m_q^2), \tag{6.29}$$

which agrees with the well-known field theory result [4,18]. The estimates (6.24)–(6.26) were compared to numerical data in Figs. 5–10 where they give the dotted magenta curves.

2. Limit of small m_q for any x

Notice that because the condensate is $\mathcal{O}(N_f N_c)$, (6.29) diverges for $x \to 0$. This signals the breakdown of the small m_q approximation. As we pointed out above, the limits $m_q \to 0$ and $x \to 0$ do not commute. This reflects properties of QCD: when $x \to 0$ the axial anomaly is effectively suppressed, the η' meson becomes light, and must also be taken into account when analyzing the physics.

From (6.11) and (6.10) we see that the susceptibility approaches its YM value $\chi_{\rm YM}$ (defined in IR units as explained above) as $x \to 0$. Working directly with this equation we can obtain an improved estimate:

[10] One can check that σ_0 is related to σ (which was defined in terms of the UV expansion of the absolute value τ) as $\sigma\cos\xi_0 = \sigma_0 + \mathcal{O}(m_q)$, and to the complex VEV defined in (3.14) as $e^{i\xi_0}\hat{\sigma} = \sigma_0 + \mathcal{O}(m_q)$.

[11] We are working around the standard solution, the rightmost cross of Fig. 3, so that the integration starts from $\bar{\theta} = 0$.

$$\chi^{-1} = \chi_{\rm YM}^{-1} - \frac{N_f^2}{\langle\bar\psi\psi\rangle|_{m_q=0} m_q}(1+\mathcal{O}(m_q)). \tag{6.30}$$

This expression is valid at small m_q but for all values of x (within the QCD like regime, $0 < x < x_c$) and agrees with chiral perturbation theory [78] (see also Sec. V).

We can also derive formulas for the free energy which are valid for all values of x. Namely, as we pointed out above, the integral in (6.22) is only relevant when x is small. But in this regime its second term is suppressed, and the first term is related to the YM topological susceptibility, so that we find[12]

$$\frac{\bar\theta}{N_f} = \xi_0 - M^3 C_a x^{-1} \chi_{\rm YM}^{-1} + \mathcal{O}(m_q) \tag{6.31}$$

whereas the relation (6.21) is unchanged and therefore implies

$$\begin{aligned} M^3 N_f N_c C_a &= \langle\bar\psi\psi\rangle|_{m_q=0} m_q \sin\xi_0 + \mathcal{O}(m_q^2) \\ &= N_f^2 \chi_{\rm YM}\left(\xi_0 - \frac{\bar\theta}{N_f}\right) + \mathcal{O}(m_q^2). \end{aligned} \tag{6.32}$$

We then compare to effective field theory results [11] given explicitly in Sec. V. Identifying the phase ϕ and the coupling a (introduced in Eqs. (5.21) and (5.26) respectively) as $\phi = \xi_0$ and

$$\frac{a}{m_\pi^2} = -\frac{N_f N_c \chi_{\rm YM}}{\langle\bar\psi\psi\rangle|_{m_q=0} m_q}, \qquad a = \frac{N_c \chi_{\rm YM}}{\hat f_\pi^2}, \tag{6.33}$$

where the latter form follows after the use of Gell-Mann-Oakes-Renner relation, the above conditions (6.32) match with (5.1) up to corrections suppressed by m_q. Moreover, imposing these conditions the differential (6.8) integrates to

$$\begin{aligned} \bar{\mathcal{E}}(\bar\theta) - \bar{\mathcal{E}}(0) &= -\langle\bar\psi\psi\rangle|_{m_q=0} m_q (1-\cos\xi_0) \\ &\quad + \frac{\chi_{\rm YM}}{2}(N_f\xi_0 - \bar\theta)^2 + \mathcal{O}(m_q^2) \end{aligned} \tag{6.34}$$

which agrees with the potential (5.33) with the above identifications.

We also remark that the solutions to the last equality in (6.32), i.e., $\xi_0(\bar\theta)$, are unique only when $|\langle\bar\psi\psi\rangle|_{m_q=0} m_q| \le N_f^2 \chi_{\rm YM}$. When this condition is violated, $\xi_0(\bar\theta)$ has several branches, which is the case for $x \ll m_q/\Lambda_{\rm UV}$. Because the condensate is negative these branches first appear near $\xi = (2n+1)\pi = \bar\theta/N_f$ as x decreases, where n is an arbitrary integer.

Finally, while we wrote the above formulas around the standard vacuum, i.e. the rightmost cross of Fig. 3, they hold also in the vicinity of other points with $m_q = 0$ (the Efimov vacua) with minor changes. That is, we need to interpret σ_0 and $\langle\bar\psi\psi\rangle$ as the values of the corresponding $m_q = 0$ solutions. In addition, the value of $\bar\theta$ should be chosen as depicted in Fig. 3 (right), so that the starting point of integration in (6.26) and (6.28) has also changed. For the susceptibility this results in a factor $(-1)^n$ in (6.29) near the nth Efimov vacuum:

$$\chi^{-1} = \chi_{\rm YM}^{-1} - \frac{(-1)^n N_f^2}{\langle\bar\psi\psi\rangle|_{n,m_q=0} m_q}(1+\mathcal{O}(m_q)), \tag{6.35}$$

where the chiral condensate is that of the nth Efimov vacuum at zero quark mass. The sign of the condensate is $-(-1)^n$ [48,55], so that both contributions to (the inverse of) χ are positive.

E. Complex Efimov spirals

It is possible to gain some analytic understanding of the structure of the solutions as the dashed line in Fig. 3 is approached where the theory flows closer and closer to the IR fixed point. That is, we can generalize the approach detailed in Sec. V of [55] to the case of nonzero C_a. First we briefly review the main points of the analysis at $C_a = 0$.

In the vicinity of the fixed point, when the BF bound is violated, the tachyon satisfies the linearized equation of motion, the solution of which can be written as a linear combination of

$$\frac{\tau_m}{\ell} \simeq \frac{m_q}{\Lambda_{\rm UV}} K_m (r\Lambda_{\rm UV})^2 \sin\left[\nu \log(r\Lambda_{\rm UV}) + \phi_m\right], \quad \left(\frac{1}{\Lambda_{\rm UV}} \ll r \ll \frac{1}{\Lambda_{\rm IR}}\right) \tag{6.36}$$

$$\frac{\tau_\sigma}{\ell} \simeq \frac{\sigma}{\Lambda_{\rm UV}^3} K_\sigma (r\Lambda_{\rm UV})^2 \sin\left[\nu \log(r\Lambda_{\rm UV}) + \phi_\sigma\right], \quad \left(\frac{1}{\Lambda_{\rm UV}} \ll r \ll \frac{1}{\Lambda_{\rm IR}}\right) \tag{6.37}$$

which have zero VEV and quark mass, respectively [the value of the quark mass and the VEV are determined by the continuation of the solutions to the UV boundary where (A6) holds]. Here $\Lambda_{\rm UV} \gg \Lambda_{\rm IR}$ since the flow becomes close to the fixed point, and the parameters ϕ_i and K_i are $\mathcal{O}(1)$ real numbers which can be determined by solving the tachyon equation of motion numerically. The parameter ν is the imaginary part of the dimension of the quark mass at the fixed point: $\nu = {\rm Im}\Delta_* = \sqrt{-m_{\tau*}^2 \ell_*^2 - 4}$, where $m_{\tau*}$ and ℓ_* are the (imaginary) bulk tachyon mass and the AdS radius

[12]The precise scaling limit which determines which terms we keep here is that $x\Lambda_{\rm UV}/m_q$ is fixed as $m_q \to 0$, but the expressions which we obtain will also remain valid for $x = \mathcal{O}(1)$ and $m_q \to 0$. Notice that the condensate is $\mathcal{O}(N_f N_c)$.

at the fixed point, respectively. The IR regular solution can be written in a similar form

$$\frac{\tau}{\ell} \simeq K_{\rm IR}(r\Lambda_{\rm IR})^2 \sin\left[\nu \log\left(r\Lambda_{\rm IR}\right) + \phi_{\rm IR}\right], \quad \left(\frac{1}{\Lambda_{\rm UV}} \ll r \ll \frac{1}{\Lambda_{\rm IR}}\right), \tag{6.38}$$

but in this case it helps to write the dimensionful quantities in IR units—then the $\mathcal{O}(1)$ parameters $K_{\rm IR}$ and $\phi_{\rm IR}$ take constant values as the fixed point is approached (i.e. as $T_0 \to T_{0c}$ from above) [55]. Expressing (6.38) as a linear combination of (6.36) and (6.37), one finds the spiral equations

$$\frac{m_q}{\Lambda_{\rm UV}} = \frac{K_{\rm IR}}{K_m}\frac{\sin\left(\phi_{\rm IR} - \phi_\sigma - \nu u\right)}{\sin\left(\phi_m - \phi_\sigma\right)} e^{-2u}$$
$$\frac{\sigma}{\Lambda_{\rm UV}^3} = \frac{K_{\rm IR}}{K_\sigma}\frac{\sin\left(\phi_{\rm IR} - \phi_m - \nu u\right)}{\sin\left(\phi_\sigma - \phi_m\right)} e^{-2u} \tag{6.39}$$

where the spiral is parametrized in terms of

$$u = \log\frac{\Lambda_{\rm UV}}{\Lambda_{\rm IR}}. \tag{6.40}$$

This kind of spiral structures is relatively common in holographic models, and has been studied in detail in a different context in [79].

There is a simple asymptotic relation between u and T_0. The IR geometry has a well-defined limit as the fixed point is approached, and the leading perturbation to the geometry is driven by the minimal distance to the fixed point [55]:

$$T_0 - T_{0c} \sim \lambda_* - \lambda_{\rm IR} \equiv \lambda_* - \lambda(r = 1/\Lambda_{\rm IR}) \sim \left(\frac{\Lambda_{\rm IR}}{\Lambda_{\rm UV}}\right)^{\delta}. \tag{6.41}$$

Here $r = 1/\Lambda_{\rm IR}$ is roughly the value of the coordinate where the growing tachyon field finally drives the flow away from the fixed point, and δ is the derivative of the holographic beta function at the fixed point, given by [48,55]

$$\delta = \sqrt{4 - \frac{9V_2\lambda_*^2}{V_0}} - 2. \tag{6.42}$$

The parameters V_i are defined though the expansion of the effective potential at the fixed point [48] as

$$V_{\rm eff}(\lambda) \equiv V_g(\lambda) - xV_{f0}(\lambda) = V_0 + V_2(\lambda - \lambda_*)^2 + \mathcal{O}((\lambda - \lambda_*)^3). \tag{6.43}$$

In terms of u, (6.41) becomes

$$u\delta \simeq -\log(T_0 - T_{0c}) + \text{const} \qquad (T_0 \to T_{0c}). \tag{6.44}$$

The spiral (6.39) admits a relatively simple generalization to nonzero $\bar{\theta}$ angle, as we will now show. It is natural to keep C_a in the IR units, i.e. $C_a/\Lambda_{\rm IR}^4$, fixed as $T_0 \to T_{0c}$. Using the UV expansions of Sec. III in the tachyon equation of motion we immediately see that the effect of finite C_a is suppressed in the UV by $\mathcal{O}(r^4)$. But one can derive a more general result which holds for all $r \ll 1/\Lambda_{\rm IR}$ and in particular near the fixed point. Namely, the equations (3.11) and (3.13) actually hold for all $r \ll 1/\Lambda_{\rm IR}$ as can be verified by inserting the behavior of the tachyon $\tau \sim r^2$ and the metric $e^A \sim 1/r$ near the fixed point in the generic equations of motion for the tachyon (3.10).

Since the complex tachyon therefore solves the same equation as the (real part of the) tachyon at $C_a = 0$, the solutions (6.36) and (6.37) are otherwise unchanged for $C_a \neq 0$, but m_q and σ should be replaced by their complex counterparts in (3.14):

$$m_q \mapsto m_q e^{i\xi_0}, \qquad \sigma \mapsto \hat{\sigma} e^{i\xi_0}. \tag{6.45}$$

Here $\hat{\sigma} = \sigma + iC_a/(2m_q\ell^5\kappa_0 W_0)$, with σ defined as the coefficient of the UV expansion of the absolute value of the tachyon in (3.17). This also means that the coefficients K_i and ϕ_i in these equations are real and independent of C_a and the $\bar{\theta}$ angle.

The flow of the tachyon in the IR (for $r \sim 1/\Lambda_{\rm IR}$), however, changes in a nontrivial manner. The tachyon is complex in the IR for generic C_a, and therefore the coefficients of (6.38) must be allowed to take complex values:

$$K_{\rm IR} \mapsto K_{\rm IR} e^{ik_{\rm IR}}, \qquad \phi_{\rm IR} \mapsto \phi_{\rm IR} + i\varphi_{\rm IR}, \tag{6.46}$$

and T_{0c} also depends on C_a. The result for the tachyon near the fixed point can be found by applying these maps to (6.38)

$$\frac{\tau e^{i\xi}}{\ell} \simeq K_{\rm IR} e^{ik_{\rm IR}} (r\Lambda_{\rm IR})^2 \{\cosh\varphi_{\rm IR} \sin[\nu \log(r\Lambda_{\rm IR}) + \phi_{\rm IR}] + i \sinh\varphi_{\rm IR} \cos[\nu \log(r\Lambda_{\rm IR}) + \phi_{\rm IR}]\}. \tag{6.47}$$

Finally, the spiral equations (6.39) generalize to

$$\frac{m_q e^{i\xi_0}}{\Lambda_{\rm UV}} = \frac{K_{\rm IR} e^{ik_{\rm IR}}}{K_m}\frac{\sin\left(\phi_{\rm IR} - \phi_\sigma - \nu u\right)\cosh\varphi_{\rm IR} + i\cos\left(\phi_{\rm IR} - \phi_\sigma - \nu u\right)\sinh\varphi_{\rm IR}}{\sin\left(\phi_m - \phi_\sigma\right)} e^{-2u}$$
$$\frac{\hat{\sigma} e^{i\xi_0}}{\Lambda_{\rm UV}^3} = \frac{K_{\rm IR} e^{ik_{\rm IR}}}{K_\sigma}\frac{\sin\left(\phi_{\rm IR} - \phi_m - \nu u\right)\cosh\varphi_{\rm IR} + i\cos\left(\phi_{\rm IR} - \phi_m - \nu u\right)\sinh\varphi_{\rm IR}}{\sin\left(\phi_\sigma - \phi_m\right)} e^{-2u}. \tag{6.48}$$

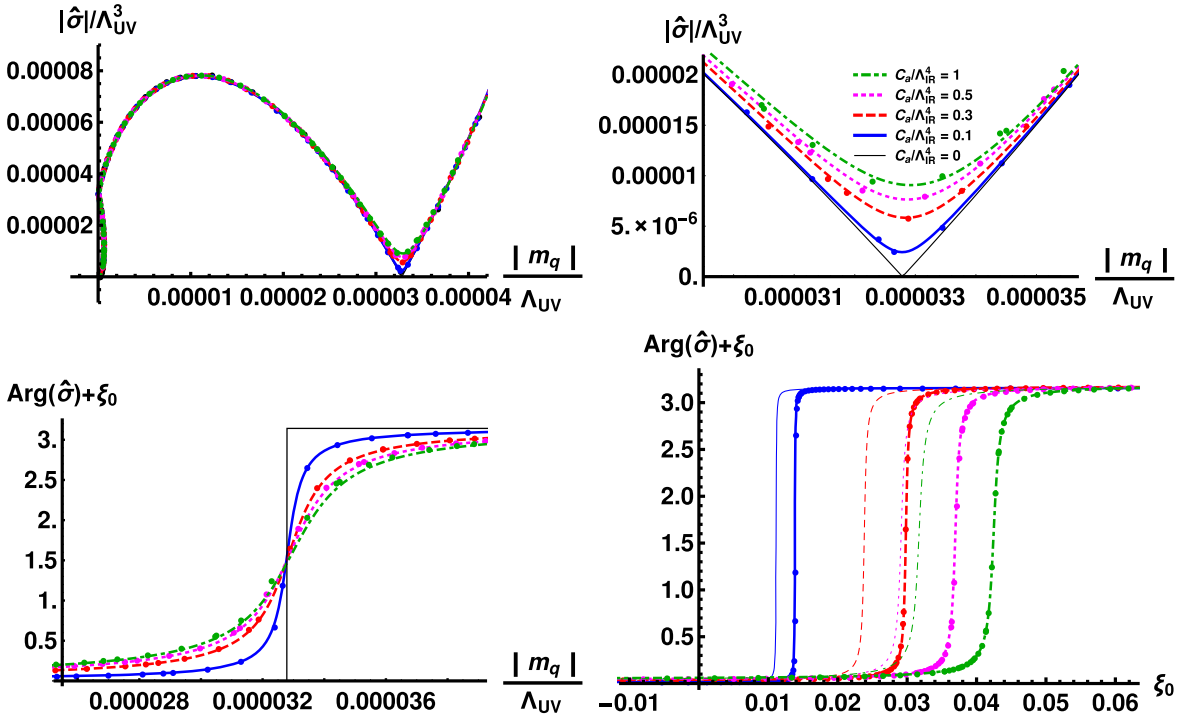

FIG. 13. Sections of the complex spiral compared with data for potentials I with $x = 2.5$. The thin black, solid blue, dashed red, dotted magenta, and dot-dashed green curves have $C_a/\Lambda_{\rm IR}^4 = 0, 0.1, 0.3, 0.5$, and 1, respectively. Top row: the absolute value of the quark mass and the condensate in two regions close to the origin of the spiral. Bottom row: the phase of the condensate in the same region as the absolute values in the top-right plot as a function of the absolute value of quark mass (left) and the phase of the quark mass (right).

These equations describe, among other things, the structure of the Efimov vacua near $C_a = 0$ as one approaches the dashed curved of Fig. 3 (left).

The equation for the phase in (3.11), $\xi' \simeq C_a/(\kappa V_{f0} e^{3A}\tau^2)$, leads to additional constraints. Inserting here the solution (6.47) or the combination of (6.36) and (6.37), recalling also the maps (6.45), gives the identities

$$\frac{C_a}{\ell_*^3 V_{f0}(\lambda_*)\kappa(\lambda_*)} = -\ell^2 K_{\rm IR}^2 \Lambda_{\rm IR}^4 \nu \cosh\varphi_{\rm IR} \sinh\varphi_{\rm IR} = \frac{C_a K_m K_\sigma \Lambda_{\rm UV}^4 \nu \sin(\phi_m - \phi_\sigma)}{2\kappa_0 W_0 \ell^3}. \quad (6.49)$$

Here the first identity constrains the C_a dependence of $K_{\rm IR}$ and $\varphi_{\rm IR}$. Equating the first and third term proves directly that $\sin(\phi_m - \phi_\sigma) > 0$, fixing the handedness of the spiral. It was pointed out in [55] that this sign is also necessary for the chirally broken vacua to dominate over the chirally symmetric vacuum.

We compare the asymptotic formulas (6.48) to numerical data for potentials I at $x = 2.5$ in Fig. 13. Since the formulas hold for small quark mass and the condensate, we plot a section of the spiral (for the absolute value of both the source and the VEV) very close to the origin, in the region where the tachyon solution has two nodes as $C_a \to 0$, so the solutions are identified as unstable (second) Efimov vacua. As it turns out, the C_a dependence is relatively mild, in particular the complex phase factor $\varphi_{\rm IR}$ remains numerically small for all values of C_a. Therefore our data and curves almost overlap as seen in the top-left plot. In order to see the dependence on C_a we zoom in the region of the top-left plot near the point where $|\hat{\sigma}|$ has a node for $C_a = 0$. The result is shown in the top-right plot. The data (dots) follows the prediction from the formulas (curves) well, even if the dependence on C_a is weak. Notice also that the various parameters of the curves in these plots were not fitted to the data but extracted directly from their definitions [e.g., in (6.47)].

The dependence on C_a can be seen more clearly in the plots on the bottom row of Fig. 13 where we show the phases of the source and the VEV in the same region as for the top-right plot. In the bottom-right plot, the curve for $C_a = 0$ is not shown because it has shrunk into a set of discrete points. For this plot, we fitted the value of the phase factor $k_{\rm IR}$ directly to the data. We did this rather than using the definition in (6.47) because the value of $k_{\rm IR}$ obtained from the definition appeared to be clearly shifted with respect to data—the spirals for these values of the phase are given by the thin curves in the plot. It is possible that this offset is a numerical effect—the construction of an IR regular tachyon solution close enough to the fixed point for it to properly obey the asymptotic formula (6.47) and the consequent four parameter fit to extract the numerical

values of the parameters is demanding due to limited numerical precision.

VII. SPECTRA OF SINGLET PSEUDOSCALAR BOUND STATES AT $\bar{\theta} = 0$

In order to compute the spectrum of mesons and glueballs one needs to study the fluctuations of all the fields of V-QCD. These fluctuations decouple into different sectors corresponding to glueballs and mesons with $J^{PC} = 0^{++}, 0^{-+}, 1^{++}, 1^{--}, 2^{++}$, where J stands for the spin and P and C for the field properties under parity and charge conjugation respectively. They can be further classified into two classes according to their transformation properties under the flavor group: flavor nonsinglet modes [expanded in terms of the generators of $SU(N_f)$] and flavor singlet modes.

The general analysis of the fluctuations for the model at vanishing $\bar{\theta}$ angle was carried out in [51]. There the quadratic action for each sector was computed, and the spectra for all but one sector were calculated numerically. In this section we will analyze the one sector left out in [51]: the flavor singlet pseudoscalar modes at vanishing $\bar{\theta}$ angle. We will restrict our study to the case $\bar{\theta} = 0$—this is the case which is closest to ordinary QCD, and at finite $\bar{\theta}$ solving the fluctuation equations would be technically very involved because the singlet scalar and pseudoscalar mesons and glueballs would all mix. This sector is made up of the pseudoscalar 0^{-+} flavor singlet meson and the 0^{-+} glueball which mix due to the axial anomaly (realized by the CP-odd sector). Since we are in the Veneziano limit, the mixing takes place at leading order in $1/N_c$. In the next section we will study the spectra for backgrounds at finite $\bar{\theta}$ angle, restricting the analysis to the flavor nonsinglet sector.

The masses of the singlet pseudoscalar states are particularly important, because they contain the physics of the η' meson, which is identified as the state with the lowest mass in this sector at small x. We will demonstrate, both analytically and numerically, that the mass of the η' meson obeys the Witten-Veneziano formula. Because of the backreaction, the pseudoscalar glueballs and mesons mix nontrivially already at small x, which affects the derivation of the Witten-Veneziano relation. We have not found a transformation (e.g., a rotation in the space of wave functions) which would remove this mixing, so we will need to study it carefully. Therefore our derivation is more involved than the typical arguments in the literature [40,42–44].

A. Pseudoscalar singlet fluctuations at $\bar{\theta} = 0$

We now write down the fluctuation equations for the pseudoscalar singlet sector. First, the vector and axial vector combinations of the gauge fields are

$$V_M = \frac{A_M^L + A_M^R}{2}, \qquad A_M = \frac{A_M^L - A_M^R}{2}. \tag{7.1}$$

They contribute to both the singlet and nonsinglet flavor sectors. Next we write the complex tachyon field as

$$T(x^\mu, r) = \tau(r) \exp\left[i\theta_T(x^\mu, r)\right], \tag{7.2}$$

where τ is the background solution, and θ_T is the pseudoscalar flavor singlet fluctuation.

The flavor singlet pseudoscalar degrees of freedom correspond to gauge invariant combinations of the longitudinal part of the flavor singlet axial vector fluctuation $A_\mu^{\|S}$, the pseudoscalar phase of the tachyon θ_T and the axion field a.

We split these fields as

$$\begin{aligned} A_\mu^{\|S}(x^\mu, r) &= -\varphi_L(r)\partial_\mu(\mathcal{T}(x^\mu)), \\ \theta_T(x^\mu, r) &= 2\varphi_\theta(r)\mathcal{T}(x^\mu), \\ a(x^\mu, r) &= 2\varphi_{\rm ax}(r)\mathcal{T}(x^\mu). \end{aligned} \tag{7.3}$$

The following combinations of the above fields

$$\begin{aligned} P(r) &\equiv \varphi_\theta(r) - \varphi_L(r), \\ Q(r) &\equiv \varphi_{\rm ax}(r) + xV_a(\lambda,\tau)\varphi_L(r), \end{aligned} \tag{7.4}$$

are invariant under the residual gauge transformations (2.18). They correspond to the pseudoscalar glueball (0^{-+}) and η' meson towers. They satisfy the coupled differential equations (see Appendix D and [51] for more details)

$$\begin{aligned} &\partial_r\left[V_f e^A G^{-1} w^2\left(-4e^{2A}\frac{V_f\kappa\tau^2}{N_a+N_b}P' + \frac{V_a'}{V_a}\frac{N_b}{N_a+N_b}P \right.\right. \\ &\left.\left. + \frac{N_b}{xV_a(N_a+N_b)}Q'\right)\right] \\ &+ 4V_f e^{3A} G\kappa\tau^2 P - 4e^{3A} Z V_a Q = 0, \end{aligned} \tag{7.5}$$

$$\begin{aligned} &\partial_r\left[e^{3A} Z\left(4xe^{2A}\frac{V_a V_f\kappa\tau^2}{N_a+N_b}P' + x\frac{V_a' N_a}{N_a+N_b}P + \frac{N_a}{N_a+N_b}Q'\right)\right] \\ &+ m^2 e^{3A} Z Q = 0, \end{aligned} \tag{7.6}$$

where the primes denote derivatives with respect to r, and N_a, N_b and G are given by the following expressions:

$$\begin{aligned} &N_a = V_f(4e^{2A}\kappa\tau^2 - m^2 w^2), \qquad N_b = 4xe^{2A} Z V_a^2 G, \\ &G = \sqrt{1 + e^{-2A}\kappa\tau'^2}. \end{aligned} \tag{7.7}$$

Notice that G is just the restriction of $\tilde{G}$ defined in (3.5) to the $\xi' = 0$ case.

B. Mass of the η' meson at small x

We start by discussing the probe limit $x \to 0$ at nonzero but small quark mass. Because the terms depending on

flavor are suppressed in the action, the fluctuation equations (7.5) and (7.6) admit solutions for which $P = \mathcal{O}(1)$, $Q = \mathcal{O}(x)$.[13] It is identified as the flavor mode at small x: to leading order in x, the P component satisfies the same fluctuation equation as the wave function for the nonsinglet pseudoscalar fluctuation described in [51]. More precisely, P is mapped to the difference $\psi_P - \psi_L$ of the radial wave function of the pion field and longitudinal gauge field as suggested by the definition (7.4), and the variable $\hat{P}$ defined in (D13) is mapped to $\hat{\psi}_P$.

Therefore one is led to expect that the flavor singlet and nonsinglet pseudoscalar mesons become degenerate as $x \to 0$. This is however not obvious since, as it turns out, the convergence towards the $x = 0$ solution is not uniform in r. In the IR there is no issue because the exponential suppression of the potentials V_f and V_a decouples the glue from the flavor for all values of x. In the UV, however, glue and flavor are nontrivially coupled at small r for any positive x (more precisely, when $r \ll \sqrt{x}$), as seen from the UV expansions in Appendix A.[14] In principle this could lead to the flavor singlet and nonsinglet mesons having different UV boundary conditions in the limit $x \to 0$ and the masses of the mesons being different. One can check by using the UV expansions from Appendix A that the boundary conditions are the same and therefore the singlet and nonsinglet states do become degenerate. In particular, η' becomes degenerate with the pions and its mass obeys the Gell-Mann-Oakes-Renner (GOR) relation as $x \to 0$ as expected from the fact that the anomaly vanishes when $x \to 0$. We will discuss this in more detail below.

1. Limit of zero x

We wish to discuss what happens at small but finite x, but it is useful to recall first how the GOR relation arises from the fluctuation equations in the limit of zero x. We rewrite the fluctuation equations (7.5) and (7.6) as a first order system (for later convenience first at finite x)

$$\hat{P} = \frac{e^{3A}}{m_f^2 - H_{PS}}[V_f \kappa \tau^2 G^{-1} P' - V_a Z(Q' + x V_a' P)], \tag{7.8}$$

$$\hat{Q} = \frac{e^{3A} Z}{m_f^2(m_f^2 - H_{PS})}\left[m_f^2(Q' + x V_a' P) - \frac{4e^{2A}\kappa\tau^2}{w^2}\frac{d}{dr}(Q + x V_a P)\right], \tag{7.9}$$

$$\hat{P}' = e^{3A}(V_a Z Q - G V_f \kappa \tau^2 P), \tag{7.10}$$

$$\hat{Q}' = -e^{3A} Z Q, \tag{7.11}$$

where

$$H_{PS} = \frac{4e^{2A}\kappa\tau^2}{w^2} + \frac{4e^{2A} x G V_a^2 Z}{V_f w^2}, \tag{7.12}$$

and m_f is the mass of the fluctuations.

As $x \to 0$ the fluctuations associated with the mesons satisfy (7.8) and (7.10) with Q and x set to zero and including only the first term in (7.12). These equations are the same as the fluctuation equations for the nonsinglet pseudoscalar mesons [51], which signals the suppression of the axial anomaly as $x \to 0$. The GOR relation is found by studying the fluctuation equations perturbatively at small m_f^2 and also taking $m_q \to 0$. When $m_f^2 = 0$ there is a solution to the system which is normalizable in the IR but not in the UV. As seen from the expansions (F14) and (F15) in Appendix A both P and $\hat{P}$ approach finite values at the boundary. It is convenient to normalize the solution such that $P \to 1$ as $r \to 0$. Then the boundary value of $\hat{P}$,

$$C_P \equiv \lim_{r\to 0} \hat{P}(r), \qquad (m_f^2 = 0) \tag{7.13}$$

can be related to the decay constant of the η' meson [up to corrections $\mathcal{O}(m_q)$]. The relation is analogous to that for the pion decay constant, found in Appendix E of [55]. Since we have taken $x = 0$ the decay constants of the pion and the η' are actually equal. After a careful comparison to the analysis of [55] we find

$$f_\pi^2 = f_{\eta'}^2 = M^3 N_f N_c C_P + \mathcal{O}(m_q), \qquad (x = 0). \tag{7.14}$$

To obtain the GOR relation we compute the leading order perturbation in m_f^2 and check when the solution becomes normalizable in the UV. As is always the case for the GOR relation (and as we will verify below) the relevant regime is close to the boundary ($r \sim \sqrt{m_q/\sigma}$), where the source and VEV terms of the tachyon are of the same order. Therefore we can take $\hat{P} \simeq$ const and neglect the logarithmic corrections to the potentials in (7.8). We obtain

$$P'(r) \simeq C_P\left(\frac{-4r}{\ell W_0 w_0^2} + \frac{m_f^2 r^3}{W_0 \kappa_0 \ell^3 \tau^2}\right). \tag{7.15}$$

Here the constants w_0, κ_0, and W_0 are the boundary values of w, κ, and V_f, respectively. We also approximated $e^A \simeq \ell/r$. The first term in (7.15) gives the weak r dependence of the $m_f = 0$ solution which can be neglected, but the second term is the important perturbation which becomes $\mathcal{O}(1)$ when $m_q \sim m_f^2$. Integrating over r and using the fact that $P \simeq 1$ when $m_f^2 = 0$ gives

[13] There is also another set of solutions which has a different x dependence and will be identified with the glueballs in the limit $x \to 0$ as we shall see below.

[14] Notice that the situation is different from the scalar sector, where the glue and flavor were decoupled also asymptotically in the UV and therefore the convergence toward $x = 0$ was uniform [51].

$$P(r) \simeq 1 - \frac{C_P m_f^2}{W_0 \kappa_0 \ell^3} \int_r^\infty \frac{\hat{r}^3 d\hat{r}}{\tau(\hat{r})^2}, \tag{7.16}$$

where the integral is dominated by the regime with $r \sim \sqrt{m_q/\sigma}$ as expected. The solution is normalizable when P vanishes at the boundary, which determines the mass of the η'. This leads to the GOR relation in the limit $x \to 0$:

$$1 \simeq \frac{C_P m_{\eta'}^2}{W_0 \kappa_0 \ell^3} \int_0^\infty \frac{\hat{r}^3 d\hat{r}}{\tau(\hat{r})^2} \simeq \frac{f_{\eta'}^2 m_{\eta'}^2}{2M^3 N_f N_c W_0 \kappa_0 \ell^5 m_q \sigma} = -\frac{f_{\eta'}^2 m_{\eta'}^2}{m_q \langle \bar{\psi}\psi \rangle}. \tag{7.17}$$

2. Small but finite x

We then discuss the $\mathcal{O}(x)$ contributions to the GOR relation for η'. At this order the coupling between the glue and the flavor can no longer be neglected and we need to study the complete system (7.8)–(7.11). But in the IR there is decoupling and we can unambiguously define the IR normalizable solutions for the glue and the flavor, denoted by $\psi^{(Q)}$ and $\psi^{(P)}$, respectively. The leading term of $\psi^{(P)}$ can be readily identified with the zero x solution discussed above. In order to determine the η' mass we need to study the normalizability of both these solutions in the UV. More precisely, we would want to find the coefficients C_- and C_1 of the non-normalizable terms of the UV asymptotic expressions in (F9) and (F11) for each of these two solutions. It is, however, easier to expand at $x = 0$ before expanding at $r = 0$ and therefore study the non-normalizable terms (F13) and (F15). Indeed by studying the expansions one sees that the non-normalizable terms in the two sets of asymptotic expressions are mapped to (linear combinations of) each other (possibly up to highly suppressed terms) when the order of limits is changed. We present here a sketch on how the $\mathcal{O}(x)$ corrections behave, and a systematic, precise treatment is done in Appendix G.

We denote the solutions defined by the UV expansions (F13) and (F15) by $\phi^{(Q)}$ and $\phi^{(P)}$, respectively. As the superscripts suggest, $\phi^{(P)}$ is the perturbative solution of the P field with vanishing Q, and $\phi^{(Q)}$ is obtained by first solving Q perturbatively, in analogy to the IR normalizable solutions. We further define

$$\begin{pmatrix} \psi^{(P)} \\ \psi^{(Q)} \end{pmatrix} = \begin{pmatrix} C_{PP} & C_{PQ} \\ C_{QP} & C_{QQ} \end{pmatrix} \begin{pmatrix} \phi^{(P)} \\ \phi^{(Q)} \end{pmatrix} + \text{UV normalizable terms}. \tag{7.18}$$

A normalizable mode can be constructed as a linear combination of $\psi^{(P)}$ and $\psi^{(Q)}$ when the determinant of the coefficient matrix vanishes.

We will sketch here how the coefficient matrix is computed—a detailed analysis will be given in Appendix G by performing a systematic expansion in both x and the (squared) bound state mass m_f^2. The elements can be obtained essentially by computing the values of P and Q near the boundary for the solutions $\psi^{(P)}$ and $\psi^{(Q)}$: as seen by comparing to the expressions (F13) and (F15), C_{IJ} is the value of J for the solution $\psi^{(I)}$ (with I, J taking the values P, Q).[15] The coupling between the glue and the flavor is irrelevant for the diagonal elements of the matrix. We have computed $\psi^{(P)}$ at leading order in x above, from which we readily obtain that $C_{PP} \simeq 1 - m_f^2/m_\pi^2$. We may normalize $\psi^{(Q)}$ such that $C_{QQ} = 1$. The backreaction of flavor on glue is suppressed by x but not vice versa, which leads to[16] $C_{PQ} = \mathcal{O}(x)$ but $C_{QP} = \mathcal{O}(x^0)$. From the fluctuation equations we see[17] that C_{QP} is enhanced as $m_q \to 0$, which will also be proven in Appendix G. Taking stock,

$$\begin{pmatrix} C_{PP} & C_{PQ} \\ C_{QP} & C_{QQ} \end{pmatrix} \simeq \begin{pmatrix} 1 - \frac{m_f^2}{m_\pi^2} & \mathcal{O}(x m_\pi^0) \\ \mathcal{O}(m_\pi^{-2} x^0) & 1 \end{pmatrix}. \tag{7.19}$$

The determinant vanishes when m_f equals the mass of the η', which leads to the expected relation

$$m_{\eta'}^2 = m_\pi^2 + \mathcal{O}(x m_\pi^0). \tag{7.20}$$

In order to compute the coefficient in the $\mathcal{O}(x)$ term of (7.20), we solve the fluctuation equations in a systematic expansion of the wave functions at small x and m_q in Appendix G. This results in the Witten-Veneziano formula for the mass of the η' meson:

$$m_{\eta'}^2 \simeq m_\pi^2 + x \frac{N_f N_c \chi_{\rm YM}}{f_\pi^2}, \tag{7.21}$$

where $\chi_{\rm YM}$ is the topological susceptibility for Yang-Mills theory. For our conventions $f_\pi^2 = \mathcal{O}(N_f N_c)$, so that the second term is indeed $\mathcal{O}(x)$.

C. Numerical results

We have computed the spectra of the singlet pseudoscalars numerically both for the potentials I and potentials II defined above in Sec. IV. The numerical study was done by using the fluctuation equations given in Appendix D as explained in [51] and in Appendix G of [55].

[15] Some care is needed because $\phi^{(Q)}$ also contains a logarithmically divergent term for P.

[16] This ensures that taking $x \to 0$ the determinant is $\propto C_{PP}$ and we will have $m_{\eta'} = m_\pi$.

[17] Solving (7.8) for P' gives $P' \sim Q'/\tau^2 + \cdots$ which leads to this enhancement.

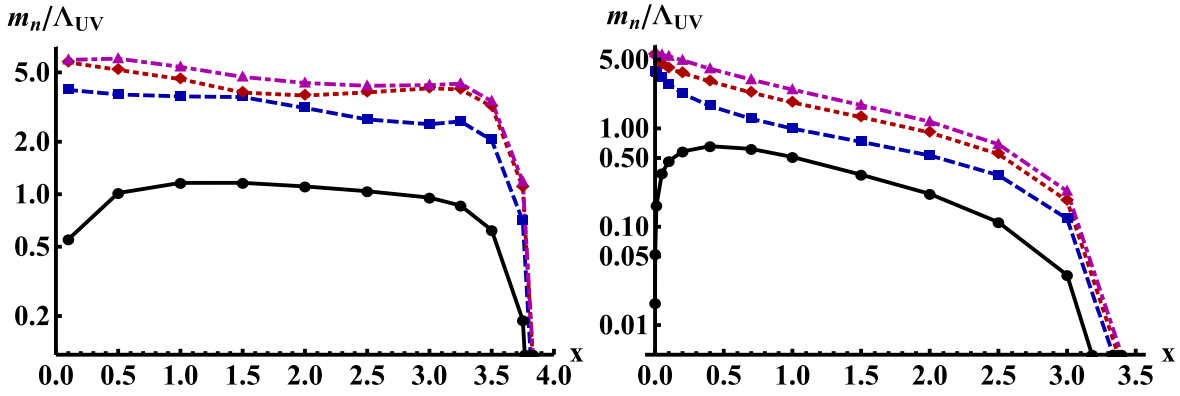

FIG. 14. Masses of the lowest four singlet pseudoscalar states in the logarithmic scale as a function of x. Left: potentials I. Right: potentials II.

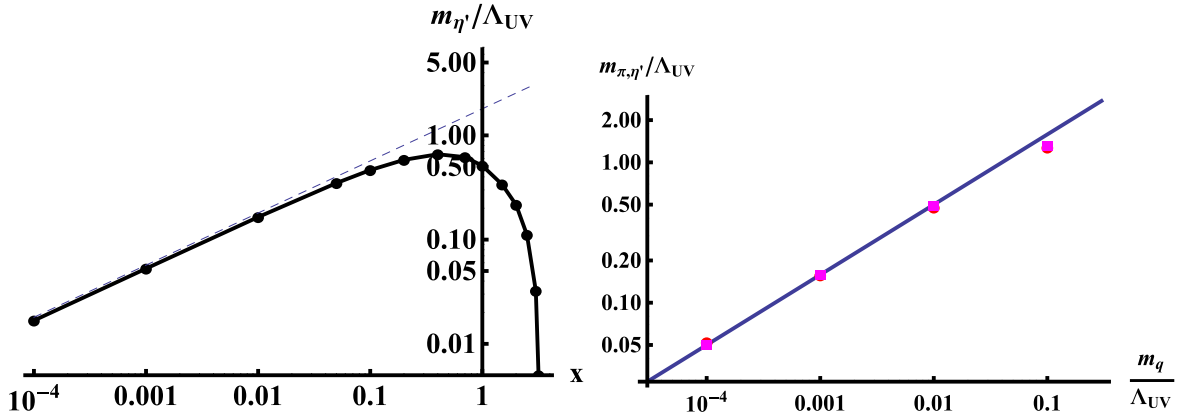

FIG. 15. The mass of the η' meson for potentials II. Left: mass of η' as a function of x in log-log scale for $m_q = 0$. The dashed blue line is a fit with the expected dependence $m_{\eta'}^2 \propto x$. Right: dependence of the mass of the η' (red circles) and the pion mass (magenta squares) on m_q at $x = 0.0001$. The blue line is a fit to the GOR relation.

The spectrum is shown in the logarithmic scale as a function of x in Fig. 14. The light η' state is best visible in the right-hand plot for small x. The third lowest state is a glueball in the limit $x \to 0$ for both potentials[18] whereas the other states are $\bar{\psi}\psi$ states. In the walking regime all masses tend to zero obeying the Miransky scaling law. Apart from the light η' meson at small x, the dependence of the spectrum on x is for both potentials very similar to that found for the singlet scalars in [51]. Notice that there is an additional interesting level crossing structure for potentials I.

We study the dependence of the mass of the η' meson on x and m_q in more detail for potentials II (for which the numerical computations are much easier then for potentials I) in Fig. 15. The left-hand plot demonstrates that the dependence on x at $m_q = 0$ is that predicted by Eq. (7.21). The right-hand plot shows the data for the η' and pion masses at very small $x = 0.0001$. The data points overlap perfectly, as predicted by Eq. (7.21). The dependence on the quark mass matches with the GOR relation (blue line).

VIII. FLAVOR NONSINGLET SPECTRA AT FINITE $\bar{\theta}$

A. Fluctuations at finite $\bar{\theta}$

We now study the quadratic fluctuations for the backgrounds with a nontrivial $\bar{\theta}$ angle studied in Sec. III. In those backgrounds both the tachyon phase ξ and the QCD axion $\mathfrak{a}$ are nonvanishing, which makes the analysis of the fluctuations, in particular the flavor singlet sector, more involved. In the following we will restrict ourselves to the analysis of the flavor nonsinglet sector. This sector consists of the flavor nonsinglet 1^{--} vector and 1^{++} axial vector mesons, and the flavor nonsinglet 0^{-+} pseudoscalar and 0^{++} scalar mesons; and these last two get mixed in a parity breaking[19] finite $\bar{\theta}$ vacuum.

[18]The mass of the glueball is actually the same for both potentials I and II because they only differ in the flavor sector.

[19]Notice that charge conjugation remains as a good quantum number, and therefore the vectors and axial vectors do not mix at finite $\bar{\theta}$.

1. Flavor nonsinglet sector

This sector involves the $SU(N_f)$ part of the vector, axial vector, scalar, and pseudoscalar mesons. The vector and axial vector fluctuations were defined in Eq. (7.1). The scalar and pseudoscalar mesons, which will mix in the presence of a nonzero phase of the tachyon, correspond to fluctuations of the complex tachyon:

$$\begin{aligned} T &= [\tau(r) + s(r,x) + \tilde{s}(r,x)] \\ &\quad \times \exp[\xi(r) + \theta_T(r,x) + \tilde{\pi}(r,x)], \\ \text{with } \tilde{s}(r,x) &= \mathfrak{s}^a(r,x)t^a, \quad \tilde{\pi}(r,x) = \pi^a(r,x)t^a. \end{aligned} \tag{8.1}$$

Only the DBI piece of the action, i.e. Eq. (2.4), contributes to the nonsinglet sector fluctuations. In Appendix E we write the resulting action up to quadratic order in the fluctuations and derive the equations of motion. We now summarize them sector by sector.

2. Scalar-pseudoscalar mesons

The fluctuations of the modulus and phase of the tachyon, and the longitudinal part of the axial vector contribute to this sector. We shall consider the following Ansatz for the three coupled fields:

$$\begin{aligned} &A_\mu^{||} = -\psi_L(r)\partial_\mu P^a(x)t^a, \qquad \tilde{s} = \psi_s(r)P^a(x)t^a, \\ &\tilde{\pi} = 2\psi_p(r)P^a(x)t^a, \end{aligned} \tag{8.2}$$

where $\partial_\mu\partial^\mu P^a(x) = m^2 P^a(x)$. As shown in Appendix E the equations of motion for these fields can be recombined into the two coupled equations (E8), (E9) for the two fields ψ_s, and $\hat{\psi}_l = e^A w^2 V_f \tilde{G}^{-1}\psi_L'$. The normalizable solutions of those equations will correspond to the scalar and pseudoscalar mesons, which mix in a parity breaking finite $\bar{\theta}$ vacuum.

3. Vector mesons

We consider the Ansatz

$$V_\mu = \psi_{\rm V}(r)\mathcal{V}_\mu^a(x)t^a, \text{ with } \partial_\nu\partial^\nu\mathcal{V}_\mu^a(x) = m_{\rm V}^2\mathcal{V}_\mu^a(x), \tag{8.3}$$

for the transverse part of the vector meson fluctuation (the longitudinal part can be set to zero). The equation of motion for V_μ resulting from the Lagrangian (E2) reduces to

$$\frac{1}{V_f w^2 e^A \tilde{G}}\partial_r\left(V_f e^A \frac{w^2}{\tilde{G}}\partial_r\psi_V\right) + m_V^2\psi_V = 0. \tag{8.4}$$

4. Axial vector mesons

We shall take the following Ansatz for the transverse part of the axial vector mesons:

$$A_\mu^\perp = \psi_{\rm A}(r)\mathcal{A}_\mu^a(x)t^a, \text{ with } \partial_\nu\partial^\nu\mathcal{A}_\mu^a(x) = m_{\rm A}^2\mathcal{A}_\mu^a(x), \tag{8.5}$$

The equation of motion for $A_\mu^\perp$ follows swiftly from the Lagrangian (E2), and in terms of this Ansatz takes the form

$$\frac{\partial_r(V_f w^2 e^A \tilde{G}^{-1}\partial_r\psi_A)}{V_f w^2 e^A \tilde{G}} - 4\frac{\tau^2\kappa e^{2A}G^2}{w^2\tilde{G}^2}\psi_A + m_A^2\psi_A = 0. \tag{8.6}$$

B. The Gell-Mann-Oakes-Renner relation at finite $\bar{\theta}$

It is possible to compute analytically the $\bar{\theta}$ dependence of the pion mass at small m_q, and to use this to write the generalization of the GOR relation at finite $\bar{\theta}$. We review here the key points of the computation and details are given in Appendix H.

The pion mass is found by analyzing the fluctuation equations for the pseudoscalar and scalar sectors in the UV and in the IR, and requiring a match of the results in the middle, where the regimes of applicability of the two results overlap when m_q is small. In the UV analysis, it is essential to use the fluctuations of the real and imaginary parts of the tachyon, in terms of which the fluctuation equations decouple when $r \ll 1/\Lambda_{\rm UV}$ and $m_q/\Lambda_{\rm UV} \ll 1$. The most important difference with respect to the computation at $\bar{\theta} = 0$ is that the background tachyon solution is replaced by the real part of the tachyon (see Appendix H for details). In the IR, or more precisely when $r \gg \sqrt{m_q/\sigma}$, it is enough to show that the mixing of the scalars and pseudoscalars is suppressed by $\mathcal{O}(m_q^2)$, and consequently the IR solutions are the same as at $\bar{\theta} = 0$.

Matching the UV and IR approximations for $\sqrt{m_q/\sigma} \ll r \ll 1/\Lambda_{\rm UV}$, where both of them are accurate, then fixes the pion mass. The only difference with respect to the result at $\bar{\theta}$ is that m_q is replaced by the source for the real part of the tachyon, i.e., $m_q\cos\xi_0 \simeq m_q\cos(\bar{\theta}/N_f)$, where we also recalled the result (6.23). The final result for the generalized GOR relation is therefore

$$f_{\pi,0}^2 m_\pi^2 = -\langle\bar{\psi}\psi\rangle|_{m_q=0} m_q\cos\frac{\bar{\theta}}{N_f} + \mathcal{O}(m_q^2), \tag{8.7}$$

where $f_{\pi,0}$ is the pion decay constant at $\bar{\theta} = 0$. The result agrees with effective field theory (see, e.g., [26]).

C. Numerical analysis

The flavor nonsinglet spectra of vector, axial-vector, pseudoscalar, and scalar mesons have been calculated for different values of quark mass, as a function of the $\bar{\theta}$ angle. The full action of the model, Eqs. (2.4) and (2.15), is expanded to quadratic order in terms of the excitation fields defined in Sec. VIII A 1. The quadratic action of the flavored excitations in a background of nontrivial $\bar{\theta}$ is presented in Eq. (E2). The vector and axial-vector excitation equations are decoupled and are given by Eqs. (8.4)

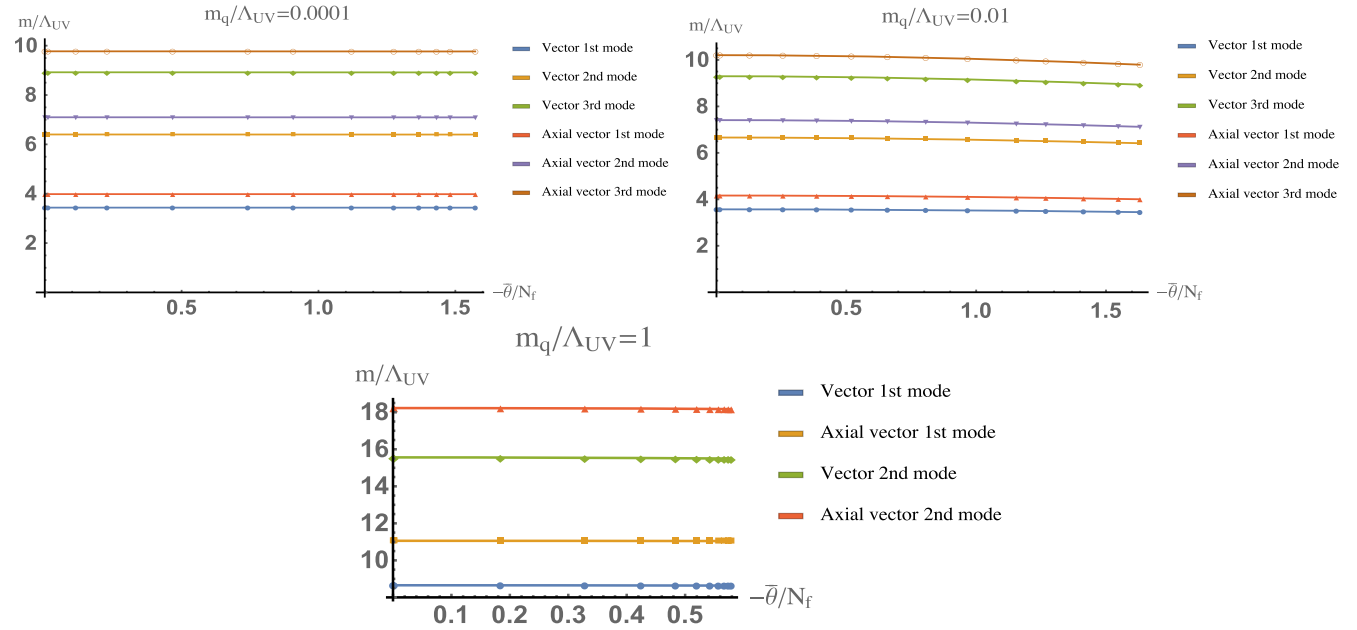

FIG. 16. The vector and axial vector masses for quark masses, $m_q/\Lambda_{\rm UV} = 0.0001$, 0.01, 1, in terms of $\bar{\theta}/N_c$ for potentials I.

and (8.6), while the pseudoscalars and scalars are coupled because of the nonzero background $\bar{\theta}$ angle, Eqs. (E4), (E5), and (E6). The numerical procedure of determining the mass spectrum, both for coupled and decoupled excitations, is described in detail in [51]. The computation consists basically of the solution of the excitation equations in the bulk spacetime with normalizable boundary conditions both at the boundary and the bottom of spacetime. The spectrum is calculated for potentials I, and for different values of quark masses $m_q/\Lambda_{\rm UV} = 0.0001$, 0.01, 1. As is depicted in Fig. 5, in case of small quark mass, for any value of the integration parameter, C_a, there are two background solutions, corresponding to two different values of $\bar{\theta}$. For larger quark mass, only the lower branch survives, and it does not turn back to the horizontal axis ($m_q/\Lambda_{\rm UV} = 1$ case). It has been found numerically that the spectrum is stable only in the lower branch of the solution. In the upper branch of solutions, it was found that one mode from the scalar channel has negative mass squared signaling an instability of the spectrum (see last plot in Fig. 19).

In Fig. 16, we plot the three lowest masses of the vector and axial-vector mesons. It observed that the vector and axial-vector masses have a mild dependence on $\bar{\theta}/N_c$. As it is expected, for larger quark masses the whole spectrum moves to higher meson masses, even though the difference in the spectrum for $m_q/\Lambda_{\rm UV} = 0.0001$ and $m_q/\Lambda_{\rm UV} = 0.01$ is small. The dependence of the pion mass on $\bar{\theta}/N_f$ is depicted in Fig. 17. The pion mass decreases with increasing $\bar{\theta}$ angle. In case of small equal quark masses, the pion mass as a function of $\bar{\theta}$ is obtained from (8.7)

$$m_\pi(\bar{\theta}) = m_\pi(0)\sqrt{\cos\left(\frac{\bar{\theta}}{N_f}\right)}. \tag{8.8}$$

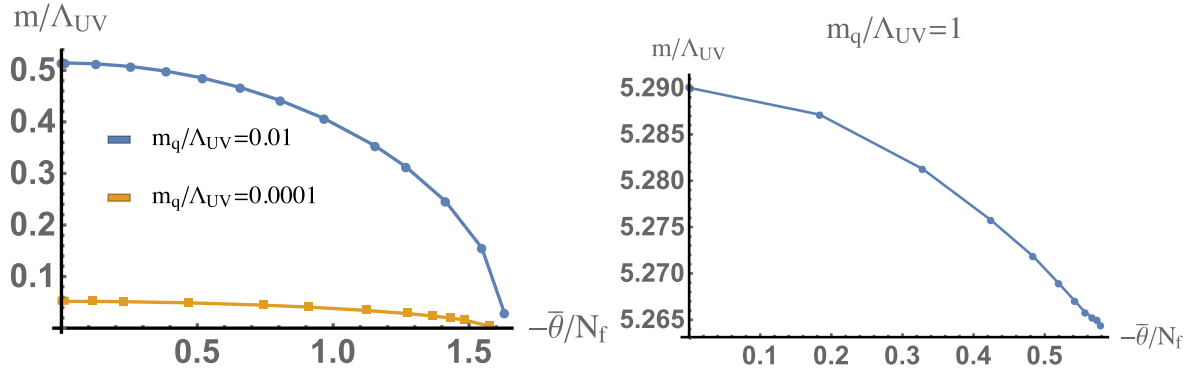

FIG. 17. The lowest mode masses of the pseudoscalar-scalar channel, for quark masses, $m_q/\Lambda_{\rm UV} = 0.0001$, 0.01 (left plot) and $m_q/\Lambda_{\rm UV} = 1$ (right plot), in terms of $\bar{\theta}/N_c$ for potentials I. Those modes correspond the pion.

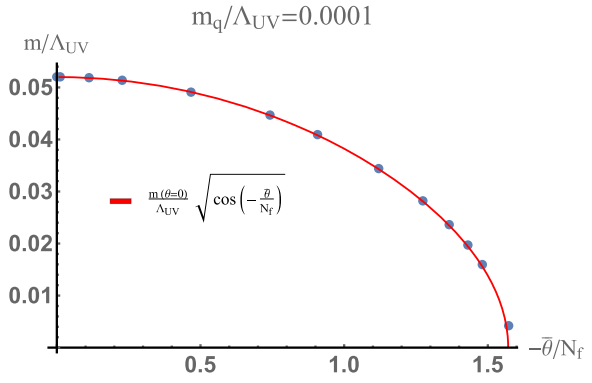

FIG. 18. The numerical result of the pion mass in terms of $\bar{\theta}$ in V-QCD is seen to be in perfect agreement with analytic formula (8.8).

In case of $m_q/\Lambda_{\mathrm{UV}} = 0.0001$, we verified the above relationship numerically as is seen in Fig. 18. Finally, the pseudoscalar-scalar masses are presented in Fig. 19. It is noticed that the states do not mix at finite $\bar{\theta}$. The lowest state corresponds to the pion, the next two to scalar excitations, and the highest to a pseudoscalar mode.

ACKNOWLEDGMENTS

We would like to thank F. Bigazzi, A. Cotrone, and K. Rummukainen for discussions. D. A. thanks the Front of Pro-Galician Scientists for unconditional support. This work was supported in part by European Union's Seventh Framework Programme under Grant Agreement (FP7-REGPOT-2012-2013-1) No. 316165 and the Advanced ERC grant SM-grav 669288. The work of D. A. is supported by the German-Israeli Foundation (GIF), Grant No. 1156. This work of I. I. is part of the D-ITP consortium, a program of the Netherlands Organisation for Scientific Research (NWO) that is funded by the Dutch Ministry of Education, Culture and Science (OCW).

APPENDIX A: UV AND IR ASYMPTOTICS OF THE BACKGROUND

In this section we will present the asymptotic form of the background fields for the choices of potentials relevant for the analysis in this work. Most of the expressions turn out to be independent of $\bar{\theta}$. For a more general analysis of the asymptotics at $\bar{\theta} = 0$ we refer the reader to Appendix D of [51].

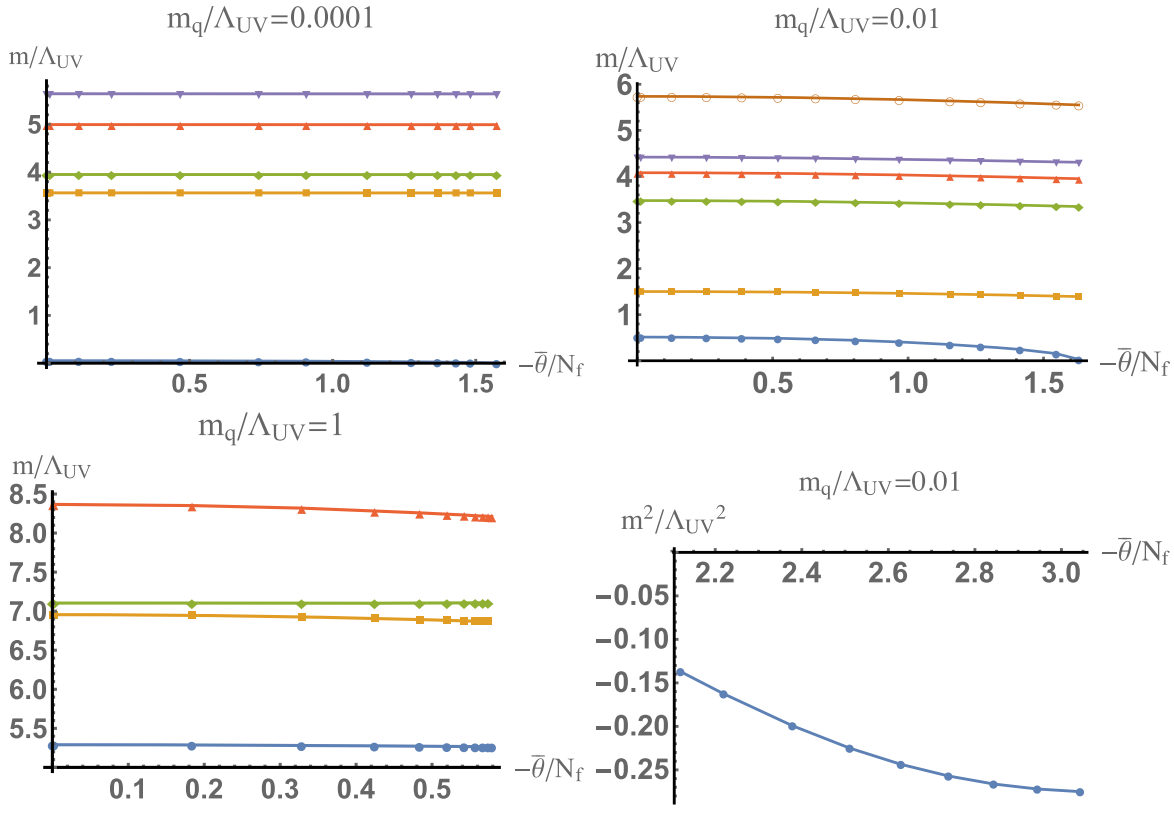

FIG. 19. The lowest mode masses of the pseudoscalar-scalar channel, for quark masses, $m_q/\Lambda_{\mathrm{UV}} = 0.0001, 0.01, 1$, in terms of $\bar{\theta}/N_c$ for potentials I. The lightest mode corresponds to the pion. In the last plot, it is shown that the pseudoscalar-scalar channel contains a mode of negative mass squared in the upper branch of solutions. The example which is shown here is for $m_q/\Lambda_{\mathrm{UV}} = 0.01$.

1. UV asymptotics

As explained in [51], in the UV ($r \to 0$) the tachyon decouples from the glue fields λ and A, whose asymptotic form is determined by the effective potential

$$V_{\rm eff}(\lambda) = V_g(\lambda) - xV_f(\lambda,0) = \frac{12}{\ell^2}[1 + V_1\lambda + V_2\lambda^2 + \cdots], \tag{A1}$$

resulting in the following solutions:

$$A(r) = -\log\frac{r}{\ell} + \frac{4}{9\log(r\Lambda)} + \frac{\frac{1}{162}\left[95 - \frac{64V_2}{V_1^2}\right] + \frac{1}{81}\log\left[-\log(r\Lambda)\right]\left[-23 + \frac{64V_2}{V_1^2}\right]}{\log(r\Lambda)^2} + \mathcal{O}\left(\frac{1}{\log(r\Lambda)^3}\right) + \mathcal{O}(m_q^2 r^2) \tag{A2}$$

$$V_1\lambda(r) = -\frac{8}{9\log(r\Lambda)} + \frac{\log\left[-\log(r\Lambda)\right]\left[\frac{46}{81} - \frac{128V_2}{81V_1^2}\right]}{\log(r\Lambda)^2} + \mathcal{O}\left(\frac{1}{\log(r\Lambda)^3}\right) + \mathcal{O}(m_q^2 r^2), \tag{A3}$$

where $\Lambda = \Lambda_{\rm UV}$ defines the UV scale of the theory. We also wrote down the size of the leading corrections due to the tachyon. Notice, in particular, that these results are independent of $\bar\theta$.

The UV scale may be defined explicitly as

$$\Lambda_{\rm UV} = \lim_{r\to 0}\frac{1}{\ell}\exp\left[A - \frac{8}{9V_1\lambda} + \left(\frac{23}{36} - \frac{16V_2}{9V_1^2}\right)\log\frac{9V_1\lambda}{8}\right]. \tag{A4}$$

In order to solve for the tachyon one inserts the asymptotic solutions for λ, and A into the equation of motion for the tachyon. We also need the UV expansions of a and κ, which read

$$\kappa(\lambda) \sim \kappa_0(1 + \kappa_1\lambda), \qquad a(\lambda) \sim a_0(1 + a_1\lambda); \quad \text{with} \quad \frac{\kappa_0}{a_0} = \frac{2\ell^2}{3}. \tag{A5}$$

We discuss the asymptotics of the tachyon at finite $\bar\theta$ in Sec. III B 1. We present here for reference the result at $\bar\theta = 0$, which reads

$$\frac{1}{\ell}\tau(r) = m_q r(-\log(r\Lambda))^{-\rho}\left[1 + \mathcal{O}\left(\frac{1}{\log(r\Lambda)}\right)\right] + \sigma r^3(-\log(r\Lambda))^{\rho}\left[1 + \mathcal{O}\left(\frac{1}{\log(r\Lambda)}\right)\right], \tag{A6}$$

with

$$\rho = -\frac{4}{3} - \frac{4\kappa_1}{3V_1}. \tag{A7}$$

2. IR asymptotics

We will only present here the discussion for the particular asymptotics of V_g that matches well with the IR properties of QCD [35].

a. λ and A

For regular potentials, the IR divergence of the tachyon decouples the tachyon and the axion from λ and A and therefore their asymptotics is independent of $\bar\theta$. For a glue potential V_g with the following IR asymptotic form[20]

$$V_g(\lambda) = v_0\left(\frac{\lambda}{8\pi^2}\right)^{4/3}\sqrt{\log\frac{\lambda}{8\pi^2}} \times\left[1 + \frac{v_1}{\log(\frac{\lambda}{8\pi^2})} + \frac{v_2}{\log^2(\frac{\lambda}{8\pi^2})} + \cdots\right], \tag{A8}$$

the asymptotic solution for the background glue fields reads

$$A = -\frac{r^2}{R^2} + \frac{1}{2}\log\frac{r}{R} + A_c + \mathcal{O}(r^{-2}), \tag{A9}$$

$$\log\lambda = \frac{3}{2}\frac{r^2}{R^2} + \lambda_c + \mathcal{O}(r^{-2}), \tag{A10}$$

with

$$A_c = -\log R - \frac{1}{2}\log v_0 + \frac{5}{4}\log 2 + \frac{3}{4}\log 3 + \frac{23}{24} + \frac{4v_1}{3}, \qquad \lambda_c = -\frac{23}{16} - 2v_1 + \log(8\pi^2). \tag{A11}$$

Here $R = 1/\Lambda_{\rm IR}$ sets the IR scale of the model. A possible explicit definition is

$$\Lambda_{\rm IR} = \lim_{r\to\infty}\frac{1}{r}\sqrt{\frac{2}{3}\log\lambda}. \tag{A12}$$

b. The tachyon

We will consider the following asymptotics for the relevant potentials

$$\kappa(\lambda) \sim \kappa_c\lambda^{-\kappa_p}(\log\lambda)^{-\kappa_\ell}, \qquad a(\lambda) \sim a_c\lambda^{a_p}(\log\lambda)^{a_\ell}, \qquad V_{f0}(\lambda) \sim v_c\lambda^{v_p}(\log\lambda)^{-v_\ell}, \tag{A13}$$

[20]The factors of $8\pi^2$ were included because this leads to simple expressions for the coefficients v_i for the potentials which we use.

where κ_c and a_c are assumed to be positive. In particular, we will focus on the special case $v_p = 10/3$, singled out by the requirement of having nonsingular $\bar{\theta} \neq 0$ backgrounds. A thorough analysis of the acceptable asymptotics with $v_p < 10/3$ was presented in Appendix D of [51]. At finite $\bar{\theta}$, the results for τ there remain unchanged, and the asymptotics of ξ can be found by substitution to (3.6). We consider two cases at $v_p = 10/3$ in the following, both leading to acceptable IR asymptotics.

1. $v_p = 10/3$, $\kappa_p = 4/3$, $\kappa_\ell > -3/2$, $a_p = a_\ell = 0$, and $v_\ell > 1 - \kappa_\ell/2$. This case results in the following asymptotic solution for the tachyon

$$\tau(r) = \tau_0 \exp\left[C_{\rm I}\left(\frac{r}{R}\right)^{3+2\kappa_\ell}(1+\mathcal{O}(r^{-2}))\right], \tag{A14}$$

with

$$C_{\rm I} = \frac{2^{1-\kappa_\ell}3^{\kappa_\ell}a_c e^{2A_c+\frac{4}{3}\lambda_c}R^2}{(3+2\kappa_\ell)(2v_\ell+\kappa_\ell-2)}. \tag{A15}$$

Substituting these asymptotics in Eq. (3.6) we obtain for ξ' in the IR

$$\begin{aligned}\xi' &\sim -C_a\left(\frac{3}{2}\right)^{v_\ell+\frac{\kappa_\ell}{2}}\frac{e^{-4A_c-\frac{8}{3}\lambda_c}}{\sqrt{\kappa_c}v_c}\frac{\tau'}{r^{2-\kappa_\ell-2v_\ell}\tau^2}\\ &= -C_a R^2 e^{-2A_c}\frac{2^{1-\frac{3}{2}\kappa_\ell-v_\ell}3^{\frac{3}{2}\kappa_\ell+v_\ell}e^{-\frac{4}{3}\lambda_c}a_c}{\tau_0(2v_\ell+\kappa_\ell-2)v_c\kappa_c^{3/2}}\left(\frac{r}{R}\right)^{3\kappa_\ell+2v_\ell}\\ &\quad\times\exp\left[-C_{\rm I}\left(\frac{r}{R}\right)^{3+2\kappa_\ell}\right],\end{aligned} \tag{A16}$$

where the prime stands now for the derivative with respect to the dimensionless variable[21] r/R. ξ' vanishes exponentially, and therefore leads to a regular background in the IR. Moreover, one can easily check that for such an exponentially vanishing ξ', all the new terms (proportional to ξ') in the tachyon equation of motion (3.10) are exponentially suppressed, and thus the asymptotic solution (A14) is not modified by a nonzero ξ'.

2. $v_p = 10/3$, $\kappa_p = 4/3$, $\kappa_\ell = -3/2$, $a_p = a_\ell = 0$, and $v_\ell > 7/4$. This case results in a tachyon diverging power like in the IR, namely

$$\tau(r) = \tau_0\left(\frac{r}{R}\right)^{C_{\rm II}}(1+\mathcal{O}(r^{-2})), \tag{A17}$$

where

$$C_{\rm II} = \frac{8\sqrt{2}a_c e^{2A_c+\frac{4}{3}\lambda_c}R^2}{3\sqrt{3}\kappa_c(4v_\ell-7)}. \tag{A18}$$

We now analyze the asymptotics of ξ'. First, the constraint (3.29), namely $e^{4A}V_{f0}\sqrt{\kappa}\tau > 0$, in terms of the IR asymptotics becomes

$$C_{\rm II} > 2v_\ell - 7/2, \tag{A19}$$

and therefore we have

$$\frac{7}{4} < v_\ell < \frac{7}{4} + \frac{C_{\rm II}}{2}, \tag{A20}$$

while the equation (3.6) for ξ' reduces to

$$\xi' \sim -\frac{C_a}{\tau_0}\left(\frac{2}{3}\right)^{\frac{3}{4}-v_\ell}\frac{e^{-4A_c-\frac{8}{3}\lambda_c}C_{\rm II}}{v_c\sqrt{\kappa_c}}\left(\frac{r}{R}\right)^{-C_{\rm II}-\frac{9}{2}+2v_\ell}, \tag{A21}$$

which vanishes powerlike (as $r \to \infty$) if the constraint (A19) is satisfied. In addition, the new terms (proportional to ξ') in the equation of motion for τ (3.10) are suppressed by powers of r. Then the leading IR asymptotic form (A17) for τ is not modified by a nonzero ξ'.

c. Special tachyon asymptotics

We have also found special asymptotic solutions which are absent at vanishing $\bar{\theta}$ angle. For such special solutions, the two terms in (3.28) have the same asymptotic behavior:

$$e^{4A}V_f\sqrt{\kappa}\tau \sim |C_a|V_a, \qquad (r\to\infty). \tag{A22}$$

Such solutions are linked to the regular tachyon solutions discussed above as follows. One may consider what happens as the single parameter τ_0 (the same parameter as T_0 in Fig. 3), which determines the normalization of the tachyon, decreases. Typically, assuming that the potentials admit a fixed point, there is a critical value τ_{0c} such that the background flows closer and closer to the fixed point as $\tau_0 \to \tau_{0c}$ from above (or more precisely, the length of the interval of the bulk coordinate where the background is close to the fixed point, increases). Then when $\tau_0 \leq \tau_{0c}$, no solution with regular UV behavior exists. But it may also happen that there is no lower boundary for τ_0 in which case one can consider the limit $\tau_0 \to 0$.

Taking $\tau_0 \to 0$ at vanishing $\bar{\theta}$ angle, one expects that there is a region with small tachyon, $\tau \ll 1$, already deep in the IR, where $\lambda \gg 1$. When there is a fixed point, for small enough τ_0 the tachyon is therefore much smaller than one when $\lambda > \lambda_*$, in the region corresponding to a positive β function. Consequently the tachyon decouples from the metric and the flow of the solution from the IR toward the UV stops without reaching the standard regular UV boundary. That is, a critical value τ_{0c} exists, below which the UV regularity is lost. But when the $\bar{\theta}$ angle is nonzero,

[21]Notice that, as can be seen from Eq. (3.3), C_a has units of R^4, and thus the combinations $C_a R^2 e^{-2A_c}$ in (A16), and $C_a e^{-4A_c}$ in (A21) are dimensionless.

the situation is different, because the tachyon is complex. When τ_0 is decreased, and τ becomes relatively small deep in the IR, the dynamics of the phase of the tachyon becomes important. As it turns out, the phase starts to evolve, backreacting on the behavior of the absolute value τ. Instead of approaching smoothly the origin, the value of the tachyon starts to rotate around it on the complex plane. The net effect is, as pointed out above, that (A22) holds, and the tachyon does not decouple. In the limit $\tau_0 \to 0$ one obtains a new asymptotic behavior, which is determined by (A22).

It is straightforward to compute this special tachyon asymptotics for any of the choices of potentials in the IR discussed above or in [51]. As an example, we present the solution for a class of potentials which includes the potentials I which were used in the numerical analysis in this article. That is, we take $\kappa_p = 4/3, \kappa_\ell = 0, a(\lambda) = \text{const}$, $V_a(\tau) = \exp(-a\tau^2 - a_l|\tau|)$, and restrict to $0 < v_p < 10/3$, in which case the regular tachyon asymptotics is an exponential [51]. The special asymptotics for the tachyon then reads

$$\tau = \frac{10 - 3v_p}{2a_l} r^2 + \frac{2v_\ell - 4}{a_l} \log(r) + \mathcal{O}\left(\left(\frac{1}{r}\right)^0\right). \tag{A23}$$

The phase of the tachyon behaves as $\xi' \sim 1/\sqrt{r}$ as $r \to \infty$, and

$$\frac{e^{8A} V_f^2 \kappa \tau^2}{C_a^2 V_a^2} - 1 \sim \frac{1}{r}, \qquad (r \to \infty), \tag{A24}$$

so that (A22) is indeed confirmed.

Notice that the special solution does not involve any additional integration constants (unlike the regular tachyon solutions which have one constant). Therefore it maps to a curve on the plane of physical parameters $(m_q/\Lambda_{\rm UV}, \bar{\theta})$. It may happen though that the solution does not admit a regular UV boundary—this is not guaranteed even if the dynamics of the complex tachyon prevents the tachyon from decoupling. Actually for the numerical values of parameters used in the numerical analysis of this article, it turns out that the special solution is always unphysical. However, if we decreased the value of a_l in (4.4) from the chosen value, the solution would be physical.

APPENDIX B: EQUATIONS OF MOTION

In this appendix we present the full equations of motion arising from the action (3.1), and discuss some of their consequences. We first write down the equations of motion for the *CP*-odd fields $\mathfrak{a}$ and A_M. They read

$$0 = \partial_M [g^{MN} \sqrt{-g} Z(\lambda) H_N], \tag{B1}$$

$$\begin{aligned} 0 = {} & 2V_a(\lambda,\tau) g^{MN} \sqrt{-g} Z(\lambda) H_N - \frac{1}{2} V_f(\lambda,\tau) \kappa(\lambda) \tau^2 (\partial_N \xi + 2A_N) \sum_{k=+,-} \sqrt{-\det \mathbf{A}_{(k)}} \left((\mathbf{A}_{(k)}^{-1})^{MN} + (\mathbf{A}_{(k)}^{-1})^{NM}\right) \\ & + \frac{1}{4} \partial_N \left[V_f(\lambda,\tau) w(\lambda) \sum_{k=+,-} k \sqrt{-\det \mathbf{A}_{(k)}} \left((\mathbf{A}_{(k)}^{-1})^{MN} - (\mathbf{A}_{(k)}^{-1})^{NM}\right) \right], \end{aligned} \tag{B2}$$

where

$$\begin{aligned} H_M &= \partial_M \mathfrak{a} + x\xi \partial_M V_a(\lambda,\tau) - 2xA_M V_a(\lambda,\tau) \\ &= \partial_M \bar{\mathfrak{a}} - x V_a(\lambda,\tau) \partial_M \xi - 2xA_M V_a(\lambda,\tau), \end{aligned} \tag{B3}$$

$\mathbf{A}_{(k)}$ were defined in (3.2), and $\bar{\mathfrak{a}} = \mathfrak{a} + x\xi V_a(\lambda,\tau)$. Due to invariance under (2.18), we have[22]

$$\frac{\delta S}{\delta \xi(x)} = x V_a \frac{\delta S}{\delta \mathfrak{a}(x)} - \frac{1}{2} \partial_M \frac{\delta S}{\delta A_M(x)}. \tag{B4}$$

Consequently the equation of motion for ξ follows from (B1) and (B2).

[22]Considering $\bar{\mathfrak{a}}$ as the axion field (rather than $\mathfrak{a}$), as we will be doing below, we obtain otherwise the same equation as (B4), but without the $\mathfrak{a}$ term.

The Einstein equations take the form

$$R_{MN} - \frac{1}{2} g_{MN} R = T^g_{MN} + T^f_{MN} + T^a_{MN}, \tag{B5}$$

where

$$T^g_{MN} = \frac{1}{2} g_{MN} \left[V_g - \frac{4}{3} \frac{(\partial_P \lambda)^2}{\lambda^2} \right] + \frac{4}{3} \frac{\partial_M \lambda \partial_N \lambda}{\lambda^2}, \tag{B6}$$

$$\begin{aligned} T^f_{MN} = {} & -\frac{x V_f}{8\sqrt{-g}} \sum_{k=+,-} \sqrt{-\det \mathbf{A}_{(k)}}\, g_{MP} \\ & \times [(\mathbf{A}_{(k)}^{-1})^{PQ} + (\mathbf{A}_{(k)}^{-1})^{QP}] g_{QN}, \end{aligned} \tag{B7}$$

$$T^a_{MN} = -\frac{1}{4} g_{MN} Z (H_P)^2 + \frac{Z}{2} H_M H_N. \tag{B8}$$

The remaining equations of motions are those of the scalars λ and τ. It is useful to keep $\bar{\mathfrak{a}}$, rather than $\mathfrak{a}$, fixed when varying the scalar fields. The equations can be written as

$$0=\frac{8}{3\lambda}\partial_M\left[\frac{g^{MN}\sqrt{-g}\partial_N\lambda}{\lambda}\right]+\sqrt{-g}\frac{dV_g}{d\lambda}-\frac{x}{2}\frac{\partial V_f}{\partial\lambda}\left(\sqrt{-\det\mathbf{A}_{(+)}}+\sqrt{-\det\mathbf{A}_{(-)}}\right)-\frac{\sqrt{-g}}{2}\frac{dZ}{d\lambda}(H_M)^2$$
$$+\sqrt{-g}Zx\frac{\partial V_a}{\partial\lambda}(\partial_M\xi+2A_M)g^{MN}H_N-\frac{1}{4}xV_f\frac{\partial\kappa}{\partial\lambda}[(\partial_M\tau)(\partial_N\tau)+\tau^2(\partial_M\xi+2A_M)(\partial_N\xi+2A_N)]\sum_{k=+,-}\sqrt{-\det\mathbf{A}_{(k)}}(\mathbf{A}^{-1}_{(k)})^{MN}$$
$$+\frac{1}{4}xV_f\frac{\partial w}{\partial\lambda}F_{MN}\sum_{k=+,-}k\sqrt{-\det\mathbf{A}_{(k)}}(\mathbf{A}^{-1}_{(k)})^{MN} \tag{B9}$$

and

$$0=\frac{1}{4}\partial_M\left[V_f\kappa\partial_N\tau\sum_{k=+,-}\sqrt{-\det\mathbf{A}_{(k)}}((\mathbf{A}^{-1}_{(k)})^{MN}+(\mathbf{A}^{-1}_{(k)})^{NM})\right]-\frac{1}{2}V_f\kappa\tau(\partial_M\xi+2A_M)(\partial_N\xi+2A_N)\sum_{k=+,-}\sqrt{-\det\mathbf{A}_{(k)}}(\mathbf{A}^{-1}_{(k)})^{MN}$$
$$-\frac{1}{2}\frac{\partial V_f}{\partial\tau}\left[\sqrt{-\det\mathbf{A}_{(+)}}+\sqrt{-\det\mathbf{A}_{(-)}}\right]+\sqrt{-g}Z\frac{\partial V_a}{\partial\tau}(\partial_M\xi+2A_M)g^{MN}H_N. \tag{B10}$$

We will now argue that the gauge field vanishes for the background solution. To see this, we consider an Ansatz where all fields depend on r only, and assume the Poincaré covariant form of the metric (2.3). Since there are other four vectors than A_μ and no sources which break the Poincaré symmetry, we expect that $A_\mu=0$. In order to verify this, we notice that for the background Ansatz $\mathbf{A}_{(\pm)}$ are diagonal up to terms involving A_μ. Therefore, as only radial derivatives are nonzero, the equations of motion for A_μ in (B2) are indeed satisfied for $A_\mu=0$. Moreover, it is convenient to choose the gauge where $A_r=0$. This still leaves the freedom of transforming $\mathfrak{a}$ and ξ by a constant ε in (2.18).

After setting the gauge fields to zero, we notice that $\mathbf{A}_{(+)}=\mathbf{A}_{(-)}$ and both matrices are symmetric so that the last term in (B2) vanishes. Inserting the r-dependent Ansatz, the only nontrivial equation is obtained for $M=r$, which simplifies to

$$V_a(\lambda,\tau)e^{3A}Z(\lambda)H_r-\frac{V_f(\lambda,\tau)\kappa(\lambda)\tau^2\xi' e^{3A}}{\tilde{G}}=0 \tag{B11}$$

with $\tilde{G}$ defined in (3.5).

APPENDIX C: ON THE PHASE DIAGRAM AT FINITE $\bar{\theta}$ ANGLE

We discuss here first the branch structure and/or uniqueness of the background solutions at finite $\bar{\theta}$ angle. In Fig. 5 and at small quark mass, there are two or zero solutions at fixed C_a and m_q, but as functions of the sources m_q and $\bar{\theta}$ the solutions are typically unique. One should notice, however, that these plots do not contain all possible solutions as we did not study the solutions near the Efimov vacua, i.e. close to the leftmost crosses of Fig. 3. The sketch of Fig. 3 suggests that the mapping from (T_0,C_a) to $(m_q,\bar{\theta})$ is bijective also in the regime of Efimov vacua. This indeed turns out to be the case for generic values of x, but (as we demonstrate in Sec. VI D) for very small values of x the mapping is not bijective: as $x\to 0$ a nontrivial branch structure as a function of $\bar{\theta}$ appears in the vicinity of the Efimov vacua.

Even at larger x where the nontrivial branch structure is absent, one should bear in mind that the $\bar{\theta}$ angle is periodic. Near different crosses of Fig. 3 we encounter backgrounds for which $\bar{\theta}$ differs by integer multiples of $2\pi N_f$, but the quark mass is the same: this corresponds to the change of phase of the tachyon by multiples of 2π and therefore the backgrounds cannot be distinguished by using UV data. Consequently, solutions at high m_q are unique, but the solutions which differ by 2π rotations of the tachyon in the UV appear at small m_q and generalize the Efimov vacua to finite $\bar{\theta}$ angle. The number of Efimov vacua grows with decreasing m_q and becomes infinite for $m_q=0$.

We argue now that the generalized Efimov vacua at finite C_a are unstable. For fixed $m_q/\Lambda_{\rm UV}\ll 1$, such Efimov vacua are found on half-rings that encircle the crosses of Fig. 3. We have shown in [48,51,55] that for $C_a=0$ the Efimov vacua are perturbatively unstable. We remind the reader that in Fig. 3, the Efimov vacua for $C_a=0$ and with fixed (absolute value of) quark mass are found on the horizontal axis for various discrete values of T_0 and the stable standard vacuum is found on the horizontal axis to the right of the Efimov vacua. For these vacua, the free energy decreases with T_0. This was proven analytically for vacua with high n (i.e. close to the dashed curve in Fig. 3) and numerically for vacua with low n. For the Efimov vacua at finite C_a, the free energy on the half-rings around the crosses is typically monotonic, as is seen from the plots of Fig. 10. When this is the case, the question of ordering the saddle points at $C_a\neq 0$ according to their energies simply boils down to the same question for the saddle points at $C_a=0$. There are also cases (as one can see from the analysis of Sec. V, and the discussion in Sec. VI D 2), in particular at small x, where

the energy is not monotonic on the half-rings. Even in this case, the variation of the free energy along the half-rings is of the order $\sim m_q|\langle\bar{\psi}\psi\rangle|_{n,m_q=0}$ where the chiral condensate is evaluated at the corresponding Efimov vacua at $m_q = 0$. Because the condensate at the Efimov vacua are strongly suppressed with respect to the standard vacuum (see, e.g., Fig. 9 in [55], where the Efimov vacua are found near the origin), this variation is too small to overcome the energy difference between the Efimov vacua and the standard vacuum.

In Sec. VIII we will also demonstrate numerically that even the solutions near the $m_q = 0$ standard vacuum (the rightmost cross in Fig. 3) are perturbatively unstable if $|\bar{\theta}| \gtrsim N_f\pi/2$. Therefore, all vacua in Fig. 3 left of the standard vacuum, i.e. for $|\bar{\theta}| \gtrsim N_f\pi/2$, are perturbatively unstable. Moreover, if we take into account all branches of solutions, which are obtained by shifting $\bar{\theta}$ by multiples of 2π, the dominant solutions are found in the immediate vicinity of the $\bar{\theta} = 0$ standard solutions [marked with the blue line in Fig. 3 (right)], as we argue in Sec. VI B.

As shown on the horizontal axis of Fig. 3 (right), $\bar{\theta}$ takes values quantized in units of πN_f on this axis, corresponding to phase shifts in units of π of the tachyon. In order to prove this, we analyze the behavior of the tachyon solution near the horizontal axis of Fig. 3. As $C_a \to 0$, the solution approaches smoothly the real valued solution having $C_a = 0$ exactly. Between the rightmost cross on the real axis and the next cross to the left in Fig. 3 (left), the (real part of the) tachyon at $C_a = 0$ has a single node at some $r = r_0$—notice that indeed such a solution has[23] $m_q < 0$ in the plot of Fig. 2. By definition τ is positive in our analysis at $C_a \neq 0$, so a change of sign in the real part of the tachyon must be realized through a shift in the tachyon phase ξ. From (3.6) we see that ξ' is positive for positive C_a, so the phase must jump by $+\pi$ at the node of the tachyon as $C_a \to 0$ from above: we have

$$\xi'(r) \to \pi\delta(r - r_0), \tag{C1}$$

where r_0 is the location of the node. By using (3.3) for the gauge invariant contribution we obtain

$$\bar{\mathfrak{a}}' = \mathfrak{a}' + x(\xi V_a)' = x\xi' V_a + \mathcal{O}(C_a) \to x\pi\delta(r - r_0) \tag{C2}$$

as $C_a \to 0$ from above, where we used the fact that $V_a = 1$ at the tachyon node [as the tachyon vanishes by definition, $\tau(r_0) = 0$]. Consequently,

$$\bar{\theta} = N_c\bar{\mathfrak{a}}_0 \to -\pi N_f. \tag{C3}$$

[23]As we discussed above, in this plot the quark mass is defined as the real part of the source for the tachyon (whereas at finite $\bar{\theta}$ we define m_q as the absolute value of the source). Therefore negative values are possible.

For solutions with more tachyon oscillations, which can be found on the horizontal axis of Fig. 3 closer to the dashed curve, one just needs to sum over the contributions from separate tachyon nodes. One finds that $\bar{\theta} \to -nN_f\pi$ as $C_a \to 0$ from above, where n is the number of nodes.

An interesting possibility is that the white region of Fig. 3 at small T_0 is absent at large C_a so that the dashed curve ends on the vertical axis. Such behavior is observed for potentials I for some (small) choices of the coefficient a_l in the function $V_a(\tau) = \exp(-a_q\tau^2 - a_l\tau)$ (but not for the choice of a_l used in the numerical studies of this article). This means that solutions exist at arbitrary small T_0, so it is natural to ask what happens in the limit $T_0 \to 0$. As it turns out, the tachyon does not vanish in this limit, but assumes an asymptotic behavior in the IR, which is different from the standard regular IR asymptotics (see Appendix A). For this special asymptotics, the two terms in (3.28) have the same IR behavior:

$$e^{4A}V_f(\lambda,\tau)\sqrt{\kappa(\lambda)}\tau \simeq |C_a|V_a(\tau) \qquad (r \to \infty). \tag{C4}$$

For potentials I with the above choice of V_a the tachyon diverges as $\tau \sim r^2$, while the phase behaves as $\sim\sqrt{r}$ at large r (see the end of Appendix A for precise treatment). This behavior is enough to decouple the tachyon from the metric, which consequently follows the usual (Yang-Mills) asymptotics. Unlike with the standard asymptotics, this tachyon asymptotics involves no free parameters, and the only free parameter for this kind of solutions is C_a. Therefore the solutions would define a curve on the $(m_q, \bar{\theta})$ plane.

APPENDIX D: FLUCTUATION EQUATIONS FOR THE SINGLET PSEUDOSCALARS AT $\bar{\theta} = 0$

In [51] the whole set of fluctuations of V-QCD was studied at $\bar{\theta} = 0$. Here we will focus on those contributing to the singlet pseudoscalar sector. We need only consider the flavor singlet axial vector, the phase of the tachyon, and the axion field.

The fluctuations of the left and right gauge fields can be written in terms of the vector and axial combinations

$$V_M = \frac{A_M^L + A_M^R}{2}, \qquad A_M = \frac{A_M^L - A_M^R}{2}, \tag{D1}$$

with the associated field strengths being V_{MN}, A_{MN}. For the axial vectors we first need to separate the transverse and longitudinal parts:

$$A_\mu(x^\mu, r) = A_\mu^\perp(x^\mu, r) + A_\mu^\parallel(x^\mu, r), \tag{D2}$$

where $\partial^\nu A_\nu^\perp(x^\mu, r) = 0$, and the longitudinal term is the divergence of a scalar function.

For the axial vector modes we need to treat the flavor nonsinglet and flavor singlet terms separately, and therefore we write

$$A_\mu^\perp(x^\mu,r)=A_\mu^{\perp F}(x^\mu,r)+A_\mu^{\perp S}(x^\mu,r),$$
$$A_\mu^\parallel(x^\mu,r)=A_\mu^{\parallel F}(x^\mu,r)+A_\mu^{\parallel S}(x^\mu,r), \tag{D3}$$

where the superscript S (F) stands for the flavor singlet (nonsinglet) part of the mode. In the following we will deal only with the longitudinal flavor singlet part of the longitudinal axial vector mode $A^{\parallel S}$, since only this part contributes to the action of the singlet pseudoscalar sector.

On the other hand, the fluctuations of the tachyon are given by

$$T=(\tau+s+\mathfrak{z}^a t^a)e^{i\theta_T+i\pi^a t^a}, \tag{D4}$$

where t^a are the generators of $SU(N_f)$. We are mostly interested in the standard vacuum for $0<x<x_c$ which gives rise to a nontrivial spectrum [51]. Therefore, the background solution $\tau(r)$ is nonzero and the phases θ_T, π^a in (D4) are well defined.

1. Flavor singlet pseudoscalar mesons

The quadratic action for all the fluctuations of V-QCD was computed in [51].

Here we will write down the two pieces contributing to the flavor singlet pseudoscalar sector: S_1 coming from the DBI piece (2.4), and S_2 from the CP-odd sector (2.15). We write each separately:

$$S_1=-M^3N_c^2\frac{x}{2}\int d^4x dr V_f(\lambda,\tau)e^A G^{-1}\times[w(\lambda,\tau)^2(\partial_r A_\mu^{\parallel S})^2+e^{2A}\kappa(\lambda,\tau)\tau^2(\partial_r\theta_T)^2+e^{2A}G^2\kappa(\lambda,\tau)\tau^2(\partial_\mu\theta_T+2A_\mu^{\parallel S})^2], \tag{D5}$$

and

$$S_2=-\frac{M^3N_c^2}{2}\int d^4x dr Z(\lambda)e^{3A}[(\partial_\mu a-2xV_a(\lambda,\tau)A_\mu^{\parallel S})^2+(\partial_r a+x\partial_r V_a(\lambda,\tau)\theta_T)^2], \tag{D6}$$

where

$$G=\sqrt{1+e^{-2A}\kappa(\lambda)\tau'^2} \tag{D7}$$

and we have set $A_r=0$.

We split the fields in the action as

$$A_\mu^{\parallel S}(x^\mu,r)=-\varphi_L(r)\partial_\mu(\mathcal{T}(x^\mu)),$$
$$\theta_T(x^\mu,r)=2\varphi_\theta(r)\mathcal{T}(x^\mu),$$
$$a(x^\mu,r)=2\varphi_{\rm ax}(r)\mathcal{T}(x^\mu). \tag{D8}$$

The following combinations of the above fields

$$P(r)\equiv\varphi_\theta(r)-\varphi_L(r),$$
$$Q(r)\equiv\varphi_{\rm ax}(r)+xV_a(\lambda,\tau)\varphi_L(r),$$
$$R(r)\equiv\varphi'_{\rm ax}(r)+x\partial_r V_a(\lambda,\tau)\varphi_\theta(r) \tag{D9}$$

are invariant under the residual gauge transformations (2.18). Only two of them are independent, and they realize the pseudoscalar glueball (0^{-+}) and η' meson towers.

Indeed, following [51] R can be eliminated from the fluctuation equations, which are found by varying Eqs. (D5) and (D6). The result may be written as

$$\partial_r\left[V_f e^A G^{-1}w^2\left(-4e^{2A}\frac{V_f\kappa\tau^2}{N_a+N_b}P'+\frac{V_a'}{V_a}\frac{N_b}{N_a+N_b}P+\frac{N_b}{xV_a(N_a+N_b)}Q'\right)\right]+4V_f e^{3A}G\kappa\tau^2P-4e^{3A}ZV_aQ=0, \tag{D10}$$

$$\partial_r\left[e^{3A}Z\left(4xe^{2A}\frac{V_aV_f\kappa\tau^2}{N_a+N_b}P'+x\frac{V_a'N_a}{N_a+N_b}P+\frac{N_a}{N_a+N_b}Q'\right)\right]+m^2e^{3A}ZQ=0, \tag{D11}$$

where N_a and N_b are given by the following expressions:

$$N_a=V_f(4e^{2A}\kappa\tau^2-m^2w^2),\qquad N_b=4xe^{2A}ZV_a^2G. \tag{D12}$$

a. Change of variables

For the analysis of the mass of the η'meson, it is useful to define the conjugate variables of P and Q:

$$\Psi=\begin{pmatrix}\hat{P}\\ \hat{Q}\end{pmatrix}=\frac{1}{N_a+N_b}\begin{pmatrix}\frac{V_fe^Aw^2}{4G}(-N_b-4e^{2A}V_f\kappa\tau^2) & \frac{V_fe^Aw^2}{4G}\frac{N_b}{xV_a}\\ e^{3A}Z(4xe^{2A}V_aV_f\kappa\tau^2-N_axV_a)m^{-2} & e^{3A}ZN_am^{-2}\end{pmatrix}\begin{pmatrix}P'\\ (Q+xV_aP)'\end{pmatrix}. \tag{D13}$$

Then the terms in the square brackets in (D10) and (D11) can be expressed in terms of $\hat{P}$ and $\hat{Q}$. Taking a suitable linear combination of these equations, differentiating once, and after some simplifications, the fluctuation equations can be written as

$$\Psi'' + C_1^{-1}\partial_r C_1 \Psi' + M\Psi = 0, \tag{D14}$$

where

$$C_1 = e^{-3A}\begin{pmatrix} \frac{1}{GV_f\kappa\tau^2} & \frac{V_a}{GV_f\kappa\tau^2} \\ \frac{V_a x}{GV_f\kappa\tau^2} & \frac{1}{Z}+\frac{V_a^2 x}{GV_f\kappa\tau^2} \end{pmatrix},$$

$$M = \begin{pmatrix} G^2m^2 - \frac{4e^{2A}(GV_a^2 xZ + G^2V_f\kappa\tau^2)}{V_f w^2} & e^{-2A}\kappa\tau'^2 m^2 V_a \\ \frac{4e^{2A}GV_a xZ}{V_f w^2} & m^2 \end{pmatrix}. \tag{D15}$$

2. Flavor singlet axial vector mesons

It was shown in [51] that the action for the singlet sector of the (transverse) axial vector modes has an extra term coming from the *CP*-odd sector. The action is given by

$$S_A = -\frac{M^3N_c^2}{2}\int d^4x dr\Big\{ xV_f(\lambda,\tau)e^A G^{-1}\Big[\frac{1}{2}G^2 w(\lambda,\tau)^2 A_{\mu\nu}A^{\mu\nu} + w(\lambda,\tau)^2\partial_r A_\mu^{\perp S}\partial_r A^{\perp S\mu} + 4\kappa(\lambda,\tau)\tau^2 e^{2A}G^2 A_\mu^{\perp S}A^{\perp S\mu}\Big] + 4x^2 Z(\lambda)e^{3A}V_a(\lambda,\tau)^2 A_\mu^{\perp S}A^{\perp S\mu}\Big\}, \tag{D16}$$

where indeed the last contribution originates from the *CP*-odd action (2.15) while all the other terms come from the flavor sector piece (2.4). Taking the following Ansatz:

$$A_\mu^{\perp S}(x^\mu, r) = \varphi_A(r)\mathcal{X}_\mu(x^\mu), \tag{D17}$$

the resulting fluctuation equation takes the form

$$\frac{1}{V_f(\lambda,\tau)w(\lambda,\tau)^2 e^A G}\partial_r(V_f(\lambda,\tau)w(\lambda,\tau)^2 e^A G^{-1}\partial_r\varphi_A) + m_V^2\varphi_A + - 4\Big[xe^{2A}\frac{Z(\lambda)V_a(\lambda,\tau)^2}{V_f(\lambda,\tau)Gw(\lambda,\tau)^2} + \frac{\tau^2 e^{2A}}{w(\lambda,\tau)^2}\kappa(\lambda,\tau)\Big]\varphi_A = 0. \tag{D18}$$

APPENDIX E: FLUCTUTIONS OF THE $\bar{\theta}$ BACKGROUNDS

In this section we will derive the equations of motion for the fluctuations in backgrounds corresponding to nonzero $\bar{\theta}$ vacua of the dual theory. As mentioned in Sec. VIII A we will only consider the flavor nonsinglet sector, which consists of the vector and axial vector mesons, together with the scalar and pseudoscalar fluctuations of the complex tachyon which we write as

$$T = [\tau(r) + s(r,x) + \tilde{s}(r,x)] \times \exp[\xi(r) + \theta_T(r,x) + \tilde{\pi}(r,x)], \quad \text{with} \quad \tilde{s}(r,x) = \mathfrak{s}^a(r,x)t^a, \quad \tilde{\pi}(r,x) = \pi^a(r,x)t^a. \tag{E1}$$

Only the DBI piece of the action, given by Eq. (2.4), contributes to the nonsinglet sector fluctuations. Up to quadratic order in the fluctuations it reads

$$\begin{aligned} S_1 = &-\frac{1}{2}M^3N_c\mathbb{T}r\int d^4x dr V_f(\lambda,\tau)e^{3A}\tilde{G}^{-1} \\ &\times\Big\{\Big[2\kappa\frac{\partial_\tau V_f}{V_f}\tau' + (\partial_\tau\kappa)\tau'(1+\tilde{G}^{-2}) - 2e^{-2A}\tilde{G}^{-2}\kappa^2\tau\tau'\xi'^2\Big]\tilde{s}\tilde{s}' \\ &+\Big[\frac{\partial_\tau^2 V_f}{V_f}e^{2A}\tilde{G}^2 + \frac{\partial_\tau V_f}{V_f}(\partial_\tau\kappa)(\tau'^2+\tau^2\xi'^2) + 2\frac{\partial_\tau V_f}{V_f}\kappa\tau\xi'^2 + \frac{\partial_\tau^2\kappa}{2}(\tau'^2+\tau^2\xi'^2) + (\partial_\tau\kappa)(1+\tilde{G}^{-2})\tau\xi'^2 \\ &-\frac{e^{-2A}}{4\tilde{G}^2}(\partial_\tau\kappa)^2(\tau'^2+\tau^2\xi'^2)^2 + \kappa\tilde{G}^{-2}(1+\kappa e^{-2A}\tau'^2)\xi'^2\Big]\tilde{s}^2 + [\kappa\tilde{G}^{-2}(1+\kappa e^{-2A}\tau^2\xi'^2)]\tilde{s}'^2 + [\kappa(1+\kappa e^{-2A}\tau^2\xi'^2)](\partial_\mu\tilde{s})^2 \\ &+[\kappa\tilde{G}^{-2}\tau^2(1+\kappa e^{-2A}\tau'^2)]\tilde{\pi}'^2 + [\kappa\tau^2(1+\kappa e^{-2A}\tau'^2)](\partial_\mu\tilde{\pi}+2A_\mu)^2 \\ &+2\xi'\Big[\frac{\partial_\tau V_f}{V_f}\kappa\tau^2 + \kappa\tau(2-\tilde{G}^{-2}e^{-2A}\kappa\tau^2\xi'^2) + \frac{\tau^2}{2}(\partial_\tau\kappa)(1+\tilde{G}^{-2})\Big]\tilde{s}\tilde{\pi}' \\ &-[2e^{-2A}\tilde{G}^{-2}\kappa^2\tau^2\tau'\xi']\tilde{s}'\tilde{\pi}' - [2e^{-2A}\kappa^2\tau^2\tau'\xi'](\partial_\mu\tilde{\pi}+2A_\mu)\partial^\mu\tilde{s} + w^2e^{-2A}\Big[\frac{\tilde{G}^2}{2}(A_{\mu\nu}A^{\mu\nu}+V_{\mu\nu}V^{\mu\nu}) + A_\mu'^2 + V_\mu'^2\Big]\Big\}. \end{aligned} \tag{E2}$$

The vector and axial vector mesons correspond to the transverse part of the fields V_μ and A_μ respectively, and their equations of motion can be readily obtained from the above Lagrangian. They are Eqs. (8.4) and (8.6) in the main text.

1. Scalar-pseudoscalar mesons

This sector consists of the fluctuations of the modulus and phase of the tachyon, and the longitudinal part of the axial vector, which we decompose as

$$A_\mu^{\parallel F} = -\psi_L(r)\partial_\mu P^a(x)t^a, \qquad \tilde{s} = \psi_s(r)P^a(x)t^a, \qquad \tilde{\pi} = 2\psi_p(r)P^a(x)t^a, \tag{E3}$$

where $\partial_\mu\partial^\mu P^a(x) = m^2 P^a(x)$. The corresponding equations of motion read:

$$\frac{\tilde{G}}{V_f e^{3A}}\partial_r\left[V_f\frac{e^{3A}}{\tilde{G}}(4P_2\psi_p' + M_1\psi_s + M_2\psi_s')\right] + m^2[4P_1(\psi_p - \psi_L) + M_3\psi_s] = 0, \tag{E4}$$

$$\frac{\tilde{G}}{V_f e^{3A}}\partial_r\left(V_f\frac{e^A}{\tilde{G}}w^2\psi_L'\right) + 4P_1(\psi_p - \psi_L) + M_3\psi_s = 0, \tag{E5}$$

$$\frac{\tilde{G}}{V_f e^{3A}}\partial_r\left[V_f\frac{e^{3A}}{\tilde{G}}(2S_3\psi_s' + S_1\psi_s + 2M_2\psi_p')\right] + 2m^2M_3(\psi_p - \psi_L) + 2m^2S_4\psi_s - S_1\psi_s' - 2S_2\psi_s - 2M_1\psi_p' = 0, \tag{E6}$$

where the different coefficients are given by

$$\begin{aligned}
P_1 &= \kappa\tau^2(1 + \kappa e^{-2A}\tau'^2), \qquad P_2 = \kappa\tilde{G}^{-2}\tau^2(1 + \kappa e^{-2A}\tau'^2),\\
S_1 &= 2\kappa\frac{\partial_\tau V_f}{V_f}\tau' + (\partial_\tau\kappa)\tau'(1 + \tilde{G}^{-2}) - 2e^{-2A}\tilde{G}^{-2}\kappa^2\tau\tau'\xi'^2,\\
S_2 &= \left[\frac{\partial_\tau^2 V_f}{V_f}e^{2A}\tilde{G}^2 + \frac{\partial_\tau V_f}{V_f}(\partial_\tau\kappa)(\tau'^2 + \tau^2\xi'^2) + 2\frac{\partial_\tau V_f}{V_f}\kappa\tau\xi'^2 + \frac{\partial_\tau^2\kappa}{2}(\tau'^2 + \tau^2\xi'^2) + (\partial_\tau\kappa)(1 + \tilde{G}^{-2})\tau\xi'^2\right.\\
&\quad \left. - \frac{e^{-2A}}{4\tilde{G}^2}(\partial_\tau\kappa)^2(\tau'^2 + \tau^2\xi'^2)^2 + \kappa\tilde{G}^{-2}(1 + \kappa e^{-2A}\tau'^2)\xi'^2\right],\\
S_3 &= \kappa\tilde{G}^{-2}(1 + \kappa e^{-2A}\tau^2\xi'^2), \qquad S_4 = \kappa(1 + \kappa e^{-2A}\tau^2\xi'^2),\\
M_1 &= 2\xi'\left[\frac{\partial_\tau V_f}{V_f}\kappa\tau^2 + \kappa\tau(2 - \tilde{G}^{-2}e^{-2A}\kappa\tau^2\xi'^2) + \frac{\tau^2}{2}(\partial_\tau\kappa)(1 + \tilde{G}^{-2})\right],\\
M_2 &= -2e^{-2A}\tilde{G}^{-2}\kappa^2\tau^2\tau'\xi', \qquad M_3 = -2e^{-2A}\kappa^2\tau^2\tau'\xi'.
\end{aligned} \tag{E7}$$

The equations (E4)–(E6) can be recombined into two equations for two variables. They read

$$\psi_s'' + \partial_r(\log C_1)\psi_s' + \frac{1}{C_1}(M + \partial_r C_3 + m^2 C_2)\psi_s + \frac{m^2}{2C_1}\left[\partial_r\left(\frac{M_2}{P_2}\right) - \frac{M_1}{P_2}\right]\hat{\psi}_l = 0, \tag{E8}$$

$$KP_2\partial_r\left(\frac{\psi_l'}{KP_1}\right) - 4e^{2A}\frac{P_2}{w^2}\hat{\psi}_l + m^2\hat{\psi}_l + K\left[P_2\partial_r\left(\frac{M_3}{P_1}\right) - M_1\right]\psi_s = 0, \tag{E9}$$

in terms of

$$\hat{\psi}_l = e^A w^2 V_f\tilde{G}^{-1}\psi_L', \tag{E10}$$

$$K = e^{3A}V_f\tilde{G}^{-1}, \qquad M = K\left(\frac{M_1^2}{2P_2} - 2S_2\right), \qquad C_1 = 2e^{3A}V_f\kappa\tilde{G}^{-3}, \tag{E11}$$

$$C_2 = 2\kappa e^{3A}V_f\frac{\tilde{G}}{G^2}, \qquad C_3 = K\left(S_1 - 2\frac{M_1M_2}{4P_2}\right). \tag{E12}$$

In addition, one can solve for ψ_p from the equation

$$\psi_p' = \frac{m^2}{4}\frac{1}{KP_2}\hat{\psi}_l - \frac{M_2}{4P_2}\psi_s' - \frac{M_1}{4P_2}\psi_s. \tag{E13}$$

APPENDIX F: UV ASYMPOTICS OF THE MESON WAVE FUNCTIONS

In this section we shall study the UV ($r \to 0$) asymptotic solutions of the system of coupled differential equations (D10)–(D11) satisfied by the wave functions of the flavor singlet pseudoscalar modes.

We will first study the system (D10)–(D11) in the UV ($r \to 0$) region. The UV asymptotics of the background were presented in Appendix A 1. We will consider the following UV asymptotics for the remaining potentials determining the action of the fluctuations:

$$V_{f0}(\lambda) \sim W_0(1 + W_1\lambda), \qquad V_a(\lambda,\tau) \sim 1 - b_0\tau^2,$$
$$Z(\lambda) \sim Z_0(1 + c_1\lambda), \qquad w(\lambda) \sim w_0(1 + w_1\lambda). \tag{F1}$$

1. Zero quark mass

The UV expansions at $m_q = 0$ are given by

$$\begin{pmatrix} P \\ Q \\ \hat{P} \\ \hat{Q} \end{pmatrix} = C_+ \begin{pmatrix} -r^{\alpha_+}(-\log(r\Lambda))^{p_+}(1 + \mathcal{O}(\log(r\Lambda)^{-1})) \\ xr^{\alpha_+}(-\log(r\Lambda))^{p_+}(1 + \mathcal{O}(\log(r\Lambda)^{-1})) \\ \frac{xr^{-2+\alpha_+}\ell^3(-\log(r\Lambda))^{p_+}Z_0}{-2+\alpha_+}(1 + \mathcal{O}(\log(r\Lambda)^{-1})) \\ \frac{xr^{-2+\alpha_+}\ell^3(-\log(r\Lambda))^{p_+}Z_0}{2-\alpha_+}(1 + \mathcal{O}(\log(r\Lambda)^{-1})) \end{pmatrix} \tag{F2}$$

$$+ C_- \begin{pmatrix} -r^{\alpha_-}(-\log(r\Lambda))^{p_-}(1 + \mathcal{O}(\log(r\Lambda)^{-1})) \\ xr^{\alpha_-}(-\log(r\Lambda))^{p_-}(1 + \mathcal{O}(\log(r\Lambda)^{-1})) \\ \frac{xr^{-2+\alpha_-}\ell^3(-\log(r\Lambda))^{p_-}Z_0}{-2+\alpha_-}(1 + \mathcal{O}(\log(r\Lambda)^{-1})) \\ \frac{xr^{-2+\alpha_-}\ell^3(-\log(r\Lambda))^{p_-}Z_0}{2-\alpha_-}(1 + \mathcal{O}(\log(r\Lambda)^{-1})) \end{pmatrix} \tag{F3}$$

$$+ C_1 \begin{pmatrix} -\frac{m^2r^{-2}(-\log(r\Lambda))^{-2\rho}}{2\ell^5\sigma^2W_0\kappa_0}(1 + \mathcal{O}(\log(r\Lambda)^{-1})) \\ -\frac{m^2r^4(-3xb_0w_0^2Z_0 + w_0^2W_0\kappa_0 + x\ell^2Z_0\kappa_0)}{2\ell^3Z_0(-2w_0^2W_0 + x\ell^2Z_0)\kappa_0}(1 + \mathcal{O}(\log(r\Lambda)^{-1})) \\ \frac{3m^2r^2w_0^2(-xb_0Z_0 + W_0\kappa_0)}{8w_0^2W_0\kappa_0 - 4x\ell^2Z_0\kappa_0}(1 + \mathcal{O}(\log(r\Lambda)^{-1})) \\ 1 - \frac{m^2r^2(-3xb_0w_0^2Z_0 + w_0^2W_0\kappa_0 + x\ell^2Z_0\kappa_0)}{8w_0^2W_0\kappa_0 - 4x\ell^2Z_0\kappa_0}(1 + \mathcal{O}(\log(r\Lambda)^{-1})) \end{pmatrix} \tag{F4}$$

$$+ C_2 \begin{pmatrix} 1 - \frac{m^2r^2\log(r\Lambda)}{8}(1 + \mathcal{O}(\log(r\Lambda)^{-1})) \\ \frac{r^6\ell^2(-\log(r\Lambda))^{2\rho}\sigma^2xW_0(\ell^2\kappa_0 - 6b_0w_0^2)}{x\ell^2Z_0 - 6W_0w_0^2}(1 + \mathcal{O}(\log(r\Lambda)^{-1})) \\ \frac{r^4\ell^5(-\log(r\Lambda))^{2\rho}\sigma^2w_0^2W_0(xb_0Z_0 - W_0\kappa_0)}{12w_0^2W_0 - 2\ell^2xZ_0}(1 + \mathcal{O}(\log(r\Lambda)^{-1})) \\ \frac{r^4\ell^5(-\log(r\Lambda))^{2\rho}\sigma^2xW_0\kappa_0(\ell^2\kappa_0 - 6b_0w_0^2)}{-4x\ell^2Z_0 + 24W_0w_0^2}(1 + \mathcal{O}(\log(r\Lambda)^{-1})) \end{pmatrix}, \tag{F5}$$

where we have defined

$$\alpha_\pm = 1 \pm \sqrt{1 + \frac{4x\ell^2Z_0}{W_0w_0^2}} \tag{F6}$$

and

$$p_\pm = \pm\frac{16x\ell^2Z_0(V_1 - c_1 - W_1 - 2w_1)}{9V_1W_0w_0^2\sqrt{1 + \frac{4x\ell^2Z_0}{W_0w_0^2}}}. \tag{F7}$$

The parameter ρ was defined in (A7) and m is the mass of the fluctuation.

2. Finite quark mass

The UV expansions at finite m_q are given by

$$\begin{pmatrix} P \\ Q \\ \hat{P} \\ \hat{Q} \end{pmatrix} = C_+ \begin{pmatrix} -r^{\alpha_+}(-\log(r\Lambda))^{p_+}(1+\mathcal{O}(\log(r\Lambda)^{-1})) \\ xr^{\alpha_+}(-\log(r\Lambda))^{p_+}(1+\mathcal{O}(\log(r\Lambda)^{-1})) \\ \frac{xr^{-2+\alpha_+}\ell^3(-\log(r\Lambda))^{p_+}Z_0}{-2+\alpha_+}(1+\mathcal{O}(\log(r\Lambda)^{-1})) \\ \frac{xr^{-2+\alpha_+}\ell^3(-\log(r\Lambda))^{p_+}Z_0}{2-\alpha_+}(1+\mathcal{O}(\log(r\Lambda)^{-1})) \end{pmatrix} \tag{F8}$$

$$+ C_- \begin{pmatrix} -r^{\alpha_-}(-\log(r\Lambda))^{p_-}(1+\mathcal{O}(\log(r\Lambda)^{-1})) \\ xr^{\alpha_-}(-\log(r\Lambda))^{p_-}(1+\mathcal{O}(\log(r\Lambda)^{-1})) \\ \frac{xr^{-2+\alpha_-}\ell^3(-\log(r\Lambda))^{p_-}Z_0}{-2+\alpha_-}(1+\mathcal{O}(\log(r\Lambda)^{-1})) \\ \frac{xr^{-2+\alpha_-}\ell^3(-\log(r\Lambda))^{p_-}Z_0}{2-\alpha_-}(1+\mathcal{O}(\log(r\Lambda)^{-1})) \end{pmatrix} \tag{F9}$$

$$+ C_1 \begin{pmatrix} \frac{m^2r^2(-\log(r\Lambda))^{2\rho}}{2\ell^5 m_q^2 W_0\kappa_0}(1+\mathcal{O}(\log(r\Lambda)^{-1})) \\ -\frac{m^2r^4(xb_0w_0^2Z_0+w_0^2W_0\kappa_0-x\ell^2Z_0\kappa_0)}{2\ell^3Z_0(-2w_0^2W_0+x\ell^2Z_0)\kappa_0}(1+\mathcal{O}(\log(r\Lambda)^{-1})) \\ \frac{m^2r^2w_0^2(xb_0Z_0-W_0\kappa_0)}{8w_0^2W_0\kappa_0-4x\ell^2Z_0\kappa_0}(1+\mathcal{O}(\log(r\Lambda)^{-1})) \\ 1-\frac{m^2r^2(xb_0w_0^2Z_0+w_0^2W_0\kappa_0-x\ell^2Z_0\kappa_0)}{8w_0^2W_0\kappa_0-4x\ell^2Z_0\kappa_0}(1+\mathcal{O}(\log(r\Lambda)^{-1})) \end{pmatrix} \tag{F10}$$

$$+ C_2 \begin{pmatrix} 1+\frac{m^2r^2\log(r\Lambda)}{-2+4\rho}(1+\mathcal{O}(\log(r\Lambda)^{-1})) \\ \frac{r^2\ell^2(-\log(r\Lambda))^{-2\rho}m_q^2W_0\kappa_0}{Z_0}(1+\mathcal{O}(\log(r\Lambda)^{-1})) \\ \frac{\ell^3(-\log(r\Lambda))^{-2\rho}m_q^2w_0^2W_0(-xb_0Z_0+W_0\kappa_0)}{2xZ_0}(1+\mathcal{O}(\log(r\Lambda)^{-1})) \\ \frac{\ell^5(-\log(r\Lambda))^{1-2\rho}m_q^2W_0\kappa_0}{1-2\rho}(1+\mathcal{O}(\log(r\Lambda)^{-1})) \end{pmatrix}. \tag{F11}$$

If we set $x \to 0$ first the expansions become

$$\begin{pmatrix} P \\ Q \\ \hat{P} \\ \hat{Q} \end{pmatrix} = C_1^{(Q)} \begin{pmatrix} \frac{2r^2}{\ell w_0^2 W_0}(1+\mathcal{O}(\log(r\Lambda)^{-1})) \\ \frac{m^2r^4}{4\ell^3Z_0}(1+\mathcal{O}(\log(r\Lambda)^{-1})) \\ -1+\frac{m^2r^2}{8}(1+\mathcal{O}(\log(r\Lambda)^{-2})) \\ 1-\frac{m^2r^2}{8}(1+\mathcal{O}(\log(r\Lambda)^{-2})) \end{pmatrix} \tag{F12}$$

$$+ C_2^{(Q)} \begin{pmatrix} \frac{2\ell^2\log(r\Lambda)Z_0}{w_0^2W_0}(1+\mathcal{O}(\log(r\Lambda)^{-1})) \\ 1+\frac{m^2r^2}{4}(1+\mathcal{O}(\log(r\Lambda)^{-1})) \\ -\frac{\ell^3Z_0}{2r^2}(1+\mathcal{O}(\log(r\Lambda)^{-1})) \\ \frac{\ell^3Z_0}{2r^2}(1+\mathcal{O}(\log(r\Lambda)^{-1})) \end{pmatrix}, \tag{F13}$$

$$\begin{pmatrix} P \\ \hat{P} \end{pmatrix} = C_1^{(P)} \begin{pmatrix} \frac{m^2 r^2 (-\log(r\Lambda))^{2\rho}}{2\ell^5 m_q^2 W_0 \kappa_0} (1 + \mathcal{O}(\log(r\Lambda)^{-1})) \\ 1 - \frac{1}{4} m^2 r^2 (1 - \frac{\rho}{\log(r\Lambda)} + \mathcal{O}(\log(r\Lambda)^{-2})) \end{pmatrix} \tag{F14}$$

$$+ C_2^{(P)} \begin{pmatrix} 1 + \frac{m^2 r^2 \log(r\Lambda)}{2(-1+2\rho)} (1 + \mathcal{O}(\log(r\Lambda)^{-1})) \\ \frac{\ell^5 (-\log(r\Lambda))^{1-2\rho} m_q^2 W_0 \kappa_0}{1-2\rho} (1 + \mathcal{O}(\log(r\Lambda)^{-1})) \end{pmatrix} \tag{F15}$$

where $Q = 0 = \hat{Q}$ for the last two functions.

APPENDIX G: PROOF OF THE WITTEN-VENEZIANO FORMULA

In order to prove the Witten-Veneziano formula we follow the strategy outlined in Sec. VII B 2. We need to compute the coefficient matrix in (7.18) at leading nontrivial order by studying the behavior of the IR normalizable solutions in the UV. To do this precisely we expand the IR normalizable solutions $\psi^{(P)}$ and $\psi^{(Q)}$ systematically at small x and m_f^2 with m_f being the mass of the fluctuation mode. We write the expansions of the various fields as

$$F = \sum_{M,N=0}^{\infty} F_{MN} m_f^{2M} x^N, \qquad (F = P, Q, \hat{P}, m_f^2 \hat{Q}). \tag{G1}$$

Notice that in addition to x and m_f^2 we have another small parameter m_q. Therefore we should study how the components F_{MN} behave at small m_q. In particular some of the components are proportional to $m_q^{-1} \sim m_\pi^{-2}$ (as we have already seen in Sec. VII B 2) and therefore subleading terms in the expansion may contribute at leading order in the η' mass. We need to identify such terms.

For the $\psi^{(P)}$ solution we expect that $Q = \mathcal{O}(x) = \hat{Q}$ and therefore we can set $Q_{0M} = 0 = \hat{Q}_{0M}$ for all M. Substituting the expansions in the fluctuation equations (7.8)–(7.11) we find

$$P'_{00} = -\frac{4e^{-A}G}{V_f w^2} \hat{P}_{00}, \qquad \hat{P}'_{00} = -e^{3A} G V_f \kappa \tau^2 P_{00}. \tag{G2}$$

We choose the IR normalizable solution which is recognized as the $m_f = 0 = x$ solution discussed in Sec. VII B 1, with the normalization $P_{00} \to 1$ and $\hat{P}_{00} \to C_P$ as $r \to 0$. Recall that C_P was related to the pion decay constant in (7.14), up to corrections suppressed by m_q and x. The other components F_{MN} can be solved iteratively from the fluctuation equations with the boundary condition that they vanish in the IR, which uniquely defines $\psi^{(P)}$.

Going higher order in m_f^2 we find that

$$P'_{10} = \frac{e^{-3A} G (w^2 \hat{P}_{00} - 4e^{2A} \kappa \tau^2 \hat{P}_{10})}{V_f w^2 \kappa \tau^2},$$
$$\hat{P}'_{10} = -e^{3A} G V_f \kappa \tau^2 P_{10}. \tag{G3}$$

Here $\hat{P}_{10}$ is not enhanced as $m_q \to 0$, but P_{10} is. The same arguments as when discussing (7.15) give[24]

$$\lim_{r\to 0} P_{10} = -\frac{C_P}{W_0 \kappa_0 \ell^3} \int_0^\infty \frac{r^3 dr}{\tau(r)^2} + \mathcal{O}(m_q^0) = -\frac{1}{m_\pi^2} + \mathcal{O}(m_q^0). \tag{G4}$$

The higher order corrections in x in the equations lead to

$$P'_{01} = -\frac{4e^{-A}G}{V_f w^2} \hat{P}_{01},$$
$$\hat{P}'_{01} = -e^{3A} (V_a^2 Z P_{00} + G V_f \kappa \tau^2 P_{01}). \tag{G5}$$

We notice that these terms are not enhanced as $m_q \to 0$ and may be neglected as their contributions are suppressed by $\mathcal{O}(x)$. Summarizing, we obtain the anticipated result

$$C_{PP} \simeq \lim_{r\to 0} (P_{00} + m_f^2 P_{10}) = 1 - \frac{m_f^2}{m_\pi^2}. \tag{G6}$$

We also obtain the exact solutions

$$\hat{Q}_{01} = 0, \qquad Q_{01} = -V_a P_{00}. \tag{G7}$$

This is remarkable since it allows us to compute the leading contribution to the mixing coefficient C_{PQ}. It is given by

$$C_{PQ} \simeq x \lim_{r\to 0} Q_{01} = -x, \tag{G8}$$

where we used the fact that $V_a \to 1$ at the boundary as required by the implementation of the axial anomaly. Again

[24]To be precise, the corrections to the integral in (G4) are larger than $\mathcal{O}(m_q^0)$ because we did not include the logarithmic corrections to the potentials, but in the final expression the corrections are indeed $\mathcal{O}(m_q^0)$ as shown in Appendix D of [55].

it may be checked that higher order terms in the series expansion contribute negligibly to C_{PQ}.

We then go on discussing the solution $\psi^{(Q)}$. The solution is defined by setting

$$\hat{Q}_{00} = \text{const} = -C_Q, \tag{G9}$$

which leads to

$$Q_{00}(r) = C_Q \int_r^\infty \frac{d\hat{r}}{e^{3A}Z}. \tag{G10}$$

Normalizing Q_{00} to unity at the boundary (so that $C_{QQ} \simeq 1$)

$$C_Q = \left(\int_0^\infty \frac{dr}{e^{3A}Z}\right)^{-1} = \frac{\chi_{\rm YM}}{M^3}, \tag{G11}$$

where $\chi_{\rm YM}$ is the (Yang-Mills) topological susceptibility. Again solving the fluctuation equations perturbatively gives

$$\begin{aligned} P'_{00} &= -\frac{e^{-3A}G(C_Q V_a w^2 + 4e^{2A}\kappa\tau^2\hat{P}_{00})}{V_f w^2 \kappa\tau^2}, \\ \hat{P}'_{00} &= e^{3A}(V_a Z Q_{00} - G V_f \kappa\tau^2 P_{00}). \end{aligned} \tag{G12}$$

As $m_q \to 0$ the most important contribution is the term $\propto C_Q$, and after integration

$$\begin{aligned} \lim_{r\to 0} P_{00}(r) &= \frac{C_Q}{W_0\kappa_0\ell^3}\int_0^\infty \frac{r^3 dr}{\tau(r)^2} + \mathcal{O}(m_q^0) \\ &= \frac{C_Q}{C_P m_\pi^2} + \mathcal{O}(m_q^0), \end{aligned} \tag{G13}$$

where we again could set V_a to unity near the boundary. Therefore $C_{QP} \simeq C_Q/C_P m_\pi^2$.

Collecting the results,

$$\begin{pmatrix} C_{PP} & C_{PQ} \\ C_{QP} & C_{QQ} \end{pmatrix} \simeq \begin{pmatrix} 1 - \frac{m_f^2}{m_\pi^2} & -x \\ \frac{C_Q}{C_P m_\pi^2} & 1 \end{pmatrix}. \tag{G14}$$

Requiring the determinant of this matrix to vanish marks the point $m_f = m_{\eta'}$, and results in the Witten-Veneziano formula

$$m_{\eta'}^2 \simeq m_\pi^2 + x\frac{C_Q}{C_P} \simeq m_\pi^2 + x\frac{N_f N_c \chi_{\rm YM}}{f_\pi^2}, \tag{G15}$$

where we used (7.14) and (G11) in the last step. Recall that for our normalization conventions $f_\pi^2 = \mathcal{O}(N_f N_c)$.

APPENDIX H: THE GELL-MANN-OAKES-RENNER RELATION AT FINITE $\bar{\theta}$

It is possible to compute the dependence of the mass of the pion on $\bar{\theta}$ in the QCD-like regime [$0 < x < x_c$ and $x_c - x = \mathcal{O}(1)$] when the quark mass m_q is small. This can be done by solving the fluctuation equations in different approximations near the boundary and in the IR and by requiring that the two results agree.

The general fluctuation equations for the scalar and pseudoscalar mesons are given in Eqs. (E9) in Appendix E. However, the (appropriately normalized) pion wave function is localized near the boundary, for $r \sim \sqrt{m_q/\sigma}$ (see computation for V-QCD at $\bar{\theta} = 0$ in Appendices E and F of [55]). In order to see how the pion wave function behaves in this neighborhood at finite $\bar{\theta}$, it is useful to rewrite the fluctuations of the tachyon using a decomposition into real and imaginary parts rather then the absolute value and phase.

To make the argument precise, we write

$$T = \tau e^{i\xi} + s_r^a t^a + i s_i^a t^a \tag{H1}$$

for the flavor nonsinglet fluctuations instead of (E1). Moreover we decompose the wave functions of the fluctuations to radial and spatial parts as in (E3) and denote the radial wave functions as ψ_r and ψ_i. When $r \ll 1/\Lambda_{\rm UV}$ and when the squared mass of the fluctuations is $\mathcal{O}(m_q)$, as we expect for the lowest mode which will be identified as the pion below, the tachyon field of (H1), and therefore also the functions ψ_r and ψ_i, satisfy the same equation (3.13) as the background:

$$\begin{aligned} &\psi''_{r/i} + \partial_r \log(e^{3A}\kappa V_{f0})\psi'_{r/i} - e^{2A}m_\tau^2\psi_{r/i} \\ &\quad = \mathcal{O}(m_q\psi_{r/i}) \qquad \left(r \ll \frac{1}{\Lambda_{\rm UV}}\right), \end{aligned} \tag{H2}$$

where the leading correction arises from the terms involving the (squared) mass of the fluctuations.

We denote the linearly independent non-normalizable and normalizable solutions of (H2) as τ_m and τ_σ, respectively, so that the background solution reads

$$\begin{aligned} \tau(r)e^{i\xi(r)} &= m_q e^{i\xi_0}\tau_m(r) + (\sigma_0 + \mathcal{O}(m_q))\tau_\sigma(r) \\ &\qquad \left(r \ll \frac{1}{\Lambda_{\rm UV}}\right). \end{aligned} \tag{H3}$$

Here we denoted the value of the VEV at $m_q = 0$ by σ_0 and dropped corrections $\mathcal{O}(m_q)$ to the VEV term as in the analysis of Sec. VI D. We have chosen the gauge where $\xi \to 0$ as $r \to \infty$, so that $\xi \simeq \bar{\theta}/N_f$ [see (6.23)]. The imaginary part of the pion mode is UV normalizable and therefore given as

$$\tau\cos(\xi)\psi_p = \tau_r\psi_p = \psi_i = C_p\tau_\sigma, \tag{H4}$$

where

$$\tau_r = \tau\cos(\xi) \simeq m_q\cos(\xi_0)\tau_m + \sigma_0\tau_\sigma \tag{H5}$$

is the real part of the background solution. Now we find that

$$\psi_p' = C_p\frac{\tau_\sigma'\tau_r - \tau_\sigma\tau_r'}{\tau_r^2} \tag{H6}$$

and therefore

$$V_{f0}\kappa e^{3A}\tau_r^2\psi_p' = C_pV_{f0}\kappa e^{3A}(\tau_\sigma'\tau_r - \tau_\sigma\tau_r'). \tag{H7}$$

This expression is constant for $r \ll 1/\Lambda_{\rm UV}$, up to correction suppressed by $\mathcal{O}(m_q)$, as can be seen analyzing (H2)—the latter form is proportional to the Wronskian (see also Appendix D in [55]). The value of the constant can be computed by taking $r \to 0$ on the right-hand side:

$$\begin{aligned} V_{f0}\kappa e^{3A}\tau_r^2\psi_p' &= C_p\lim_{r\to 0}(\tau_\sigma'\tau_r - \tau_\sigma\tau_r') \\ &= 2C_pW_0\kappa_0\ell^5 m_q\cos\xi_0. \end{aligned} \tag{H8}$$

To complete the computation of the pion mass we need to make contact with the fluctuations in the IR. We note that the tachyon background depends on m_q smoothly when written as a complex field:

$$\tau e^{i\xi} = \tau_0 + \mathcal{O}(m_q), \tag{H9}$$

where τ_0 is the (real) background at $m_q = 0$. As τ_0 does not have nodes in the IR, the phase ξ is $\mathcal{O}(m_q)$. The phase is the source of parity violation, and therefore the mixing between the scalar and pseudoscalar fluctuations is controlled by it. That is, all coefficients of the mixing terms in the fluctuation equations (E4)–(E6) in Appendix E are $\mathcal{O}(m_q)$ in the IR. Therefore we can choose a basis with an IR normalizable mode, relevant for the pion, which has $\psi_p = \mathcal{O}(1)$ and $\psi_s = \mathcal{O}(m_q)$. Taking stock, the fluctuation equation (E4) for the pion mode becomes

$$\begin{aligned} &\frac{1}{GV_f\kappa\tau^2e^{3A}}\partial_r\left(\frac{V_f\kappa\tau^2e^{3A}}{G}\psi_p'\right) + m^2(\psi_p - \psi_L) \\ &= \mathcal{O}(m_q^2) \qquad \left(r \gg \sqrt{\frac{m_q}{\sigma_0}}\right), \end{aligned} \tag{H10}$$

where the precise range of validity can be seen by inserting the UV expression (H3) into the fluctuation equations. This implies that in the IR the fluctuation equation takes the same form as for $\bar\theta = 0$. In particular, there is not dependence on $\bar\theta$, apart from possible dependence through the mass of the fluctuation m.

When $m = 0$ exactly, the solutions to (H10) are given by

$$\frac{V_f\kappa\tau^2e^{3A}}{G}\psi_p' = \text{const}, \qquad \psi_p = \text{const}. \tag{H11}$$

The first solution is non-normalizable in the IR, but the second solution is normalizable (when $m_q = 0$ also it is identified as the pion mode). For m small but nonzero the terms mix so that the normalizable mode is constant to leading order in m but also includes a component $\propto m^2$ corresponding to the first term which can be computed by integrating (H10).

When $\sqrt{m_q/\sigma_0} \ll r \ll 1/\Lambda_{\rm UV}$ we can match the UV and IR behavior of the fluctuations, construct the pion mode, and determine its mass. From the IR analysis we learned that the pion is dominated by the second solution in (H11), but there is also a small component corresponding to the first solution [which can be obtained in principle by integrating (H10)], which satisfies

$$V_f\kappa\tau^2e^{3A}\psi_p' = k_pm_\pi^2\psi_p + \mathcal{O}(m_q^2) \qquad \left(\sqrt{\frac{m_q}{\sigma_0}} \ll r \ll \frac{1}{\Lambda_{\rm UV}}\right), \tag{H12}$$

where the proportionality coefficient k_p is independent of m_q and $\bar\theta$. Notice that for $r \ll 1/\Lambda_{\rm UV}$ we were able to approximate $G = 1$ and that (H10) implies that the left-hand side of (H12) is indeed constant in this regime. Comparing to the result of the UV analysis in (H8) (noticing that $C_p \simeq \psi_p$ and $\tau_r \simeq \tau$) we see that

$$k_pm_\pi^2 = 2W_0\kappa_0\ell^5m_q\cos\xi_0 + \mathcal{O}(m_q^2). \tag{H13}$$

As k_p was independent of m_q and $\bar\theta$, we find that $m_\pi^2 \propto m_q\cos\xi_0$. Comparing to the GOR relation at $\bar\theta = 0$ [55], the proportionality constant is found to be $k_p = f_{\pi,0}^2/M^3N_fN_c\sigma_0$, where $f_{\pi,0}$ is the pion decay constant at $\bar\theta = 0$. The final result therefore reads

$$f_{\pi,0}^2m_\pi^2 = -\langle\bar\psi\psi\rangle|_{m_q=0}m_q\cos\frac{\bar\theta}{N_f} + \mathcal{O}(m_q^2), \tag{H14}$$

where we inserted (6.23) and the relation between the condensate and σ_0.

[1] S. Weinberg, The U(1) problem, Phys. Rev. D **11**, 3583 (1975).

[2] R. J. Crewther, Effects of topological charge in gauge theories, Acta Phys. Austriaca Suppl. **19**, 47 (1978).

[3] G. 't Hooft, Symmetry Breaking through Bell-Jackiw Anomalies, Phys. Rev. Lett. **37**, 8 (1976).

[4] R. J. Crewther, Chirality selection rules and the U(1) problem, Phys. Lett. B **70**, 349 (1977).

[5] E. Witten, Instantons, the quark model and the $1/n$ expansion, Nucl. Phys. **B149**, 285 (1979).

[6] G. Veneziano, U(1) without instantons, Nucl. Phys. **B159**, 213 (1979).

[7] E. Witten, Current algebra theorems for the U(1) Goldstone boson, Nucl. Phys. **B156**, 269 (1979).

[8] P. Di Vecchia, An Effective Lagrangian with No U(1) Problem in CP^{n-1} Models and QCD, Phys. Lett. **85B**, 357 (1979).

[9] C. Rosenzweig, J. Schechter, and C. G. Trahern, Is the effective Lagrangian for QCD a sigma model?, Phys. Rev. D **21**, 3388 (1980).

[10] P. Di Vecchia and G. Veneziano, Chiral dynamics in the large n limit, Nucl. Phys. **B171**, 253 (1980).

[11] E. Witten, Large N chiral dynamics, Ann. Phys. (N.Y.) **128**, 363 (1980).

[12] K. Kawarabayashi and N. Ohta, The problem of η in the large N limit: effective Lagrangian approach, Nucl. Phys. **B175**, 477 (1980).

[13] N. Ohta, Vacuum structure and chiral charge quantization in the large N limit, Prog. Theor. Phys. **66**, 1408 (1981); Erratum, Prog. Theor. Phys. **67**, 993(E) (1982).

[14] E. Vicari and H. Panagopoulos, Theta dependence of SU(N) gauge theories in the presence of a topological term, Phys. Rep. **470**, 93 (2009).

[15] C. Bonati, M. D'Elia, H. Panagopoulos, and E. Vicari, Θ dependence of 4D SU(N) gauge theories at finite temperature, *Proc. Sci.*, LATTICE2013 (2014) 136 [arXiv:1309.6059].

[16] C. Bonati, M. D'Elia, and A. Scapellato, θ dependence in $SU(3)$ Yang-Mills theory from analytic continuation, Phys. Rev. D **93**, 025028 (2016).

[17] C. Bonati, M. D'Elia, P. Rossi, and E. Vicari, θ dependence of 4D $SU(N)$ gauge theories in the large-N limit, Phys. Rev. D **94**, 085017 (2016).

[18] M. A. Shifman, A. I. Vainshtein, and V. I. Zakharov, Can confinement ensure natural CP invariance of strong interactions?, Nucl. Phys. **B166**, 493 (1980).

[19] R. D. Peccei and H. R. Quinn, CP Conservation in the Presence of Instantons, Phys. Rev. Lett. **38**, 1440 (1977).

[20] S. Weinberg, A New Light Boson?, Phys. Rev. Lett. **40**, 223 (1978).

[21] F. Wilczek, Problem of Strong p and t Invariance in the Presence of Instantons, Phys. Rev. Lett. **40**, 279 (1978).

[22] J. E. Kim, Weak Interaction Singlet and Strong CP Invariance, Phys. Rev. Lett. **43**, 103 (1979).

[23] A. R. Zhitnitsky, On possible suppression of the axion hadron interactions, Yad. Fiz. **31**, 497 (1980) [Sov. J. Nucl. Phys. **31**, 260 (1980)].

[24] M. Dine, W. Fischler, and M. Srednicki, A simple solution to the strong CP problem with a harmless axion, Phys. Lett. **104B**, 199 (1981).

[25] C. Vafa and E. Witten, Parity Conservation in QCD, Phys. Rev. Lett. **53**, 535 (1984).

[26] G. Grilli di Cortona, E. Hardy, J. P. Vega, and G. Villadoro, The QCD axion, precisely, J. High Energy Phys. 01 (2016) 034.

[27] D. E. Kharzeev, L. D. McLerran, and H. J. Warringa, The effects of topological charge change in heavy ion collisions: "Event by event P and CP violation", Nucl. Phys. **A803**, 227 (2008); K. Fukushima, D. E. Kharzeev, and H. J. Warringa, Chiral magnetic effect, Phys. Rev. D **78**, 074033 (2008).

[28] E. V. Shuryak, Suppression of instantons as the origin of confinement, Phys. Lett. **79B**, 135 (1978); D. J. Gross, R. D. Pisarski, and L. G. Yaffe, QCD and instantons at finite temperature, Rev. Mod. Phys. **53**, 43 (1981).

[29] V. A. Kuzmin, V. A. Rubakov, and M. E. Shaposhnikov, On the anomalous electroweak baryon number nonconservation in the early universe, Phys. Lett. **155B**, 36 (1985); P. B. Arnold and L. D. McLerran, Sphalerons, small fluctuations, and baryon number violation in electroweak theory, Phys. Rev. D **36**, 581 (1987); A. R. Zhitnitsky, Local P violation effects and thermalization in QCD: Views from quantum field theory and holography, Nucl. Phys. **A886**, 17 (2012); G. D. Moore and M. Tassler, The sphaleron rate in SU(N) gauge theory, J. High Energy Phys. 02 (2011) 105.

[30] I. Iatrakis, S. Lin, and Y. Yin, Axial Current Generation by P-odd Domains in QCD matter, Phys. Rev. Lett. **114**, 252301 (2015); The anomalous transport of axial charge: Topological vs non-topological fluctuations, J. High Energy Phys. 09 (2015) 030.

[31] A. Jimenez-Alba, K. Landsteiner, and L. Melgar, Anomalous magnetoresponse and the Stckelberg axion in holography, Phys. Rev. D **90**, 126004 (2014).

[32] U. Gürsoy and A. Jansen, (Non)renormalization of anomalous conductivities and holography, J. High Energy Phys. 10 (2014) 092; U. Gursoy and J. Tarrio, Horizon universality and anomalous conductivities, J. High Energy Phys. 10 (2015) 058.

[33] E. Witten, Theta Dependence in the Large N Limit of Four-Dimensional Gauge Theories, Phys. Rev. Lett. **81**, 2862 (1998).

[34] E. Witten, Anti-de Sitter space, thermal phase transition and confinement in gauge theories, Adv. Theor. Math. Phys. **2**, 505 (1998).

[35] U. Gürsoy and E. Kiritsis, Exploring improved holographic theories for QCD: Part I, J. High Energy Phys. 02 (2008) 032; U. Gürsoy, E. Kiritsis, and F. Nitti, Exploring improved holographic theories for QCD: Part II, J. High Energy Phys. 02 (2008) 019; E. Kiritsis, Dissecting the string theory dual of QCD, Fortschr. Phys. **57**, 396 (2009); U. Gürsoy, E. Kiritsis, L. Mazzanti, G. Michalogiorgakis, and F. Nitti, Improved holographic QCD, Lect. Notes Phys. **828**, 79 (2011).

[36] U. Gürsoy, E. Kiritsis, L. Mazzanti, F. Nitti, Deconfinement and Gluon Plasma Dynamics in Improved Holographic QCD, Phys. Rev. Lett. **101**, 181601 (2008); U. Gürsoy, E. Kiritsis, L. Mazzanti, and F. Nitti, Holography and thermodynamics of 5D dilaton-gravity, J. High Energy Phys. 05 (2009) 033.

[37] F. Bigazzi, A. L. Cotrone, and R. Sisca, Notes on theta dependence in holographic Yang-Mills, J. High Energy Phys. 08 (2015) 090.
[38] J. L. F. Barbon and A. Pasquinucci, Aspects of instanton dynamics in AdS/CFT duality, Phys. Lett. B **458**, 288 (1999).
[39] S. Dubovsky, A. Lawrence, and M. M. Roberts, Axion monodromy in a model of holographic gluodynamics, J. High Energy Phys. 02 (2012) 053.
[40] J. L. F. Barbon, C. Hoyos-Badajoz, D. Mateos, and R. C. Myers, The holographic life of the eta-prime, J. High Energy Phys. 10 (2004) 029.
[41] M. Kruczenski, D. Mateos, R. C. Myers, and D. J. Winters, Towards a holographic dual of large-N(c) QCD, J. High Energy Phys. 05 (2004) 041.
[42] A. Armoni, Witten-Veneziano and from Green-Schwarz, J. High Energy Phys. 06 (2004) 019.
[43] T. Sakai and S. Sugimoto, Low energy hadron physics in holographic QCD, Prog. Theor. Phys. **113**, 843 (2005).
[44] R. Casero, E. Kiritsis, and A. Paredes, Chiral symmetry breaking as open string tachyon condensation, Nucl. Phys. **B787**, 98 (2007).
[45] I. Iatrakis, E. Kiritsis, and A. Paredes, An AdS/QCD model from Sen's tachyon action, Phys. Rev. D **81**, 115004 (2010); An AdS/QCD model from tachyon condensation: II, J. High Energy Phys. 11 (2010) 123.
[46] F. Bigazzi and A. L. Cotrone, Holographic QCD with dynamical flavors, J. High Energy Phys. 01 (2015) 104.
[47] M. B. Green, J. A. Harvey, and G. W. Moore, I-brane inflow and anomalous couplings on d-branes, Classical Quantum Gravity **14**, 47 (1997).
[48] M. Järvinen and E. Kiritsis, Holographic Models for QCD in the Veneziano Limit, J. High Energy Phys. 03 (2012) 002.
[49] T. Alho, M. Järvinen, K. Kajantie, E. Kiritsis, and K. Tuominen, On finite-temperature holographic QCD in the Veneziano limit, arXiv:1210.4516.
[50] D. Arean, I. Iatrakis, M. Järvinen, and E. Kiritsis, V-QCD: Spectra, the dilaton and the S-parameter, Phys. Lett. B **720**, 219 (2013).
[51] D. Arean, I. Iatrakis, M. Järvinen, and E. Kiritsis, The discontinuities of conformal transitions and mass spectra of V-QCD, J. High Energy Phys. 11 (2013) 068.
[52] T. Alho, M. Järvinen, K. Kajantie, E. Kiritsis, C. Rosen, and K. Tuominen, A holographic model for QCD in the Veneziano limit at finite temperature and density, J. High Energy Phys. 04 (2014) 124; Erratum, J. High Energy Phys. 02 (2015) 033.
[53] T. Alho, M. Järvinen, K. Kajantie, E. Kiritsis, and K. Tuominen, Quantum and stringy corrections to the equation of state of holographic QCD matter and the nature of the chiral transition, Phys. Rev. D **91**, 055017 (2015).
[54] I. Iatrakis and I. Zahed, Spectral functions in V-QCD with matter: Masses, susceptibilities, diffusion, and conductivity, J. High Energy Phys. 04 (2015) 080.
[55] M. Järvinen, Massive holographic QCD in the Veneziano limit, J. High Energy Phys. 07 (2015) 033.
[56] F. Bigazzi, R. Casero, A. L. Cotrone, E. Kiritsis, and A. Paredes, Non-critical holography and four-dimensional CFT's with fundamentals, J. High Energy Phys. 10 (2005) 012.
[57] R. Casero, C. Nunez, and A. Paredes, Towards the string dual of $N = 1$ SQCD-like theories, Phys. Rev. D **73**, 086005 (2006); C. Nunez, A. Paredes, and A. V. Ramallo, Unquenched flavor in the gauge/gravity correspondence, Adv. High Energy Phys. **2010**, 196714 (2010).
[58] O. Bergman, S. Seki, and J. Sonnenschein, Quark mass and condensate in HQCD, J. High Energy Phys. 12 (2007) 037; A. Dhar and P. Nag, Sakai-Sugimoto model, tachyon condensation and chiral symmetry breaking, J. High Energy Phys. 01 (2008) 055; Tachyon condensation and quark mass in modified Sakai-Sugimoto model, Phys. Rev. D **78**, 066021 (2008); N. Jokela, M. Järvinen, and S. Nowling, Winding effects on brane/anti-brane pairs, J. High Energy Phys. 07 (2009) 085.
[59] P. Kraus and F. Larsen, Boundary string field theory of the D anti-D system, Phys. Rev. D **63**, 106004 (2001); T. Takayanagi, S. Terashima, and T. Uesugi, Brane-anti-brane action from boundary string field theory, J. High Energy Phys. 03 (2001) 019.
[60] U. Gürsoy, I. Iatrakis, E. Kiritsis, F. Nitti, and A. O'Bannon, The Chern-Simons diffusion rate in improved holographic QCD, J. High Energy Phys. 02 (2013) 119.
[61] M. Järvinen and F. Sannino, Holographic conformal window: A bottom up approach, J. High Energy Phys. 05 (2010) 041.
[62] J. M. Kosterlitz and D. J. Thouless, Ordering, metastability and phase transitions in two-dimensional systems, J. Phys. C **6**, 1181 (1973).
[63] V. A. Miransky and K. Yamawaki, Conformal phase transition in gauge theories, Phys. Rev. D **55**, 5051 (1997); Erratum, Phys. Rev. D **56**, 3768(E) (1997).
[64] K. Yamawaki, M. Bando, and K.-i. Matumoto, Scale Invariant Technicolor Model and a Technidilaton, Phys. Rev. Lett. **56**, 1335 (1986).
[65] D. Kutasov, J. Lin, and A. Parnachev, Conformal phase transitions at weak and strong coupling, Nucl. Phys. **B858**, 155 (2012).
[66] D. Kutasov, J. Lin, and A. Parnachev, Holographic walking from tachyon DBI, Nucl. Phys. **B863**, 361 (2012); M. Goykhman and A. Parnachev, S-parameter, technimesons, and phase transitions in holographic tachyon DBI models, Phys. Rev. D **87**, 026007 (2013).
[67] J. Alanen and K. Kajantie, Thermodynamics of a field theory with infrared fixed point from gauge/gravity duality, Phys. Rev. D **81**, 046003 (2010); J. Alanen, K. Kajantie, and K. Tuominen, Thermodynamics of quasi conformal theories from gauge/gravity duality, Phys. Rev. D **82**, 055024 (2010); J. Alanen, T. Alho, K. Kajantie, and K. Tuominen, Mass spectrum and thermodynamics of quasiconformal gauge theories from gauge/gravity duality, Phys. Rev. D **84**, 086007 (2011).
[68] R. Alvares, N. Evans, and K.-Y. Kim, Holography of the conformal window, Phys. Rev. D **86**, 026008 (2012); T. Alho, N. Evans, and K. Tuominen, Dynamic AdS/QCD and the spectrum of walking gauge theories, Phys. Rev. D **88**, 105016 (2013); J. Erdmenger, N. Evans, and M. Scott, Meson spectra of asymptotically free gauge theories from holography, Phys. Rev. D **91**, 085004 (2015).
[69] D. B. Kaplan, J.-W. Lee, D. T. Son, and M. A. Stephanov, Conformality lost, Phys. Rev. D **80**, 125005 (2009).

[70] N. Evans and M. Scott, Hyperscaling relations in the conformal window from dynamic AdS/QCD, Phys. Rev. D **90**, 065025 (2014).

[71] D. D. Dietrich, Mass-dependent beta-function, Phys. Rev. D **80**, 065032 (2009); Quasionformality and mass, Phys. Rev. D **82**, 065007 (2010).

[72] L. Del Debbio and R. Zwicky, Hyperscaling relations in mass-deformed conformal gauge theories, Phys. Rev. D **82**, 014502 (2010).

[73] U. Gürsoy, E. Kiritsis, L. Mazzanti, and F. Nitti, Improved holographic Yang-Mills at finite temperature: Comparison with data, Nucl. Phys. **B820**, 148 (2009).

[74] J. Schechter, Effective Lagrangian with two color singlet gluon fields, Phys. Rev. D **21**, 3393 (1980).

[75] E. Kiritsis, W. Li, and F. Nitti, Holographic RG flow and the quantum effective action, Fortschr. Phys. **62**, 389 (2014).

[76] E. Kiritsis, W. Li, and F. Nitti, On the gluonic operator effective potential in holographic Yang-Mills theory, J. High Energy Phys. 04 (2015) 125.

[77] P. Nath and R. L. Arnowitt, The U(1) problem: Current algebra and the theta vacuum, Phys. Rev. D **23**, 473 (1981).

[78] H. Leutwyler and A. V. Smilga, Spectrum of Dirac operator and role of winding number in QCD, Phys. Rev. D **46**, 5607 (1992).

[79] N. Iqbal, H. Liu, and M. Mezei, Semi-local quantum liquids, J. High Energy Phys. 04 (2012) 086; Quantum phase transitions in semi-local quantum liquids, arXiv:1108.0425; Lectures on holographic non-Fermi liquids and quantum phase transitions, arXiv:1110.3814.